

UNCLASSIFIED

AD 296 861

*Reproduced
by the*

**ARMED SERVICES TECHNICAL INFORMATION AGENCY
ARLINGTON HALL STATION
ARLINGTON 12, VIRGINIA**



UNCLASSIFIED

NOTICE: When government or other drawings, specifications or other data are used for any purpose other than in connection with a definitely related government procurement operation, the U. S. Government thereby incurs no responsibility, nor any obligation whatsoever; and the fact that the Government may have formulated, furnished, or in any way supplied the said drawings, specifications, or other data is not to be regarded by implication or otherwise as in any manner licensing the holder or any other person or corporation, or conveying any rights or permission to manufacture, use or sell any patented invention that may in any way be related thereto.

296 861

63-2-4
14

296861

ASD-TDR-62-1045

DESIGN AND DEVELOPMENT OF A LIQUID METAL FUEL CELL

TECHNICAL DOCUMENTARY REPORT NO. ASD-TDR-62-1045

December 1962

Directorate of Aeromechanics
Aeronautical Systems Division
Air Force Systems Command
Wright-Patterson Air Force Base, Ohio

CATALOGUED BY ASTIA
AS AD NO.

Project No. 8173, Task No. 817303 FEB 27 1963

RECEIVED
TISIA A

(Prepared under Contract No. AF33(657)-7847
by the Allison Division, General Motors Corporation,
Indianapolis, Indiana;
Dr. B. Agruss, H. R. Karas, and V. L. Decker, authors.)

NOTICES

When Government drawings, specifications, or other data are used for any purpose other than in connection with a definitely related Government procurement operation, the United States Government thereby incurs no responsibility nor any obligation whatsoever; and the fact that the Government may have formulated, furnished, or in any way supplied the said drawings, specifications, or other data, is not to be regarded by implication or otherwise as in any manner licensing the holder or any other person or corporation, or conveying any rights or permission to manufacture, use, or sell any patented invention that may in any way be related thereto.

Qualified requesters may obtain copies of this report from the Armed Services Technical Information Agency, (ASTIA), Arlington Hall Station, Arlington 12, Virginia.

Copies of this report should not be returned to the Aeronautical Systems Division unless return is required by security considerations, contractual obligations, or notice on a specific document.

FOREWORD

This report was prepared by the Research Group of the Allison Division of General Motors Corporation on Air Force Contract AF33(657)-7847, Task No. 817303 (Fuel Cells); Project No. 8173 (Static Energy Conversion Technology). The work was administered under the direction of the Flight Accessories Laboratory, Aeronautical Systems Division. Mr. F. J. Brock was the project engineer for ASD until 7 September 1962 when he was succeeded by Captain G. Starkey.

The work began on 2 January 1962 on a basic contract to result in the design and development of a stack of liquid metal cells having a power output of 310 watts at approximately 3.5 volts using the potassium-mercury liquid metal system. As work progressed, necessary background information was compiled and preliminary cell and stack designs were completed. Results from the first controlled cell experiments indicated some major materials problems, and a concerted effort was made to fully define problem areas. When it became apparent that solution of problems associated with the sintered oxide ceramic matrix was of a long-term nature, the contract was amended (Supplemental Agreement, USAF, AFSC, ASD, WPAFB, Ohio, dated 16 August 1962, Modification No. SA Nr. 1, AF33(657)-7847) to eliminate the 310-watt requirement and focus the effort on (1) proof of electrochemical and regenerative feasibility, (2) the study of a new concept in a matrix-electrolyte combination---the composite matrix, and (3) further seal development work. This report is being submitted to fulfill part of the contract commitment.

The Liquid Metal Cell Project is managed by Dr. B. Agruss, Section Head, Applied Chemistry. Dr. Agruss, V. L. Decker, and H. R. Karas are responsible for the work at Allison. Management direction includes Mr. T. F. Nagey, Director of Research, and Dr. R. E. Henderson, Chief of Applied Physics.

This is the final report under Contract AF33(657)-7847. The contractor's report number is EDR 3100.

ABSTRACT

The electrochemical, physical, and chemical characteristics of potassium and potassium-mercury amalgams lend themselves to the successful operation of a liquid metal cell for space power. During the first year's work, substantial progress was made in the study and operation of potassium-mercury cells and in pointing up problem areas requiring solution. Six different types of cells were run, some utilizing a ceramic matrix while others operated on a differential density principle. Certain cells were operated with flowing cathode metal, so that steadiness of operation and regenerative capability could be studied. Results confirmed this regenerative capability up to 60 mw/cm^2 , the operating level of the experiment. Liquid metal cell life was extended to as long as 550 hours to date. Current densities of 227 ma/cm^2 and power densities of 91 mw/cm^2 were achieved.

Composite matrices composed of $6\text{-}\mu$ MgO particles were produced, and electrical conductivities of discs of various electrolyte/MgO ratios were measured. Results conform to requirements of liquid metal cell systems.

Preliminary measurements of those ceramic properties necessary for the design of a reliable cell seal were completed. Required support equipment was constructed.

Publication of this technical documentary report does not constitute Air Force approval of the report's findings or conclusions. It is published only for the exchange and stimulation of ideas.

TABLE OF CONTENTS

<u>Section</u>		<u>Page</u>
I	Introduction	1
II	Theory	3
III	Materials	7
	Metals	7
	Ceramics for Matrices and Insulators	8
	Pure Ceramics (Chemical Properties).	9
	Pure Sintered Ceramics (Physical Properties)	12
	Porous Ceramics	14
	Liquid Metal Reactants	16
	Electrolyte.	22
	Miscellaneous Materials for Special Purposes	25
IV	The Matrix	27
	Analysis of Porous Media	27
	Geometrical Parameters	27
	Resistivity Relationships	29
	Methods of Measuring Porous Media Parameters	30
	Ionic Conductivity	32
	Conductivity Measurement	32
	Electrolyte Impregnation and Retention.	44
	Impregnation Test Procedures	44
	Electrolyte Retention.	45
V	Liquid Metal Cells	47
	Flat-Type Circular Cell.	47
	Single Cup Cell—Static Type	58
	Double Cup Cell	58
	Differential Density Cell—Static Type	60
	Single Cup Cell—Flowing Type	62
	Differential Density Cell—Flowing Type	63
	Rectangular Cell.	63
VI	Experimental Results	67
	Conductivity Measurements	67
	Formation Factor (Effective Electrode Area)	67
	Electrolyte Matrix Conductivity Measurement.	69

<u>Section</u>		<u>Page</u>
	Seal Studies	75
	Compressive Strengths of Selected Ceramics	75
	Seal Experiment	78
	Results of Cell Work	78
	Detailed Comments on Cell Runs.	80
VII	Problem Areas and Solutions	105
	Generalized Problem Areas.	105
	Particular Problem Areas at the First Level and Their Solutions (Proposed or Accomplished)	105
	Selection of Materials for Cell Construction.	105
	Matrix.	106
	Electrolyte	112
	Impurities.	113
	Seals	114
	Resistances	116
	Recommendations	116
VIII	Support Equipment	117
	Mercury Feed	117
	Potassium Feed	122
	Heat Balance Flowmeter	123
	Evaluation of Flow Equipment.	126
IX	Design of a Multicell Stack.	129
	Estimation of Performance	129
	Stack Design.	130
X	Accomplishments and Technical Position	137
XI	References	141

LIST OF ILLUSTRATIONS

<u>Figure</u>		<u>Page</u>
1	EMF vs Composition for K-Hg System	5
2	Schematic Diagram of an Operating Cell	6
3	Density of Amalgam as a Function of Composition	16
4	Amalgam Viscosity vs Composition	17
5	Phase Diagram of K-Hg System	17
6	Electrical Resistivity of K-Amalgam vs Composition.	18
7	Electrical Resistivity of K-Amalgam vs Temperature	19
8	Solubility of Potassium Monoxide in Potassium Metal	22
9	Phase Diagram of KOH-KBr System.	23
10	Phase Diagram of KOH-KI System.	23
11	Phase Model of KOH-KBr-KI System	24
12	Tortuosity Concept.	28
13	Plastic Conductivity Cell.	33
14	Specific Conductance of 0.1 N and 1.0 N KCl	33
15	Fused Electrolyte Conductivity Cells	35
16	Capillary Cell Conductivity Apparatus.	37
17	Schematic of Modified Wheatstone Bridge	39
18	Parasitic Bridge Currents	40
19	Oscilloscope Trace of Polarization Effect.	42
20	Schematic of Constant Current Conductivity Apparatus	43
21	Vacuum Impregnation Tank for Small Specimens	45
22	Vacuum Impregnation Tank for Large Specimens	45
23	Bottom Half of Circular Cell.	47
24	No. 5186 Matrix and A-402 Gasket	48
25	Top Half of Circular Cell	48
26	Cell in Press	49
27	Detail of Bottom Half of Circular Cell.	50
28	Detail of Top Half of Circular Cell	51
29	Detail of Cell Profile and Intermediate-Type Cells	52
30	Press Assembled.	53
31	Press—Top Plate	54
32	Press—Bottom Plate	55
33	Press—Transite Insulating Plate	56
34	Press—Load Plate.	56
35	Press—Small Parts	57
36	Single Cup Cell—Static Type	59
37	Double Cup Cell	59
38	Differential Density Cell—Static Type	60

<u>Figure</u>		<u>Page</u>
39	Three Cells in Laboratory Settings	61
40	Single Cup Cell—Flowing Type	62
41	Flowing Single Cup Cell in Operation	62
42	Differential Density Cell—Flowing Type	64
43	Rectangular Cell with Matrix in Place.	65
44	Rectangular Cell Outside of Press.	65
45	Detail of Rectangular Cell	66
46	Aqueous Electrolyte Formation Factor Cells	68
47	Electrolyte-Matrix Conductivity Apparatus	70
48	Conductance of 31/69 Percent Composite Matrix	72
49	Conductance of 33/67 Percent Composite Matrix	72
50	Conductance of 33/67 Percent Composite Matrix	73
51	Conductance of 35/65 Percent Composite Matrix	74
52	Seal Testing Equipment	76
53	Shorted Matrix	81
54	Voltage-Time Curve for Double Cup Cell	82
55	Voltage-Current Curve for Double Cup Cell.	83
56	Freezing of Electrolyte in Double Cup Cell	84
57	Resistance Measurement with Cathode Ray Oscilloscope	84
58	Single Electrode Measurements in Double Cup Cell with Sintered Discs	84
59	Single Electrode Measurements in Double Cup Cell with Sintered Discs	85
60	Voltage-Time Curve for (Differential Density) Cell 11	86
61	Voltage-Current Curve for (Differential Density) Cell 11.	86
62	Voltage-Time Curve for (Differential Density) Cell 17	87
63	EMF vs Concentration of K and Hg	92
64	Operating Characteristics of Flowing Single Cup Cell (18)	94
65	Operating Characteristics of Flowing Single Cup Cell (18)	95
66	Operating Characteristics of Flowing Single Cup Cell-MgO Matrix (19).	98
67	Operating Characteristics of Flowing Single Cup Cell-MgO Matrix (19).	99
68	Flowing Differential Density Cell	101
69	Operating Characteristics of Differential Density Cell (21).	102
70	Differential Density Cell (22) Prior to Operation	103
71	Microstructure of Alumina Disc Prior to Impregnation.	107
72	Microstructure of Alumina Disc After Impregnation	107
73	Microstructure of Alumina Disc After 40 Hours	107
74	Alumina Unexposed to Electrolyte	108

<u>Figure</u>		<u>Page</u>
75	Alumina Immediately After Impregnation	108
76	Alumina After 14 Days Exposure to Electrolyte.	108
77	Magnesia Unexposed to Electrolyte	109
78	Magnesia Immediately After Impregnation	109
79	Magnesia After 14 Days Exposure to Electrolyte	109
80	Sandwich Matrix Design	111
81	Porous Cup Showing Evidence of Metal Penetration.	113
82	Effect of Impure Materials on Cell Life	114
83	Hot Trap Detail.	115
84	Mercury Feed System	118
85	Detail of Mercury Weir	119
86	Detail of Consecutive Mercury Weir.	120
87	Close-up of Mercury Weirs in Operation	121
88	Close-up of Exit End of Three Cell Stack with Mercury Flow	121
89	Detail of Potassium Weir	122
90	Heat Balance Flowmeter	124
91	Improved Heat Balance Flowmeter	124
92	Temperature Differential vs Flowrate for Mercury Metal	125
93	Flowmeter Response and Cell Feed Rate	127
94	Top View of 310-Watt Stack	131
95	Schematic of Feed System for Liquid Metal Cell Stack	132
96	Schematic of Exterior Electrical Connections.	134
97	View of Assembled Three-Cell Stack and Feed System.	136
98	Program Schedule	139

LIST OF TABLES

<u>Table</u>		<u>Page</u>
I	Important Properties of Metals Useful in Liquid Metal Cell Construction	8
II	Important Physical Properties of Pure Sintered Ceramics Useful in Liquid Metal Cell Construction	12
III	Important Thermal and Electrical Properties of Pure Sintered Ceramics Useful in Liquid Metal Cell Construction	12
IV	Physical Characteristics of A-402 Impervious Alumina	13
V	Physical Characteristics of RR Impervious Alumina	13
VI	Physical Characteristics of M-208 Impervious Magnesia.	13
VII	Physical Characteristics of 5186 Porous Alumina	14
VIII	Physical Characteristics of LA Porous Aluminas.	14
IX	Physical Characteristics of No. 139 Porous Alumina.	15
X	Physical Characteristics of M Porous Magnesia	15
XI	Physical Characteristics of LM-833 Porous Magnesia	15
XII	Properties of Mercury Metal	20
XIII	Properties of Metallic Potassium	21
XIV	Wheatstone Bridge Frequency Dependence	41
XV	Formation Factors of Various Porous Aluminum Oxides.	69
XVI	Formation Factor Comparison.	69
XVII	Measured Compressive Strengths of Morganite Porous Magnesia	76
XVIII	Measured Compressive Strengths of LM-833 Porous Magnesia	77
XIX	Measured Compressive Strengths of M-208 Impervious Magnesia	77
XX	Measured Compressive Strengths of A-402 Impervious Alumina	77
XXI	Single Cell Performance	79
XXII	Performance of Cell 22	103

GLOSSARY OF TERMS

A, LA, LM, M, and RR---Terms used in conjunction with some number to refer to a manufacturer's product designation

Anolyte---The fluid contained within the anode compartment of an electrochemical device

Catholyte---The fluid contained within the cathode compartment of an electrochemical device

Cell---A single cell consisting of an anode chamber, electrolyte or electrolyte-matrix, and a cathode chamber

Cell Unit---A number of cells in electrical series to provide a basic package of given operating voltage

Cell Stack---A group of cell units arranged in such a manner as to provide a package of given wattage

Kovar---A nickel-cobalt-iron alloy known for its low thermal expansion

Matrix---A porous structure which forms the foundation and physical limits of a liquid impregnant

Spinel---A ceramic compound of the formula $MgO \cdot Al_2O_3$

Silicone Rubber---A synthetic elastomer consisting of cross-linked chains of a basic-O-SiR₂-bonding (capable of higher temperature regimes than most rubbers)

Weir---A dam-like device used to maintain a liquid at some fixed level

LIST OF SYMBOLS AND DEFINITIONS

<u>Symbol</u>	<u>Description</u>
A	Area (or representation of a liquid metal, where appropriate)
B	Representation of a liquid metal
D	Diameter
E	Reversible electrical potential
F	Faraday
(F)	Formation Factor
$\Delta G, \Delta \bar{G}$	Free energy, partial molar free energy
ΔH	Enthalpy
I	Current
I_k	Constant current
K	Cell constant
$^{\circ}\text{K}$	Degrees Kelvin
K_e	Equilibrium constant
L	Length of straight path
L_e	Length of tortuous path
M	Mass
N	Mole fraction
P	Actual porosity
P_e	Effective porosity
R	Gas constant
R_e	Electrical resistance
ΔS	Entropy
T	Absolute temperature
V	Voltage
V_o	Open circuit voltage
V_c	Cell or operating voltage
Vol	Volume
W	Power
a	Activity
cal	Calorie
cm	centimeter
d	Density
d_m	Density of porous body
d_B	Bulk density
g, gm	Grams
k	Conductivity
l	Length of straight path
ln	Natural logarithm

<u>Symbol</u>	<u>Description</u>
mv	Millivolts
n	Electron charge
p	Pressure
(s)	Solid
sec	Second
t	Time
t_e	Length of straight path
x	Concentration of stoichiometric ratio
y	Stoichiometric ratio
z	Flow rate
a	Activity coefficient
η_c	Voltage efficiency, V_c/V_o
θ	Wetting angle
μ	Microns
$\mu\mu f$	Micromicrofarads
ρ	Electrical resistivity
ρ_e	Electrical resistivity of pure electrolyte
σ	Surface tension
τ	Tortuosity
ϕ	Actual porosity
Ω	Ohms

I. INTRODUCTION

In the late 1950's a comprehensive survey was made of the fuel cell literature.¹ * From this survey it was noticed that very little work was being done on regenerative systems---a surprising observation considering the preponderance of thermal energy available from both solar and nuclear sources. It was then suggested that thermal and electrochemical regenerative systems should be studied.² Pursuing these leads further, it was decided to determine the problems associated with such systems and what inorganic compounds would lend themselves to thermal regeneration. A survey of the literature for thermally decomposable inorganic compounds³ revealed only about 20 compounds suitable for thermally regenerative systems based on more or less practical criteria, while another evaluation⁴ based on thermodynamic and kinetic data produced only two suitable reactions for inorganic compounds. A general systems analysis⁵ revealed that the greatest improvement in efficiency of regenerative systems could be accomplished by reductions in polarization and electrolyte resistance losses. It is known that the kinetics of liquid metal electrodes in contact with fused salts is extremely rapid.⁶ Also the conductivity of fused salts is possibly two to five times greater than the conductivity of the best aqueous electrolytes.⁷ With these improvements as a goal, work was initiated at Allison to develop the liquid metal cell (LMC).

The liquid metal cell is a thermally regenerative static power converter in which heat is converted directly into electrical energy. No reaction mass is consumed in the generation of the electrical energy. The LMC power converter system contains no moving parts and allows complete control over output electrical energy to be accomplished by external electrical devices. These features make the LMC attractive for use with nuclear reactor or radioisotope thermal sources necessary for missions of long duration.

Application of the LMC power converter is attractive for such space missions as Voyager, Mariner, orbiting space stations, or any mission where electrical energy is required over long time periods at a high reliability confidence level. In particular, missions which utilize the SNAP II reactor are adaptable to the LMC power converter because electrical output, reactor temperature level, and converter system size, weight, and volume are compatible with the proposed SNAP II power converter system requirements. The LMC can provide significant reductions in system weight due to the dual capability of the LMC to provide electrical power and, at the the same time, particle gamma shielding.

As a consequence, the long-range program has been directed toward the following system goals:

- Capable of one year reliable space operation with a power output of 5 kw at 28 volts
- Capable of remote, unattended start-up and shutdown in space operation
- Capable of withstanding the vibration, shock, and acceleration experienced during prelaunch, launch, and orbit of a space vehicle

*Superscripts refer to references in Section XI

- High power-to-mass values
- Shelf life of six months

Manuscript released by the authors December 1962, for publication as an ASD Technical Documentary Report.

II. THEORY

When metals react to form alloys, solutions, and compounds, an exchange of energy takes place which may manifest itself in the form of heat. These reactions can be analyzed by standard thermodynamic principles.⁸ For instance, the heat of the reaction may be expressed as

$$\Delta H = \Delta G + T\Delta S. \quad (1)$$

Two methods—calorimetric or electrochemical—are used to evaluate the terms of Equation (1). The former measures enthalpy, ΔH , and entropy, ΔS , from which the free energy, ΔG , can be calculated. The latter measures ΔG and ΔS , and ΔH is calculated according to the Gibbs-Helmholtz equation:

$$E = -\frac{\Delta H}{nF} + T\left(\frac{dE}{dT}\right) \quad (2)$$

where

$$\Delta S = -nF\left(\frac{dE}{dT}\right) \quad (3)$$

and

$$\Delta G = -nFE. \quad (4)$$

The free energies involved can be measured in galvanic cells in which the anode is formed of the more electronegative metal and the cathode is formed of the alloy. The cation of the electrolyte is the ionized form of the anode metal. The cell is represented schematically as



The galvanic cell (S) is a special case of a general type called a concentration cell, which is represented by



in which A and B may be a wide variety of metals and a_1 and a_2 are the activities of A in each electrode. The energy associated with Scheme (G) can be expressed as

$$-\Delta\bar{G} = nFE = -RT \ln \frac{a_2}{a_1} \quad (7)$$

where $\Delta\bar{G}$ is the partial molar free energy of species A.

The simple concentration cell (S) has the energy associated with the assimilation of one mole of A by a large amount of A_{a_2} (B). The energy is expressed by Equation (5) but, in this case, the activity, a_1 , by definition is unity; therefore, the cell potential is

$$E = - \frac{RT}{nF} \ln a_2. \quad (6)$$

The activity is defined by

$$a = \gamma N_A \quad (7)$$

where (a) can never be greater than unity, γ is the activity coefficient, and N_A is the mole fraction of species A. Hence, alloying reactions with high molar free energies yield high voltages and the cell potential declines logarithmically with an increase of the concentration of A in the alloy.

In a cell constructed as in (S), comprising two liquid metal electrodes and a molten electrolyte, the open circuit voltage will be governed by Equation (6) and the cell voltage by

$$V = V_O - IR_e \quad (8)$$

where V_O is the open circuit voltage from Equation (6), V is the operating voltage at current I , and R_e is the cell resistance.

Because liquid metal electrodes are used, electron transfer and metal diffusion should be very rapid. This means that the cell should operate with little polarization loss; the electrical losses should be limited to IR_e (i. e., ohmic resistance) losses almost entirely. The exchange currents at metal electrodes in molten salts can be extremely high,⁶ which permits high current densities with very small amounts of activation polarization. Also, the cation of the molten electrolyte has a transference number of nearly unity; hence, there should be no concentration polarization in the electrolyte. There can be some concentration polarization at the alloy electrode-electrolyte interface at high current densities where metal A can be discharged faster than surface tension effects and diffusion can remove it, resulting in a thin, high alloy concentration layer. Because of the rapid diffusion rates at these high temperatures in liquid metals and the stirring effect caused by the change in surface tension, this polarization should occur only at high current densities, but here the IR_e drop would greatly overshadow the small polarization effect. Hence, the only significant voltage loss in a liquid metal cell of this type should be the IR_e loss in the electrolyte. These IR_e losses are minimal and much lower than those encountered in aqueous systems because molten salts have conductivities of the order of 1-5 mhos, while the best aqueous electrolyte conductivities are in the range of 0.5-0.9 mho.

Based on carefully screened data,⁹ Figure 1 shows the effect of a change in amalgam composition as it would affect the open circuit voltage of the liquid metal cell. With the cell in operation, the load voltage would be a function of the current drawn and the electrolyte-matrix resistance as given in Equation (8).

If compounds were formed, however, the activity of A in the alloy would be governed by the free energy of formation of the compound. For the reaction



the equilibrium constant is expressed by

$$K_e = \frac{a_{AxBy}}{a_A^x \cdot a_B^y} \quad (10)$$

$$\text{and } \Delta G (\text{formation}) = - RT \ln K_e \quad (11)$$

Since it is desired that the activity of the free A metal in the alloy be low to maintain a high potential, the free energy of formation should be large—which demonstrates the difference between a liquid metal system involving compound formation and a simple liquid metal concentration cell in which the activity of free A atoms is expressed merely by the relative number of moles of A dissolved in B. The cell emf is directly related to the free energy of formation of the compound by the relationship

$$E = - \frac{RT}{xnF} \left[\frac{\Delta G (\text{formation})}{RT} + \ln \frac{a_{AxBy}}{a_A^x a_B^y} \right] \quad (12)$$

Equation (12) is derived from (11) by substituting Equation (10) for K_e and (6) for a_A . This shows that for a specified concentration of A in B, compounds with the highest free energies of formation will result in the highest cell voltage.

In addition, because of the high energy of formation, there will be a composition range wherein the change in activity of A will be small over a relatively large concentration change, resulting in a high, relatively steady voltage. In contrast, the emf of an ideal solution will change logarithmically with concentration and there will be no constant emf portion. Hence, those systems departing the most from ideality through compound formation will yield high, steady voltages over wide composition ranges.

Actual operation of a single cell within the stack is shown schematically in Figure 2.

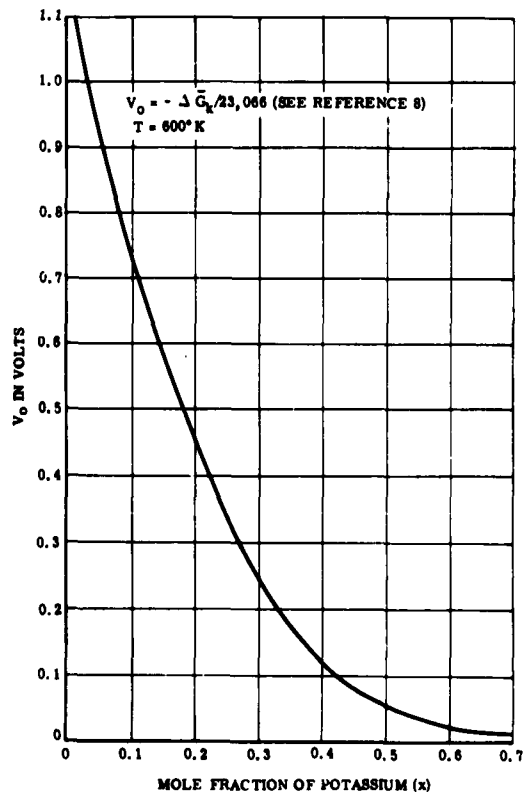


Figure 1. EMF vs Composition for K-Hg System

In Figure 2, A and A_xB_y are chambers containing A and A_xB_y , respectively, separated by a porous ceramic matrix. The electrolyte is a molten salt (consisting of a cation of metal A and some anions) soaked into the matrix. (This electrolyte is chosen mainly on the criteria of proper melting point range, lack of reaction with the liquid metals, matrix, or container, and the absence of thermal decomposition.) As the cell commences operation, the following reaction takes place:

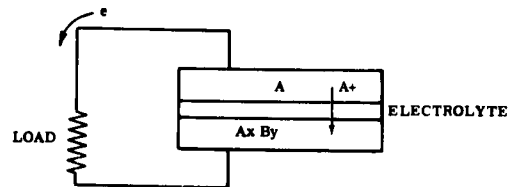


Figure 2. Schematic Diagram of an Operating Cell

1. A gives up an electron and becomes the ion A^+ .
2. The ion A^+ migrates into the electrolyte and displaces a cation, A^+ , of the electrolyte.
3. The electron passes through the load in the external circuit furnishing electrical power and unites at the electrolyte A_xB_y interface with the cation, A^+ , forming the neutral atom A.
4. A reacts with the alloy A_xB_y , forming the alloy $A_x'B_y$.

The amount of current or voltage available from a cell of this type is a function of the electrode area, electrolyte-matrix resistance, and other intracell resistances.

The potassium-mercury liquid metal cell is a concentration cell and can be operated according to Equations (S) or (G). If for the moment (G) is assumed, then there is amalgam in both anode and cathode compartments. As current is drawn, the potassium-rich amalgam in the anode chamber loses potassium to the cathode and, consequently, becomes richer in mercury. The mercury-rich amalgam in the cathode compartment takes on more and more potassium. It can be seen from Figure 1 that with no flow of mercury through the cathode, the emf of the cell would decrease as current is drawn. By flowing fresh mercury-rich amalgam into the cathode, the composition level is maintained and a steady emf can be obtained.

III. MATERIALS

METALS

The following criteria should be considered in the choice of containment metals for a cell system:

1. Compatibility with mercury, alkali metals, and electrolyte
2. Thermal expansion
3. Density
4. Cost
5. Machinability and joining
6. Behavior in space environment

The Liquid Metals Handbook¹⁰ lists the results of tests run on the resistance of materials to attack by mercury and by sodium and sodium-potassium alloys. It is pointed out that while there are some materials which are resistant to mercury in static systems, care must be used in selection since dynamic mercury systems significantly affect the corrosion properties of metals. At low flow rates (as would be encountered in a liquid metal cell), corrosion can be very serious. Therefore, most reliance was placed on those tests which were run in dynamic rather than static systems.

There are two classes of metals which seem to lend themselves most readily to use in the liquid metal cell system—ferrous and nonferrous. The ferrous metals of primary interest would be (1) the low carbon steels, which show good resistance in dynamic systems from temperatures of 673 to 923°K, depending on the particular formulation, (2) stainless steels of the ferritic type, and (3) a few of the proprietary alloys. Nonferrous metals showing promise would include tungsten, listed as having good properties to 873°K, molybdenum to 873°K, and chromium to 823°K (as measured in a static system). The literature also indicates that low carbon steels have good resistance up to 673°K, while the addition of small amounts of chromium, silicon, titanium, and molybdenum can increase this resistance up to 873°K.¹⁰

The ferritic steels, which are high chromium stainless types with little or no nickel present, showed good results in static tests but were not tested in dynamic systems. These steels would comprise the 400 series stainless steels. The 300 series stainless or austenitic steels which are high in nickel and chromium showed poor resistance to attack by mercury in dynamic systems. As to the attack by sodium or sodium-potassium alloys, carbon steels are listed as having good resistance to 723°K, while the ferritic stainless steels show good resistance up to 903°K. Reference 10 lists the possibilities of corrosion inhibitors being added directly to the mercury to reduce attack on ferrous alloys, but at this time the effect of these additives on the operation of the liquid metal cell system is uncertain.

Testing of the nonferrous metals previously listed showed that they had good resistance to both the sodium-potassium alloys and to the pure mercury. With the exception of chromium, these tests were in dynamic systems. Table I is a compilation of the important properties of metals useful in constructing the liquid metal cell.^{11,12}

TABLE I							
Important Properties of Metals Useful in Liquid Metal Cell Construction*							
Material	Density (gm/cm ³)	Coefficient of Thermal Expansion (cm/cm/°K)	Thermal Conductivity, 293°K (cal/cm ² /cm/sec/°K)	Electrical Resistivity (microhm-cm) (273-293°K)	Melting Point (°K)	Temperature of Maximum Use	
						NaK (°K)	Hg (°K)
Low Carbon Steel**	7.8	10-12 × 10 ⁻⁶ (293-373°K)	0.108	20	1703	723	673
Ferritic Stainless Steels (400 series)**	7.7	10-12 × 10 ⁻⁶ (273-811°K)	0.057	57	1723	903	823
Chromium	7.2	6.2 × 10 ⁻⁶ (293°K)	0.160	12.9	2163	823	823
Columbium	8.6	7.3 × 10 ⁻⁶ (293°K)	0.125	12.5	2741	-	-
Molybdenum	10.2	5.5 × 10 ⁻⁶ (298-773°K)	0.340	5.2	2898	873	903
Tungsten	19.2	4.5 × 10 ⁻⁶ (273-573°K)	0.397	5.7	3683	873	903

*Properties listed at near ambient temperatures are shown for a comparative basis. It is to be understood that interrelationships could change as higher temperature regimes are attained.

**Varies with particular composition or preparation

Chromium, molybdenum, columbium, or tungsten might be desirable materials to use in some respects. The specific gravity of tungsten and the difficulties in joining refractory metals, added to the fact that 410 stainless steel has a thermal expansion coefficient close to that of alumina which was used in the initial phase of this program, made the use of 410 stainless material desirable from the standpoint of service availability, price, and weight. Consequently, this was the major material used for this program. Changes in design or a switch from alumina to other matrix ceramics could affect the choice of metal used in cell construction. The materials listed in Table I are satisfactory on the basis of current information and form a group of available materials from which selection can be made on the basis of expansivity, thermal or electrical conductivity, etc.

CERAMICS FOR MATRICES AND INSULATORS

The main criteria in the choice of ceramic materials would be:

1. Compatibility with the mercury-potassium amalgam and electrolyte systems
2. (For matrices) Apparent porosity, pore size, and distribution of the pores among the three possible types—pores open on both ends, pores open on one end, and pores closed on both ends. The maximum porosity attainable would be desirable because this would lend itself to absorption of the greatest amount of electrolyte in the pores

open on both ends. However, a retention of the electrolyte under a differential head is important, and, for this reason, it would be critical to control the pore size so that maximum electrolyte retention can be attained.

3. Availability
4. Stability against thermal shock
5. Cost

Any characterization of the properties of oxide ceramics is an extremely difficult task. Chemical, physical, or mechanical properties are highly dependent on the nature of preparation of the finished material, the extent of sintering, the presence of impurities, the type of binder used to hold the particles together, the porosity (as reflected in the surface area), and the degree of wetness or dryness. In the interests of clarity, tabulation of properties will be made on three bases:

1. Expected behavior of the basic, pure ceramic material (this would involve the chemical behavior of the pure powder, or of a dense, sintered solid in which no binder is used)
2. Physical properties of highly dense, sintered bodies (this would give a reasonable comparison in a standard condition between the various materials considered)
3. Available information on porous ceramics, which may or may not incorporate a binding material (this would summarize some of the materials tested for compatibility and offer a means by which the change in properties on the assumption of porosity may be determined)

Pure Ceramics (Chemical Properties)

Present indication is that an oxide-type ceramic will be required for durability as a matrix material in the liquid metal cell. Initial work made use of alumina (see Section VII, Problem Areas and Solutions) to prove the feasibility of the liquid metal cell as a regenerative system for electrical power, based on the immediate availability of aluminas in needed forms, sizes, porosities, etc. It has since been indicated that the useful life of porous alumina elements may be very short. Among the many oxide ceramics in existence, the following are deemed the best for consideration in the present cell configuration:

- Magnesia MgO
- Spinel Al₂O₃·MgO
- Thoria ThO₂

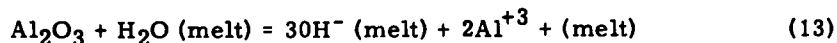
Others considered and rejected for long-term use with the present electrolyte (KOH-KBr-KI) are:

- Alumina Al_2O_3
- Zirconia ZrO_2
- Boron Nitride B_3N
- Beryllia BeO
- Calcia CaO

A more detailed discussion of the oxide ceramics considered is given in the following.

- Alumina—Compatibility with mercury is good up to 873°K .¹⁰ Compatibility with alkali metals is good to 773°K .¹⁰ Ryshkewitch¹⁰ states that potassium induces some attack on alumina, and Reference 10 speaks of the attack of alkali metals on aluminas in which silica, SiO_2 , is used as a binder. Smith¹⁴ discusses the corrosion of ceramics in fused hydroxides (a constituent of the electrolyte system used in the liquid metal cell). Smith points out the following:

1. The oxide-type ceramic has only a negligible tendency to capture an oxide ion from a hydroxyl ion in the salt and therefore should stand up fairly well. Aluminum oxide, being more amphoteric than magnesia, should be more readily attacked.
2. The two biggest factors in determining whether there is attack are the presence of water and the presence of a silica binder. Silica is listed by Smith¹⁴ as being readily attacked by fused hydroxides. The attack by water would take place according to Equation (13).



Smith further states that ceramics impregnated with a hydroxide will disintegrate when washed with water since the hydroxide quickly forms hydrates or hydrated carbonates with appreciable volume expansion.

Ryshkewitch¹³ states that there is no recognizable corrosive action on sintered alumina by molten alkali halides at temperatures up to 1273°K .

- Zirconia—Zirconia is soluble in molten alkali hydroxides¹³ forming alkali-meta-zirconate, K_2ZrO_3 .
- Boron Nitride—Reports of behavior in molten alkali hydroxides were conflicting in nature, so a sample of unbound B_3N was run in the electrolyte. The material disintegrated.

- Beryllia—Beryllia is more amphoteric in nature than alumina.
- Calcia—Calcia is difficult to handle because of its extreme hygroscopic tendencies. A slow reaction with molten sodium hydroxide is reported at temperatures as low as 623°K.
- Magnesia—Compatibility with mercury is good up to 873°K.¹⁰

Compatibility with alkali metals is good up to 473°K¹⁰ with the area above that unknown, although Ryshkewitch¹³ states "The chemical behavior of magnesia is determined by the position of magnesium in the periodic table. The element is a weak representative of the earth alkali metals. Accordingly, magnesia is a weak base, particularly at high temperatures. Therefore, a sintered magnesia body is not, or almost not attacked by basic substances, such as alkalis, and alkali carbonates, even in prolonged action in the molten state."

Smith¹⁴ mentions the testing of magnesia in fused alkali hydroxides at "substantial temperatures" with no evidence of reaction.

Magnesia may react at elevated temperatures with free halogens which might be released by the thermal decomposition of the electrolyte according to Equation (14).¹³



In the presence of carbon, magnesia chlorination begins at 473°K.

Magnesia is more sensitive to thermal shock than is alumina.

- Spinel—Magnesium meta-aluminate, $\text{MgO} \cdot \text{Al}_2\text{O}_3$, offers some possibility as a ceramic material that would combine the best features of magnesia and alumina—the corrosion resistance approaching that of magnesia and the thermal shock resistance better than that of magnesia.
- Thoria—Compatibility with mercury should present no problem. Compatibility data for reactions with alkali metals are scarce. Thoria is known to react with alkalis at temperatures of 1673°K in a closed, pressurized vessel.¹³

Thoria should be the least reactive of all the materials mentioned with molten alkali salts (see Section VI, Experimental Results).

Of the three oxide ceramics—magnesia, spinel, and thoria—thoria is the most

subject to thermal shock and great care would be needed in its preparation to remove residual firing stresses.

Pure Sintered Ceramics (Physical Properties)

Densified ceramics will be needed for use as gaskets or other structural members in a liquid metal cell. Some design information should be available for this purpose. Use of oxide ceramics as matrices requires some means for estimating relative properties of these ceramics as porous bodies—even though it is acknowledged that the properties will be strongly affected by methods of preparation. It is with this in mind that the physical properties are summarized in Tables II and III.

TABLE II				
Important Physical Properties of Pure Sintered Ceramics Useful in Liquid Metal Cell Construction ¹³				
<u>Material</u>	<u>Theoretical Specific Gravity (gm/cm³)</u>	<u>Compressive Strength (kg/cm²)</u>	<u>Tensile Strength, (kg/cm²)</u>	<u>Melting Point (°K)</u>
Alumina	3.96-3.98	15,000 (673°K)	2560 (573°K)	2323
Magnesia	3.57	< Alumina	< Alumina	3073
Spinel	3.60	16,000 (573°K)	1200 (573°K)	2408
Thoria	10.05	11,000 (673°K)	1000 (298°K)	3573

Note: The tensile strength of heat treated steel is 4500 kg/cm² at 673°K

TABLE III				
Important Thermal and Electrical Properties of Pure Sintered Ceramics Useful in Liquid Metal Cell Construction ¹³				
<u>Material</u>	<u>Specific Resistivity (ohm-cm)</u>	<u>Specific Heat (cal/gm/°K)</u>	<u>Thermal Conductivity (cal/cm²/cm/sec/°K)</u>	<u>Coefficient of Thermal Expansion (cm/cm/°K)</u>
Alumina	>10 ⁸ (1103°K)	0.258 (303-1173°K)	0.0538 (473°K) 0.0314 (673°K)	7.3 × 10 ⁻⁶ (298-773°K)
Magnesia	10 ⁹ (803°K)	0.277 (303-1173°K)	0.038 (573°K)	12.0 × 10 ⁻⁶ (573°K)
Spinel	10 ⁸ (673°K)	0.194 (303°K)	0.032 (573°K)	6.7 × 10 ⁻⁶ (298-1073°K)
Thoria	10 ⁹ (823°K)		0.020 (473°K) 0.014 (673°K)	9.7 × 10 ⁻⁶ (96% dense)

Three impervious ceramic materials have been used for construction in the program to date. Their properties are summarized in Tables IV, V, and VI.

TABLE IV			
Physical Characteristics of A-402 Impervious Alumina ¹⁵			
Typical Chemical Analysis			
Al ₂ O ₃	99.0%	CaO	0.3%
MgO	0.3%	SiO ₂	0.2-0.4%
Fe ₂ O ₃	0.03%	Alkali (Na ₂ O)	0.03%
TiO ₂	Trace		
Temperature of Maximum Use—2173°K			
Specific Gravity—3.80 (pure oxide, 3.97) gm/cm ³			
Apparent Porosity—0%			
Specific Heat—0.27 cal/gm/°K			
Coefficient of Thermal Expansion ¹⁶ — 5.9×10^{-6} cm/cm/°K			

TABLE V	
Physical Characteristics of RR Impervious Alumina ¹⁷	
Chemical Analysis—Al ₂ O ₃ , 99.7 + %	
Temperature of Maximum Use—2223°K	
Specific Gravity—3.78 gm/cm ³	
Coefficient of Thermal Expansion— 8.8×10^{-6} cm/cm/°K	

TABLE VI			
Physical Characteristics of M-208 Impervious Magnesia ¹⁵			
Typical Chemical Analysis			
MgO	99.0% min	Fe ₂ O ₃	0.15% max
SiO ₂	0.2% max	B	0.003% max
CaO	0.2% max	R ₂ O ₃	0.35% max
Temperature of Maximum Use—2000°K			
Specific Gravity—3.0 (pure oxide, 3.57) gm/cm ³			
Apparent Porosity—15%			

Porous Ceramics

In the early stages of this program, compatibility studies were made to determine gross compatibilities of various materials. Over 30 different alumina and magnesia materials were tested. Many samples disintegrated completely, while a few indicated materials possibilities. On the basis of these initial studies, additional compatibility tests were made (see Section VII, Problem Areas and Their Solutions). The materials, along with their properties, which have been used in the program to date are given in Tables VII and VIII

TABLE VII			
Physical Characteristics of No. 5186 Porous Alumina ¹⁵			
Typical Chemical Analysis			
Al ₂ O ₃	98.85%	CaO	0.01%
SiO ₂	0.70%	MgO	0.02%
Fe ₂ O ₃	0.11%	TiO ₂	0.02%
Na ₂ O	0.28%	K ₂ O	0.01%
Bulk Density—3.0 gm/cm ³			
Temperature of Maximum Use—2008-2038°K			
Thermal Expansion— 10×10^{-6} (303-1773°K)			
Apparent Porosity—24%			

TABLE VIII	
Physical Characteristics of LA Porous Aluminas ¹⁵	
Typical Chemical Analysis (partial)	
Al ₂ O ₃	99.6%
SiO ₂	<0.2%
Fe	5 ppm
Apparent Porosity—40-45%	
Pore Size—LA-830, 10 μ \pm 2; LA-831, 25 μ \pm 3; LA-832, 40 μ \pm 4	

The LA and LM materials have just been made available and are still considered as a laboratory-type ceramic rather than a production type. In the initial compatibility studies on the ceramic specimens, no noticeable effect on strength was noted after submersion periods of 336 hours in the electrolyte. Physical characteristics of No. 139 porous alumina, M porous magnesia, and LM-833 porous magnesia are given in Tables IX, X, and XI.

TABLE IX			
Physical Characteristics of No. 139 Porous Alumina ¹⁵			
Typical Chemical Analysis			
Al ₂ O ₃	98.8%	CaO	0.01%
SiO ₂	0.70%	MgO	0.02%
Fe ₂ O ₃	0.12%	TiO ₂	0.02%
Na ₂ O	0.32%	K ₂ O	0.01%
Bulk Density—2.5 gm/cm ³			
Temperature of Maximum Use—1920°K			
Thermal Expansion—9.9 × 10 ⁻⁶ (303-1773°K)			
Apparent Porosity—36%			

TABLE X	
Physical Characteristics of M Porous Magnesia ¹⁷	
MgO—98.6%	
Bulk Density—2.13 gm/cm ³	
Temperature of Maximum Use—2673°K	
Thermal Expansion—13.5 × 10 ⁻⁶	
Apparent Porosity—40%	

TABLE XI			
Physical Characteristics of LM-833 Porous Magnesia			
Typical Chemical Analysis			
MgO	99.0% min	Fe ₂ O ₃	0.15% max
SiO ₂	0.2% max	R ₂ O ₃	0.35% max
CaO	0.2% max	B	0.003% max
TiO ₂	0.1%		
Apparent Porosity—40-45%			
Pore Size	LM-833 20μ; LM-919 5μ; LM-918 10μ;		
	LM-920 19μ (48% porosity)		

The apparent porosity given is determined by dividing the actual density of the material by the density (Table II) of the pure oxide. The apparent porosity represents the three possible types of pores—those open on both ends, open on one end, and totally enclosed. The pores that are open either on both ends or on one end can be determined by an absorption method.¹⁸

A comparison of Tables II and VII through XI shows the extent to which the physical configuration or chemical formulation of a porous body can affect such properties as thermal expansion.

LIQUID METAL REACTANTS

The compilation of literature on amalgams is incomplete due to the scarcity of literature on the subject.

A 90 percent (mole) potassium amalgam versus pure mercury in the cell will give an open circuit emf of approximately 1.2 volts (Figure 1). Figure 3 indicates that as current is drawn, the depletion of potassium in the anode will lead to an increase in density of the anode amalgam, while the amalgam in the cathode will be decreasing in density as potassium is added to the raw mercury. The linearity of density with temperatures may be extrapolated over a fairly wide range of values.¹⁹ The increase and decrease in respective densities will cause no problem. To maintain a constant mass flow rate through the cell, there will be a concurrent adjustment in the volume flow rate. Figure 4 is a plot of amalgam viscosity versus composition.²⁰ Figure 5⁸ shows that any place in the system where the mole percent of mercury is likely to approach 67 percent, the mercury must be maintained at temperatures above 533°K to keep the system molten. Such a condition could exist at the electrolyte-mercury interface where the mercury-rich amalgam would conceivably be formed.

Figure 6²¹ indicates the change in electrical resistivity that occurs with a change in concentration of potassium amalgam. Figure 7²² indicates the effect of temperature on resistivity.

The properties of mercury and potassium are listed in Tables XII and XIII.

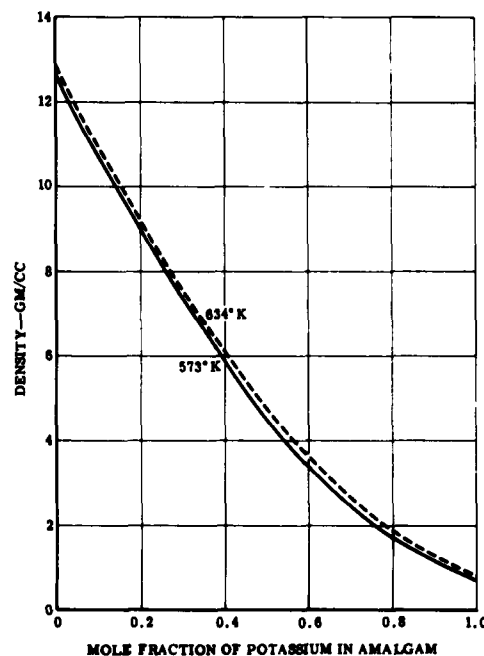


Figure 3. Density of Amalgam as a Function of Composition

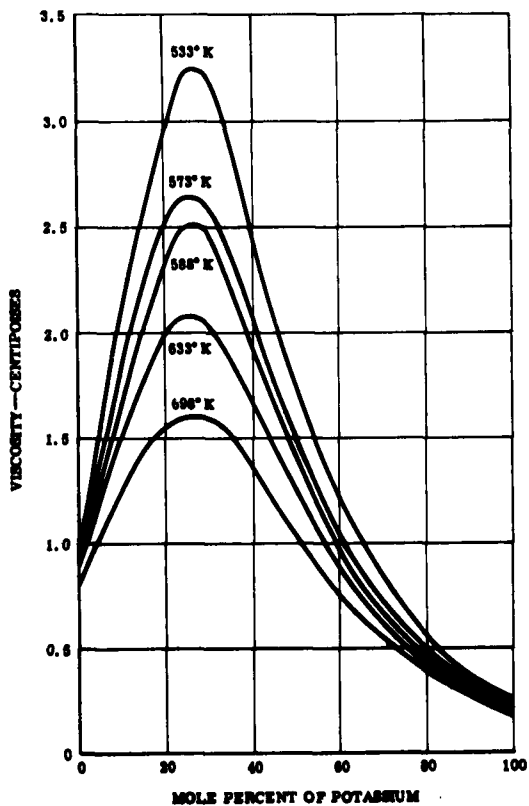


Figure 4. Amalgam Viscosity vs Composition

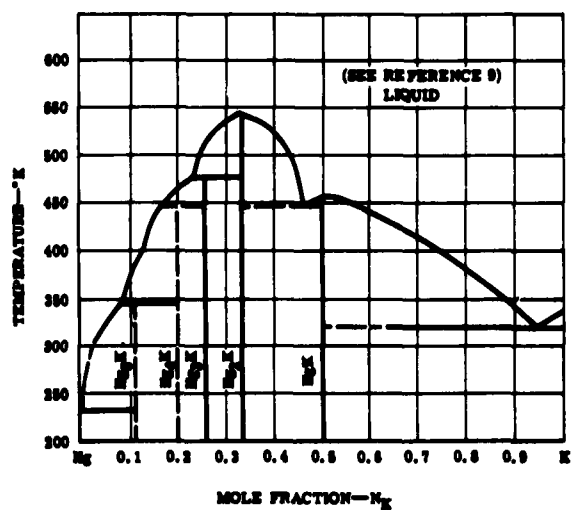


Figure 5. Phase Diagram of K-Hg System

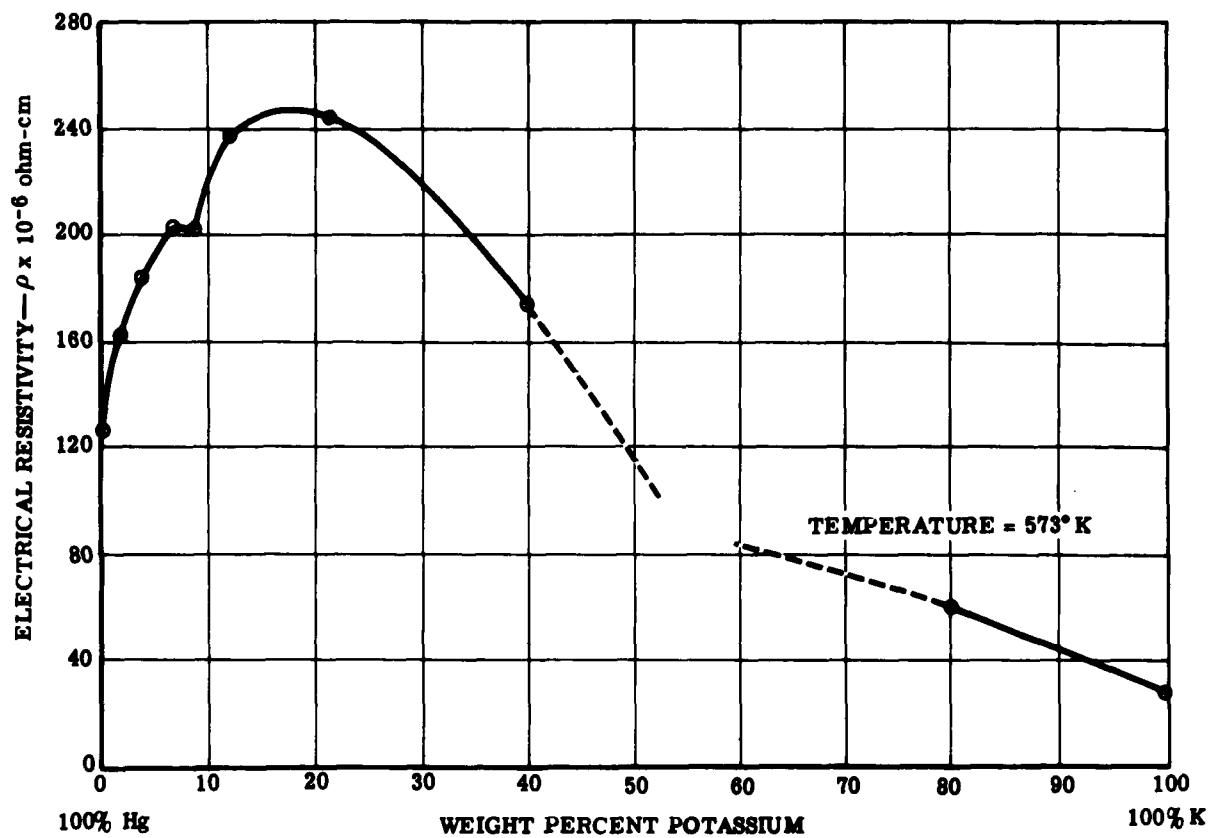


Figure 6. Electrical Resistivity of K-Amalgam vs Composition

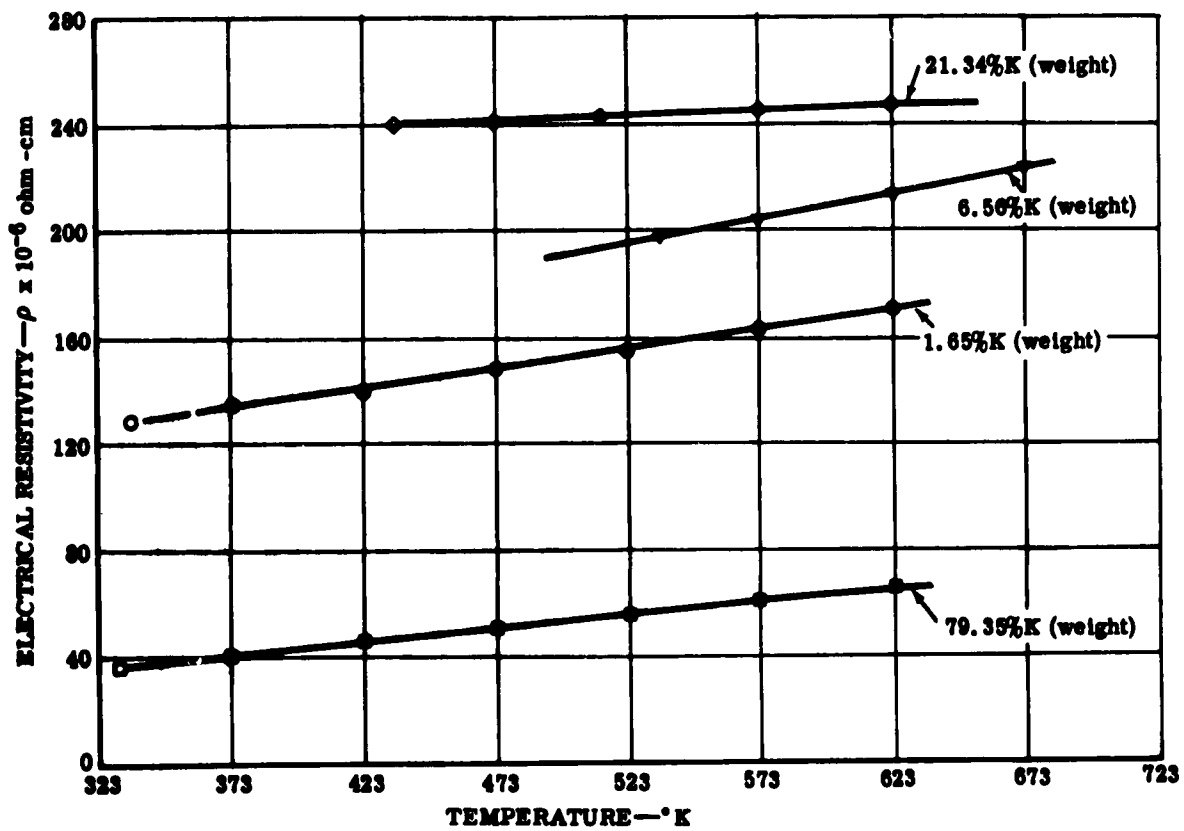


Figure 7. Electrical Resistivity of K-Amalgam vs Temperature

TABLE XII

Properties of Mercury Metal²²

Melting Point—234.13°K

Latent Heat of Fusion—2.8 cal/gm

Boiling Point—630°K

Latent Heat of Vaporization—69.7 cal/gm

Density—12.881 gm/cm³ (573°K)

Volume Change in Fusion—3.6% of solid

Vapor Pressure

(mm Hg)(°K)

1	399.2
10	457.0
100	534.7
200	563.7
400	596.0

Heat Capacity

(cal/gm/°K)(°K)

0.03334	273
0.03279	373
0.03245	473
0.03234	573
0.03256	723

Thermal Conductivity

(cal/sec/cm/°K)(°K)

0.0196	273
0.0231	333
0.0261	393
0.0279	433
0.0303	493

Resistivity

(microhms)(°K)

98.4	323
103.2	373
114.2	473
127.5	573
135.5	623

Surface Tension

(dynes/cm)(°K)

465	293
454	385
436	473
405	573
394	627

TABLE XIII

Properties of Metallic Potassium

Melting Point—336.7°K
 Latent Heat of Fusion—14.6 cal/gm
 Boiling Point—1033°K
 Latent Heat of Vaporization—496 cal/gm
 Vapor Pressure—1 mm Hg at 615°K
 Density—0.783 at 523°K
 Surface Tension—86 dynes/cm (373°-423°K)
 Volume Change on Fusion—2.41% of solid

Heat Capacity		Viscosity	
(cal/gm/°K)	(°K)	(centipoises)	(°K)
0.1956	348	0.515	342.6
0.1887	473	0.331	440.4
0.1826	673	0.258	523.0
		0.191	673.0

Thermal Conductivity		Resistivity	
(cal/sec/cm/°K)	(°K)	(microhms)	(°K)
0.1073	473	13.16	337
0.1013	573	18.70	423
0.0956	673	25.00	523
		28.20	573
		31.40	623

Solubility of Potassium in Fused Hydroxides²³

	(753°K)	(873°K)
7.8-8.9 gm/100 gm		3-4 gm/100 gm
	(923°K)	(973°K)
2-2.7 gm/100 gm		0.5-1.3 gm/100 gm

Handling metallic potassium with the intent of maintaining any degree of purity is a difficult and tedious procedure. Not only is it highly reactive with moisture or air, but it is exceedingly difficult to procure potassium which does not have dissolved oxides. Figure 8²⁴ is a plot of potassium monoxide solubility in potassium metal as it varies with temperature. The curve follows the relationship:

$$\text{Weight percent O}_2 = 0.0865 - 0.0006089t + 0.000007714t^2 \quad (15)$$

where $t = ^\circ\text{C}$ for the range 75 to 305 $^\circ\text{C}$.

To convert to weight percent potassium monoxide, multiply by 5.875. Various techniques are reported²⁵ for the purification of potassium using a titanium or zirconium sponge. These techniques do not work well in an amalgam since both titanium and zirconium show some solubility in mercury and their effect on the system is unknown at this time. The reaction of potassium with water is well known by nature of its violence. In the presence of a minute amount of oxygen, a clean potassium surface will quickly cloud over with oxide and, under the proper conditions, may form an explosive peroxide.

ELECTROLYTE

The electrolyte is a molten salt mixture containing potassium as the common cation. This electrolyte was chosen initially on the criteria of proper melting point; lack of reaction with the liquid metals, matrix, or container; the absence of thermal decomposition; and good electrical conductivity. During the experimental phase of work it was found that there was some reaction involved with liquid metals and cell materials (see Sections VI and VII) which greatly complicated the development of the liquid metal cell. Three electrolyte systems were considered—two were binary systems and one was a ternary system. The binary systems consist of (1) potassium hydroxide-potassium bromide, which shows a eutectic of 573 $^\circ\text{K}$ at a composition of 65 mole percent potassium hydroxide, and (2) a mixture of potassium hydroxide-potassium iodide, which shows a eutectic composition of 72 mole percent potassium hydroxide melting at 523 $^\circ\text{K}$. The ternary system KOH-KBr-KI has been used for cell work to date. The eutectic composition is approximately 70 mole percent KOH, 15 mole

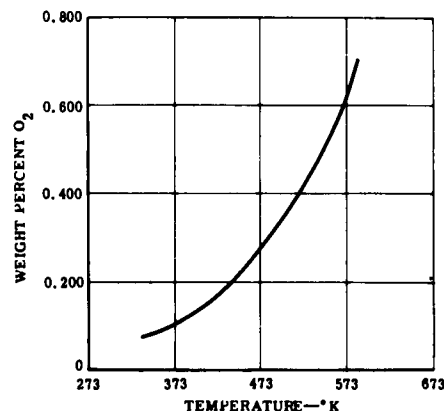


Figure 8. Solubility of Potassium Monoxide in Potassium Metal

percent KBr, 15 mole percent KI, and has a melting point, when dry, of 493°K. Phase diagrams²⁶ of the binary systems are shown in Figures 9 and 10. A three-dimensional model of the ternary system is shown in Figure 11.

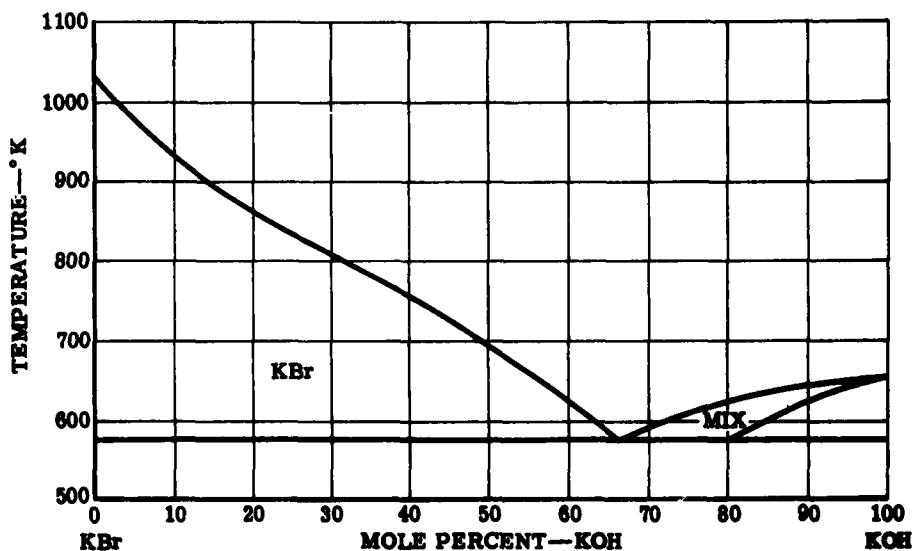


Figure 9. Phase Diagram of KOH-KBr System

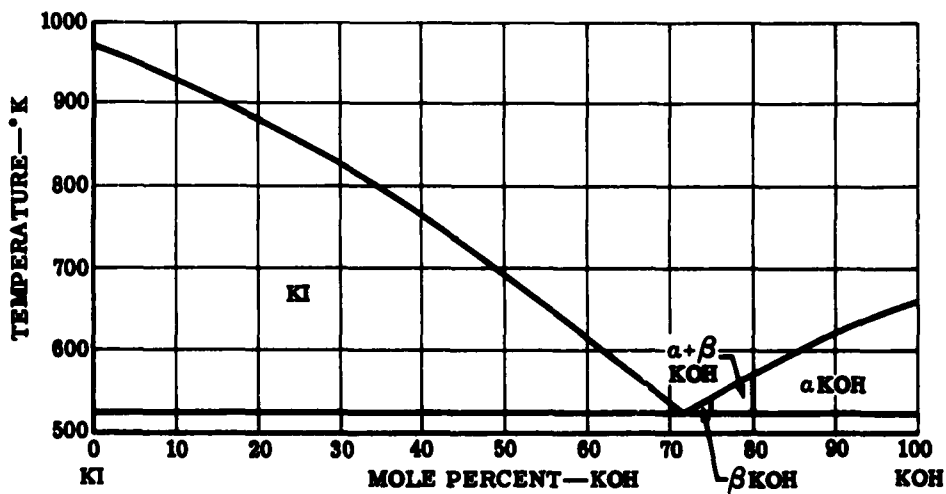


Figure 10. Phase Diagram of KOH-KI System

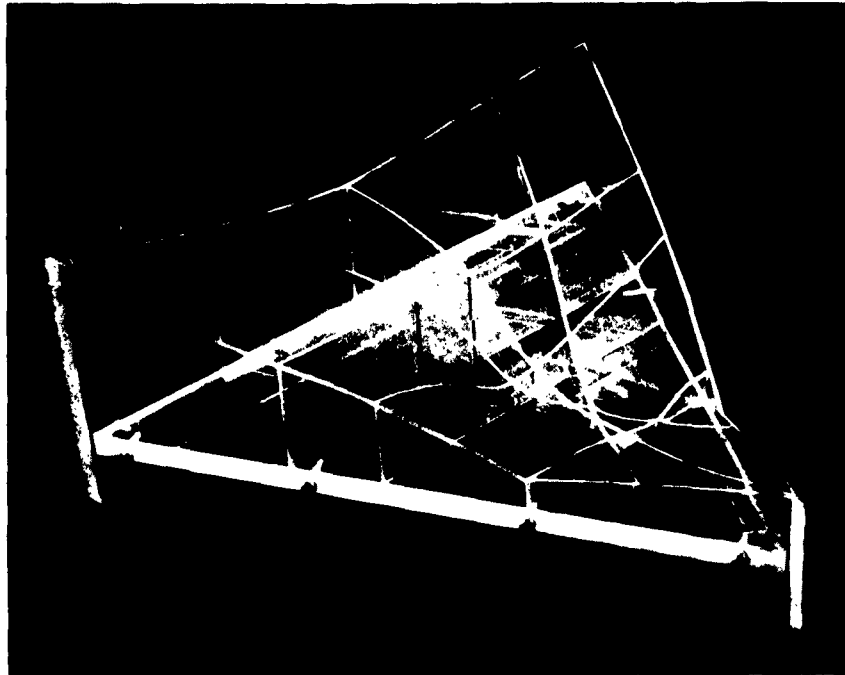


Figure 11. Phase Model of KOH-KBr-KI System

The allowable melting point range of the electrolyte system is limited by the minimum temperature as determined from the potassium-mercury phase diagram (Figure 5) at 553°K, while the upper end of the melting point range must not exceed the boiling point of mercury.

All three of the systems mentioned fall within these requirements--the potassium hydroxide-potassium bromide system is the highest melting system; the ternary (potassium hydroxide-potassium bromide-potassium iodide) system is the lowest melting system. Selection of an electrolyte would then be based on the following considerations:

1. The further the cell operating temperature from the melting point of the electrolyte, the better the conductivities expected.
2. The further the melting point of the electrolyte system from the boiling point of mercury, the less danger of overheating due to heat generated within the cell.
3. The lower the percentage of potassium hydroxide in the system, the less corrosion there should be on the ceramic and metal portions of the cells.

The ternary system fits these qualifications best and is therefore the one chosen for the present work. The noneutectic mixture of 60 percent (mole) potassium hydroxide-20 percent (mole) potassium bromide-20 percent (mole) potassium iodide was used initially, but later work indi-

cated the desirability of going to the eutectic mixture of 70-15-15, respectively. This electrolyte has a resistivity of approximately 1 ohm-cm (ρ) at cell temperature and contains less potassium hydroxide than either of the binary systems. Tests on reagent grade potassium hydroxide have shown that dewatering of this hygroscopic material at 623°K in an argon inerted atmosphere evolved an average of 11.5 percent water, while a vacuum treatment at the same temperature evolved 17.3 percent water. Since water has been found to be detrimental to the life of the ceramics, it is important in the preparation of any electrolyte system that it be adequately dewatered under vacuum.

MISCELLANEOUS MATERIALS FOR SPECIAL PURPOSES

A silicone rubber is now available in laboratory batches which shows good resistance to alkali metals at temperatures up to 623°K for periods of at least several weeks. On contact with the ternary electrolyte, however, it quickly decomposes with evolution of gases and forms a scum throughout the electrolyte container. At temperatures above 623°K, the material loses its elasticity and tends to part under the least tensile strain. It has been useful in cup-type cells where it can be maintained in a cooler portion of the cell. If the seal is undisturbed, it maintains its integrity even after the loss of tensile properties. Several interesting possibilities remain for this material.

Gold has been found to be useful in applications involving high temperatures and electrolyte contact. It has been particularly useful as a reference electrode. Attempts were made to use gold-plated O-rings for sealing flat-type cells, but it was found that the electrolyte undercut the porous gold layer.

Teflon can be useful in preparation of electrolytes, provided that its maximum temperature of use, 533°K, is not exceeded. It must not be brought into contact with alkali metals due to possibility of a violent, toxic reaction.

The compatibility of Kovar was checked in a mercury loop at 623°K for 425 hours with no detectable weight loss. This might be a promising material for future cell construction because of its thermal expansion coefficient which approaches that of dense ceramics.

IV. THE MATRIX

Some means is needed to maintain separation of the anolyte, electrolyte, and catholyte in the liquid metal cell. As will be discussed in Section V, separation is possible by means of differences in the densities of the three components, but for a space capable system, a more positive means of separation is necessary. The amalgams and electrolyte have limited mutual solubility, but since all are liquid it is necessary to prevent mechanical mixing and subsequent failure of the cell. The proposed means for accomplishing this is to employ a nonconducting porous medium to interstitially hold the electrolyte. The alliance of the molten electrolyte and this porous medium, called the matrix,²⁷ operates as an effective means of separation between the liquid metal electrodes while providing a mode of ionic conduction between them.

In considering matrix configurations, two of the possible ones available are the consolidated (a porous piece of ceramic in which the individual particles have been sintered together forming a rigid body), and the unconsolidated (a mixture of electrolyte and ceramic powder in definite proportion held together by surface forces, forming a body of very low plasticity). In the consolidated type there is an actual cementation between particles, while the unconsolidated type relies strictly on adhesive forces between the electrolyte-ceramic combination. These matrices have been used successfully with other fuel cell systems.²⁸ These two matrix types were the only ones actively explored for purposes of this contract.

ANALYSIS OF POROUS MEDIA

The texture of the porous matrix is very important since it directly affects ionic conductivity and electrolyte impregnation and retention. The texture or pore space geometry of a porous body consists of a system of voids and interconnecting passages. The complexity of such systems is made evident by the fact that theoretically derived relationships which attempt to express the dependence of electrical resistivity and fluid flow properties on pore space geometry have been generally unsatisfactory. The failure of these derived relationships lies generally in the deviation between the assumed pore space geometry and that actually present in the porous medium in question. These quantities, however, are measurable and previous successes at relating them have been predominantly through the empirical approach.

Geometrical Parameters

The parameters which receive most frequent use in the analysis of porous media are porosity, tortuosity, formation factor, permeability, and specific surface. The first three parameters are used more frequently in resistivity studies while the latter two are more common to fluid flow relationships.

Porosity

Two types of porosity are of interest---actual and effective. Actual porosity is defined as the ratio of the void volume to that of the porous body. Effective porosity, generally less than actual porosity, is defined as the ratio of interconnecting channels and void volumes. In comparing the two, the effective porosity is generally no less than 95 percent of the actual porosity for bodies of 20 percent actual porosity and greater.

Tortuosity

Tortuosity is defined as the ratio of the tortuous length traversed by migrating ions in going from one parallel plane to another to the actual distance measured perpendicular to the planes. It is obvious that in porous media, in general, the distance traveled is not the same for all ions due to the interconnecting passages and constrictions which occur in the complex interstices. Thus, this concept of tortuosity is a statistical average with no complete physical description other than that implicit in the relationships with which it is involved. Figure 12 illustrates the concept of tortuosity.

Formation Factor

The concept of formation factor was first introduced by Sundberg.²⁰ It is given as the ratio of the resistivity of an electrolyte impregnated body to the resistivity of the electrolyte. The formation factor (F) is independent of the saturating electrolyte if complete impregnation of the effective pores is realized and if available ion concentrations are sufficient to render surface conduction effects negligible.

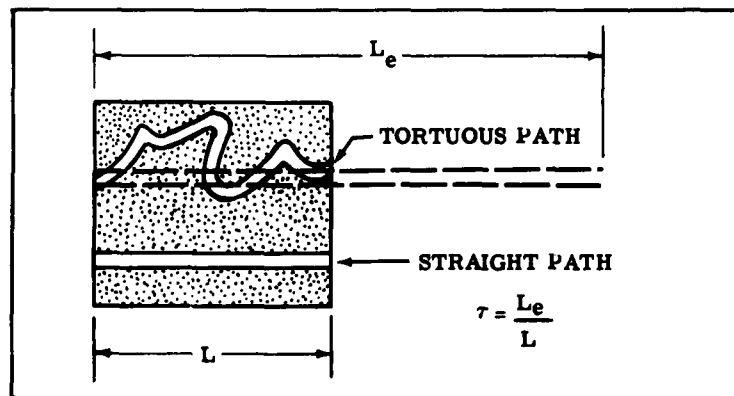


Figure 12. Tortuosity Concept

Permeability

The permeability concept was introduced by Darcy (1865) as a result of theoretical studies of laminar flow through porous media. His efforts resulted in the following expression:

$$Q = -K'A(P_2 - P_1 + gh)/h \quad (16)$$

where Q is the volume flow per unit time, A and h are the dimensions of the porous medium, and the term in parentheses is a measure of the drop in head across the porous body.

The constant, K' , which depends upon the properties of both the fluid and porous medium, is known as the permeability. Its units are generally expressed as Darcys or cm^2 , where the conversion is:

$$1 \text{ Darcy} = 9.87 \times 10^{-9} \text{ cm}^2 \quad (17)$$

Specific Surface

Specific surface relates the internal area of a porous medium to a particular volume associated with the bulk. Depending upon application, it is taken as the ratio of internal surface area to medium volume or internal surface area to void volume.

Resistivity Relationships

The resistivity of an electrolyte saturated porous medium is defined as the resistance of a unit cube of the material, provided the medium is isotropic. The formation factor, (F), for a porous medium can be derived theoretically in the following manner.

Consider a rectangular parallelepiped of electrolyte with two electrode faces of area A and a separation distance of L . The resistance, R_e , of this block for an electrolyte resistivity of ρ is

$$R_e = \rho \frac{L}{A} \quad (18)$$

The resistance, R'_e , of a porous block of identical geometry, saturated with the electrolyte of resistivity ρ is

$$R'_e = \rho \frac{L'}{A'} \quad (19)$$

The tortuous channels and constrictions increase the equivalent thickness of the block by $L' - L$ due to the increased current path length. The area cross section presented to current is reduced by the imposition of the porous body, resulting in the lesser area, A' . The ratio of R_e^i and R_e or formation factor results in the following expression:

$$\frac{R_e^i}{R_e} = \frac{L'/L}{A'/A} \quad (20)$$

Since L'/L is defined as tortuosity (τ), Equation (20) becomes:

$$(F) = \frac{\tau}{A'/A} \quad (21)$$

It can be shown that the product of tortuosity and the area ratio A'/A is equal to the effective porosity, P_e .

$$P_e = \tau \frac{A'}{A} \quad (22)$$

Therefore, Equation (21) may be written as:

$$(F) = \frac{\tau^2}{P_e} \quad (23)$$

Equation (23) shows that formation factor or resistance ratio is directly proportional to the square of tortuosity and inversely proportional to the effective porosity. The separation between unconsolidated and consolidated porous media is made evident by this equation. The basic difference between the two lies in the fact that tortuosity can be an order of magnitude greater for consolidated porous bodies than for unconsolidated porous bodies.³⁰ Therefore, the formation factor varies significantly between the two forms, the consolidated showing a higher resistance for the same effective porosity.

Methods of Measuring Porous Media Parameters

The empirical and certain of the theoretical relationships require knowledge of the actual value of the porous media parameters. Many methods have been devised to measure these quantities. The following descriptions of measurement methods are aimed at presenting some of the more important measurement processes.

Porosity

The method most generally used for measuring porosity is the gas expansion method. The basic principle of this method is the measurement of the volume of entrained gas in the void space. The procedure involves the placement of a known bulk volume of the porous material and a gas

in a container of known volume. Connecting this container to an evacuated container of known volume results in an expansion of the gas in the originally pressurized container containing the porous medium to a new total system pressure. By observing initial and final pressures, the volume of gas entrained initially in the porous medium can be calculated from the gas laws. The ratio of the entrained gas volume to bulk volume is the effective porosity.

Density methods depend upon an accurate determination of the bulk volume or upon volumetric displacement in a nonwetting fluid. If the density, d_m , of the constituent material of the porous medium is known and the bulk density, d_B , has been determined, then actual porosity is related as follows:

$$P = 1 - \frac{d_B}{d_m} \quad (24)$$

A method which has received some use employs saturation of the porous body with a fluid of known density. The difference in unsaturated and saturated weight is attributed to the additional weight of the entrained fluid. The volume of liquid contained is then simply the ratio of fluid weight to fluid density.

Tortuosity

An interesting method of measuring tortuosity, described by Winsauer,³¹ is by timing the ion migration under a potential gradient through the tortuous channels of a porous body of known thickness and comparing this with that required for ion migration in a nontortuous system of equal thickness. The potential gradient must be sufficiently high to maintain migration velocity much greater than diffusion velocity. Winsauer derives the following expression for tortuosity, τ , in terms of tortuous transit time, t' , and straight transit time, t :

$$\frac{L'}{L} = \tau = \sqrt{t'/t} \quad (25)$$

The conditions of the procedure dictate that the resistivity of the entrained electrolyte remain essentially constant during the course of ion migration. This is accomplished by employing a "filler" electrolyte that has ion mobility and resistivity similar to that of the ions to be timed. The differentiation between the tracer and filler is made chemically. The experiment is initiated by introducing the tracer at one surface of the porous sample and observing changes in tracer-ion concentration with time at the opposite surface. In practice, Winsauer first saturated a core sample with sodium nitrate solution, then placed the core in contact with a sodium chloride solution. The chloride ion was then permitted to migrate through the sample. Corrections are made to bring ion diffusion rates to a unit area basis. The unity tortuous calibration system consists of an aggregation of right cylinders or tubes which present straight paths along their axis to current flow. The ratio between the slopes of concentration versus time plots yields the value of tortuosity squared.

Formation Factor

Formation factor is obtained by determining the resistivity of a porous medium impregnated with an electrolyte of known resistivity. The ratio of porous medium resistivity to electrolyte resistivity is the formation factor.

IONIC CONDUCTIVITY

A given electrolyte-matrix in a liquid metal cell presents a finite resistance to the current in the cell. This resistance is a measure of the number and mobility of free-charge carriers in the electrolyte. The rate of migration of charge carriers, which depends upon the emf gradient within the electrolyte, affects the resistance, since this represents the rate at which the charge is delivered through the electrolyte. It is evident from an analysis of porous media that the internal resistance of electrolyte matrices having different porosities and tortuosities will, in general, be different. Low porosity implies that there is more inert material in a given volume which effectively reduces the average concentration of charge carriers and, as a result, increases the resistance. The effect of higher tortuosity and thicker electrolyte matrices is to reduce the per-unit voltage gradient which reduces the migration rate and increases the internal resistance.

The term commonly used for expressing current-carrying properties of electrolytes is ionic conductivity. Ionic conductivity is numerically equal to the reciprocal of the resistance of the electrolyte matrix. The ionic conductivity of an electrolyte matrix is most important since it determines current density and, for this reason, sets the physical size and mass of a liquid metal cell of specified power capacity.

Conductivity Measurement

The apparatus which is employed to contain the electrolyte and which provides the means of electrical contact is known as a conductivity cell. The conductivity cell is generally placed in a controlled environment, such as an ice bath or furnace, to facilitate temperature control. Two types of equipment were used in this project to measure the internal resistance of the conductivity cell. One method employs a modified Wheatstone bridge and the other a special constant-current apparatus. The following discussion describes the conductivity measurement apparatus in more detail.

Conductivity Cells

The conductivity cell configuration depends on what method is to be used in determining the cell constant on the electrolyte in question, and on the measurement equipment employed. A conductivity cell, for which the cell constant is to be calculated from dimensions, must have a regular geometrical configuration of uniform cross section along the known current path to facilitate taking the dimensions. A conductivity cell of this type is shown in Figure 13.

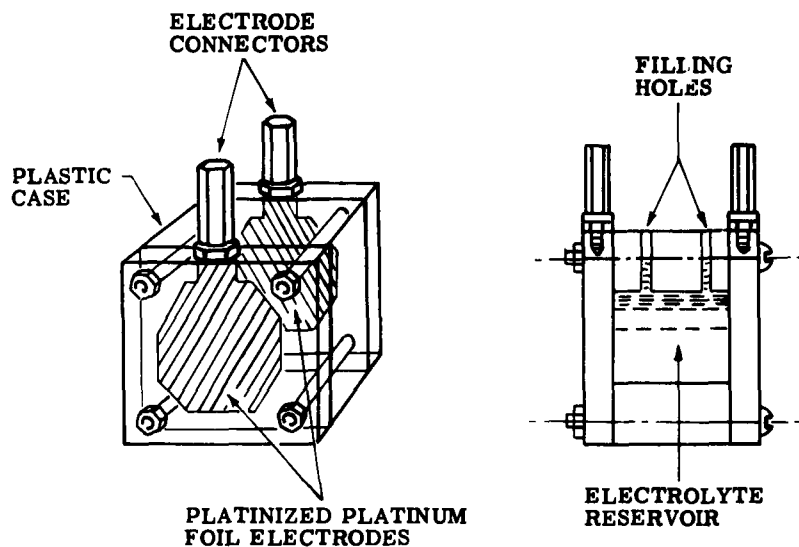


Figure 13. Plastic Conductivity Cell

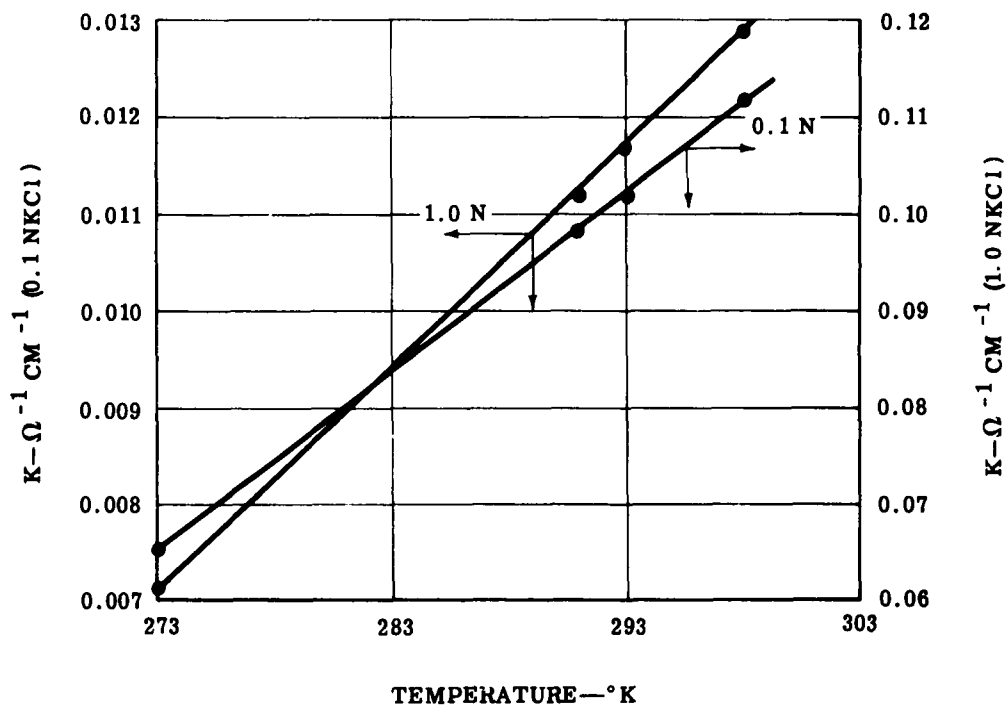


Figure 14. Specific Conductance of 0.1 N and 1.0 N KCl

This cell was used in experiments to check the validity of the measurement equipment designed for the project. The electrolyte used was 0.1 N KCl, which is widely used as a standard. The specific conductivities of 0.1 N KCl and 1.0 N KCl are plotted in Figure 14. The electrolyte is introduced through one of the two vertical passages which intersect the reamed hole in the

center section. The second vertical passage allows entrained air to escape during filling. The electrodes used should be platinized platinum foil. The electrodes cover the entire end area of the electrolyte cylinder and are pressed between two plastic caps which are fastened with small bolts through the assembly. The cell constant is equal to the length, or thickness, of the center section divided by the area of the bore and, in this case, is equal to 0.9018 cm^{-1} . The resistance of this cell can be directly calculated using Equation (26), since both the cell constant and the specific conductivity are known quantities.

$$R_e = \frac{K}{k} \quad (26)$$

where

- R_e = resistance in ohms
- K = cell constant in cm^{-1}
- k = conductivity in $\Omega^{-1} \text{ cm}^{-1}$

The validity of an experimental measurement method can be checked by comparing the measured resistance of this cell with the calculated quantity.

A conductivity cell, which is to have the cell constant resolved by calibration with a standard electrolyte of known conductivity, such as aqueous KCl, does not require that the geometry of the current path be known. It does require that the geometry of this path remain constant from the time of calibration to the time it is used with an unknown. The two conductivity cells used in this project for the determination of the specific conductivity of the fused electrolyte of potassium salts are shown in Figure 15. Both cells require calibration with a standard electrolyte.

Cell configurations depend upon the electrolyte sample. Contrary to working with fused salts, aqueous solutions for low temperature range measurements do not require the use of refractory materials. Compatibility with the electrolyte is of prime importance since reactions occurring within the cell would conceivably bias the measurement because of decreased electrode contact area or changes in electrolyte structure.

The two methods employed in this investigation to measure resistance influenced the cell configuration. The modified Wheatstone bridge performs best when the resistance of the cell is high (100 to 1000 ohms), while the constant-current method is more applicable to low resistance measurements (1.0 to 10.0 ohms). A high resistance cell has a high cell constant and a low resistance cell has a low cell constant.

The capillary cell in Figure 15 is fabricated from densified alumina. The fine capillaries in this cell result in a high resistance configuration suitable for use in the Wheatstone bridge circuit. The cell is of one-piece construction with the exception of the gold electrodes. This property ensures constant current path geometry, increasing the reliability of the cell constant calibration.

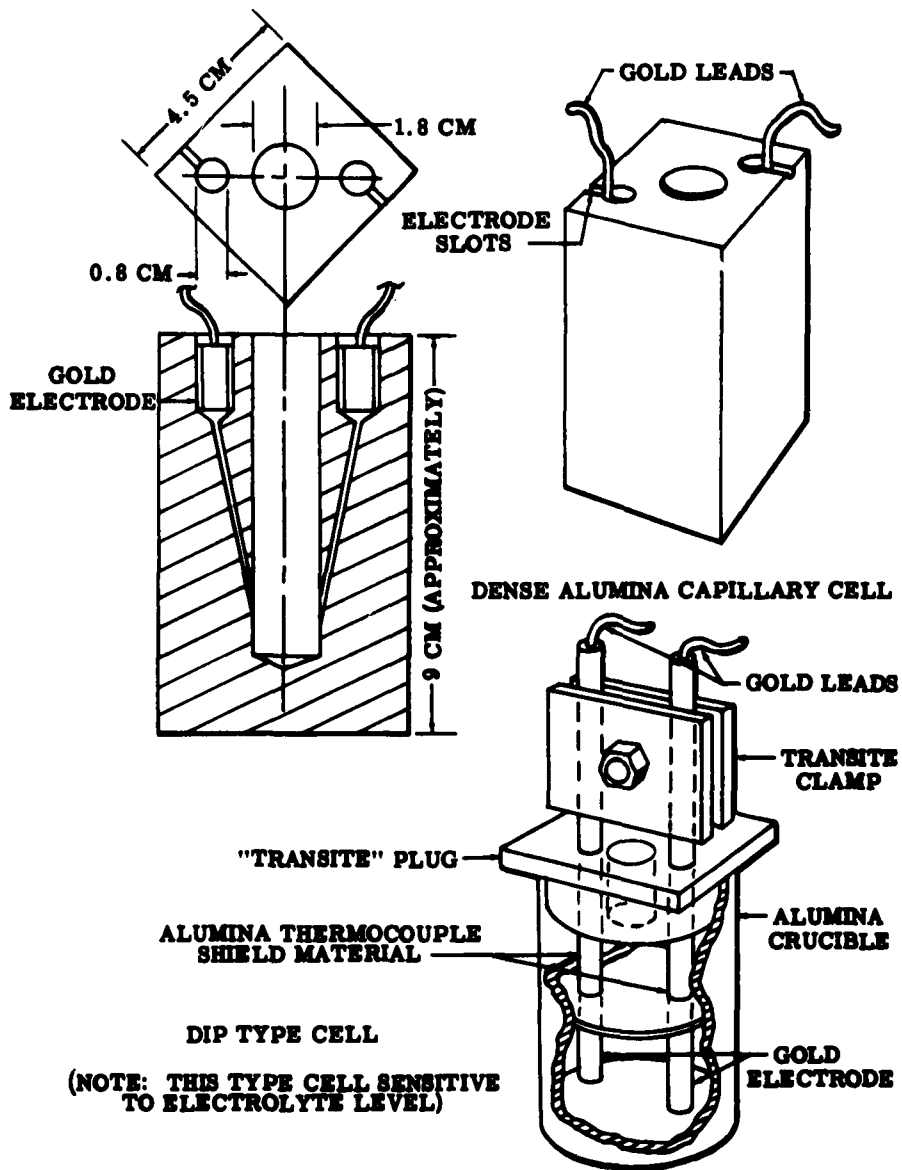


Figure 15. Fused Electrolyte Conductivity Cells

The electrode reservoirs containing the gold cylindrical electrodes give good low resistance electrical contact with the electrolyte capillaries. Slight variations in contact area in the reservoirs, as a result of electrolyte level changes or electrode contamination, produce a percentage change in contact resistance. The overall effect is negligible, however, since the reservoirs are so much lower in resistance than the capillaries. As a result of this property, capillary cells provide greater accuracy than do low resistance cells.

The capillary cell was fabricated from low-fired aluminum oxide (A402-LF, Norton Company), and dispatched to Norton Company, Worcester, Massachusetts, for densification. The densification treatment consisted of heating for 15 hours at 1123°K and then heating for 25 hours at 2023°K.

Arndt and Ploetz³² investigated the conductivity of KOH and recommended the use of silver or, preferably, gold as electrodes. They contended that platinum is strongly attacked by molten potassium alkali. Their experiments were conducted in an open vessel. Gold electrodes were used in the capillary cell since the potassium iodide in the KOH-KBr-KI electrolyte reacts with the silver. The gold electrodes were rolled from rectangular segments of 0.015-in., 24-karat gold having gold wire leads welded to them by torch peening. The cell assembly and furnace are shown in Figure 16. A dense aluminum oxide cap is held by compression on the top of the capillary cell. The electrode leads are taken out through slots cut in the top surface of the cell proper. The ground surfaces between the cap and the cell proper prevent the electrolyte, which has a tendency to creep, from producing a film shunt across the top and between electrodes. Trouble has been experienced in preventing electrolyte depletion due to creep along the gold electrode leads. Argon gas is introduced at the bottom of the cell container and allowed to escape through fixture holes in the tapered "Transite" plug to which is fastened the cell clamp and thermocouple harness. The thermocouple harness consists of a section of cylindrical tubing which contains four 1/4-20 machine screws spaced to contact the four vertical sides of the cell proper. Each screw is drilled along its axis and a chromel-alumel thermocouple is inserted to bear against the capillary cell.

Problematic Procedures Encountered

Certain areas were investigated early in the project which proved to yield negative results. These areas involved the first approach to working with fused electrolytes and their conductivity cells. The evaluation of the conductivity cells with which difficulties were encountered will be given first, followed by a discussion of the problems encountered in using fused standard electrolytes for the determination of cell constants.

The first unsuccessful conductivity cell consisted of a section of alumina thermocouple tubing of the type which has a double bore. Platinum wires placed in the bores served as electrodes. The ends of the platinum wires came to within 3 in. of the bottom of the 12-in. section of thermocouple tubing. This dip-type capillary cell was then dipped into an alumina crucible containing a fused electrolyte. The fine wire of electrolyte which rose in each of the capillaries

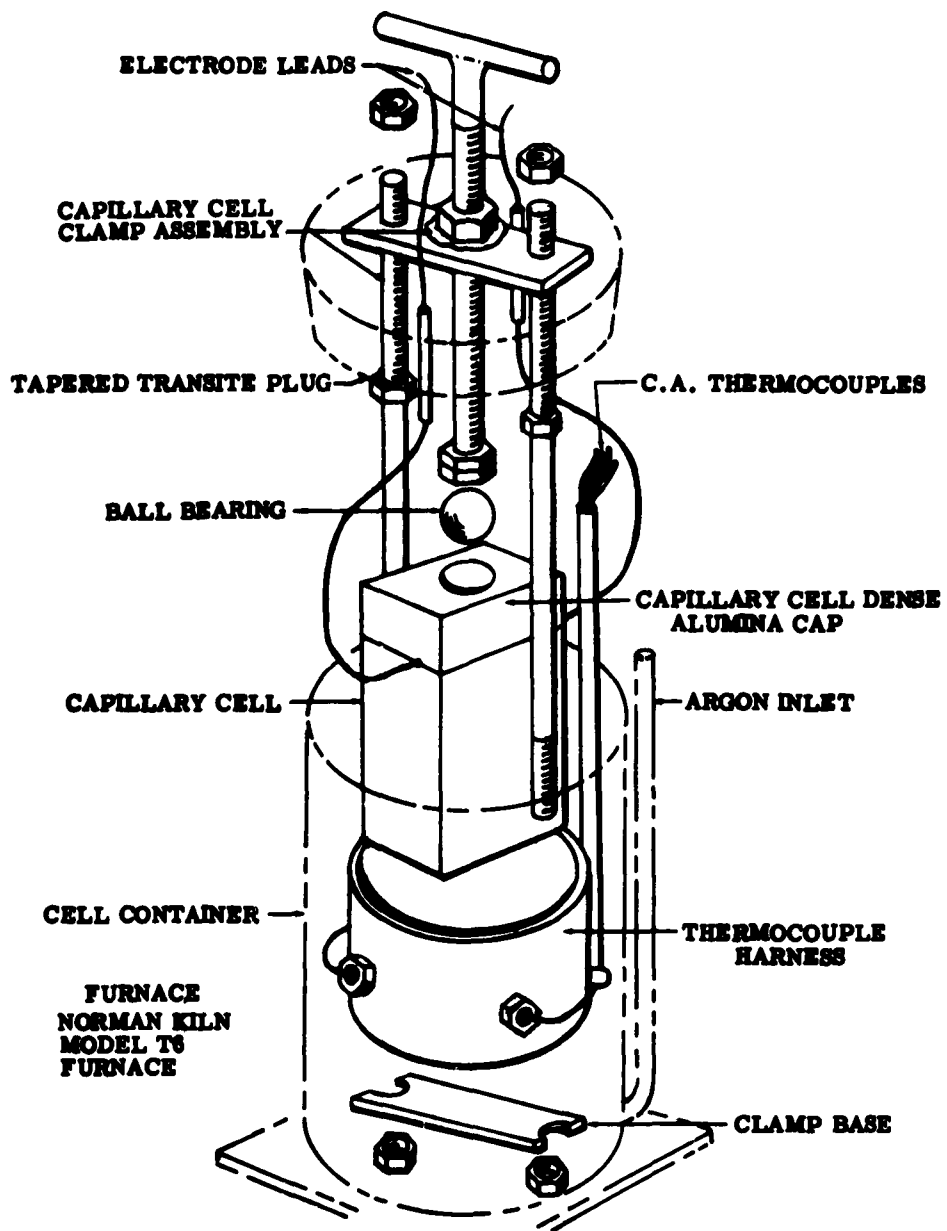


Figure 16. Capillary Cell Conductivity Apparatus

formed a high-resistance "U" between the electrode wires. It was conceived that a high-resistance cell of this type should work well with a Wheatstone bridge. However, this cell would not demonstrate reproducible results and it was finally decided that capillary rise within the cell was altering the length of the electrolyte wire during the course of the experiment.

A conductivity cell was then designed using larger inner diameter, high purity alumina tubing to reduce the effect of capillary rise. This cell was also a dip type with platinum wire electrodes. Difficulties with reproducibility were encountered as with the previous cell. High percentage changes in cell resistance were attributed to slight changes in contact area between the fused electrolyte and the electrode wires. These problems led to the final capillary cell design, shown in Figure 15, which has electrode reservoirs with much greater diameters than the capillaries. This condition results in small percentage changes in the cell resistance with changes in electrode reservoir contact area.

The use of fused electrolytes as standards for calibrating fused electrolyte conductivity cells is desirable since doing so duplicates the environmental conditions in which the cells are designed to operate. The fused electrolytes employed in the initial effort to determine cell constants were stannous chloride and silver nitrate. These were used because data on their conductivities were available at temperatures near 598°K.

Stannous chloride proved difficult to handle because of trouble encountered in removing the water of hydration. The hydrate of stannous chloride melts at 311°K, forming a yellowish liquid. Increasing the temperature removes the water, forming a voluminous mass which then deflates to a form resembling a volcanic ash. This anhydrous form melts at 519°K with some sputtering as inner portions expand. These obvious handling problems led to the investigation of silver nitrate as a possible standard.

Silver nitrate proved to be much better from the handling standpoint, but it showed gradual decomposition with time at 598°K. Decomposition was also evidenced when the silver nitrate was allowed prolonged exposure to light.

The inherent difficulties presented by fused salts soon indicated that a more reliable determination of the cell constants could be achieved by using aqueous electrolytes at lower temperatures. The change in a cell constant with temperature can be estimated by calculating the thermal expansion using available coefficients if higher precision is desired. This was not done in this case.

Modified Wheatstone Bridge

The conductance of electrolytic solutions or molten electrolyte is generally determined with an alternating current Wheatstone bridge. Many circuits incorporating features which meet the problems encountered in electrolytic conductance measurements were studied independently by Jones³³ and Shedlovsky.³⁴ Their recommendations are the basis for most of the precision

conductance bridges in use today. The bridge used in this study was of the type constructed by Edelson and Fuoss,³⁵ based essentially upon a Shedlovsky circuit. A schematic diagram of the bridge is shown in Figure 17.

The Campbell-Shackelton ratio box (Leeds and Northrup Model No. 1553) contains a matched pair of ratio arms, Wagner ground arms, variable capacitance compensation, and a shielded input transformer. This unit is mounted in a completely shielded box and is assembled into the bridge without alteration. A shielded decade resistance box (STD) and a lead connection to the conductivity cell complete the bridge proper. The detector (General Radio Model 1232-A) is a tuned amplifier and null detector whose output is applied to the vertical input of an oscilloscope. The audio oscillator is a Hewlitt Packard Model 200T.

The operation of the Wheatstone bridge is discussed in the following. The alternating voltage is applied at points A and C. The ratio arms have a ratio of unity so that when the standard re-

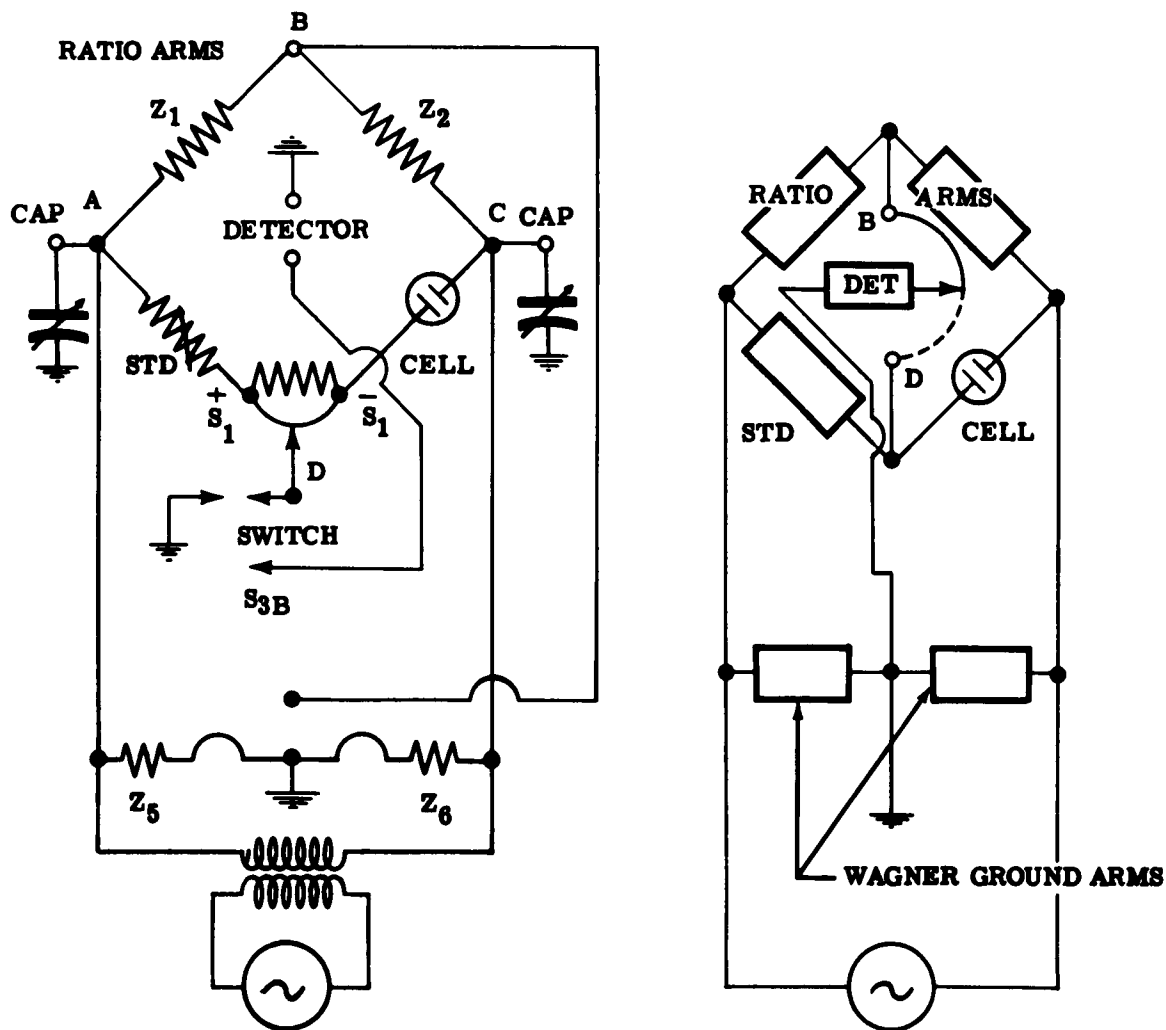


Figure 17. Schematic of Modified Wheatstone Bridge

sistance is adjusted to bring the potential at B equal to that at D, the voltage drop across the standard is equal to the voltage drop across the conductivity cell. Obviously, at this condition, the resistance of the standard is equal to that of the cell, since the series connection between the standard and the cell results in the current being the same in both.

One of the requirements in a precision bridge setup is that a Teflon or polyethelene insulation be used on all external leads. The purpose of shielding is to make the earth admittances of bridge elements definite in amount and type so that their effect is known. The admittance is predominantly capacitive since the leakage conductance of bridge wiring is usually negligible. The admittance current or parasitic current in the bridge circuit of Figure 18 is a condition commonly called the "head effect," because originally the detector consisted of headphones and the operator's head furnished the capacitive path to ground. The parasitic currents are a result of the potential differences between bridge branch points and earth.

The parasitic currents are supplementary to the desired bridge currents circulating in the network due to the applied voltage between A and B. The parasitic currents upset the balance and cannot be eliminated by adjusting Y_1 , Y_2 , Y_3 , or Y_4 . This effect can be eliminated only by making branch points B and D remain permanently near earth potential. The Wagner ground modification makes this possible.

The lead resistance effects in the bridge can be eliminated by first balancing the bridge using direct current. A slidewire (R) is included in the ratio box for this purpose. The slidewire adds resistance to either the decade resistance arm (STD) or the unknown arm (cell). In the procedure for calibration, a ten-ohm or equivalent standard resistor of accurately known resistance is connected in the unknown arm. The decade resistance box is then set to read the same resistance. A six- or nine-volt battery is then placed between bridge points B and D. The calibration for lead resistance is then made by adjusting the slidewire (R) for zero deflection on the galvanometer.

Capacitive reactance in the bridge arms must be balanced to make the bridge sensitive to small changes in the resistive component of the arm impedances. A ganged variable capacitor (CAP) is included in the ratio box and its connection in the circuit is shown in Figure 17. If more capacitance compensation is needed, a shielded 500- $\mu\mu$ f variable capacitor may be connected across the standard resistance decade box.

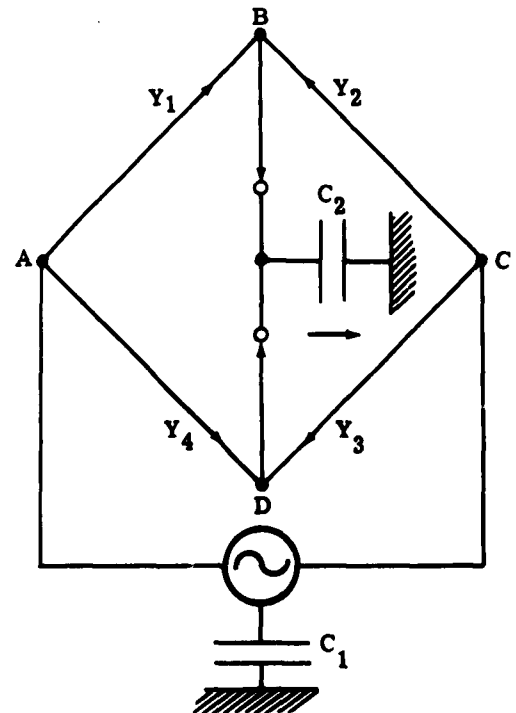


Figure 18. Parasitic Bridge Currents

The bridge is balanced by adjusting capacitance and resistance alternately with switch S_3 in position D. This balances the unknown arms against the Wagner ground arms. The Wagner ground arms are next balanced similarly with switch S_3 in position B. This procedure is continued until no difference in balance exists between positions B and D. The bridge is then in balance.

The frequency dependence of the bridge is illustrated by the data in Table XIV. The resistance value for a 10K-ohm resistor changed 0.03 percent in going from 1000 to 10,000 cps.

TABLE XIV Wheatstone Bridge Frequency Dependence	
<u>Frequency (cps)</u>	<u>Resistance (10K)</u>
250	9410.0 Ω
1,000	9408.7 Ω
2,000	9408.7 Ω
10,000	9405.6 Ω
20,000	9395.5 Ω
100,000	9165.0 Ω

Constant Current Apparatus

The constant current method of measuring the resistance of a conductivity cell employs the measurement of the voltage drop across the conductivity cell when a constant direct current is passed through the cell. The resistance is simply calculated from Ohm's law. A factor which acts to complicate the use of this method is polarization. Polarization, in an electrochemical sense, is a phenomenon which shows up externally as an increase in resistance above the true value and is due to special action within the electrolyte. The nature of polarization is that it takes a finite time to occur. The true resistance of the cell may be calculated from the potential drop across the cell if determined at the instant a switch is closed, allowing a constant current to flow through the cell. The effect of time on polarization is indicated by observing the potential drop increase toward a saturation point. This is illustrated in Figure 19.

The constant-current apparatus designed around the forestated principle is shown schematically in Figure 20. This circuitry is based upon a similar method employed by Dr. S. M. Selis and J. L. Griffin at the General Motors Research Laboratories. For this method, two 45-volt Burgess batteries are connected in parallel and placed in series with a current limiting resistor (R_1), a calibration resistor (R_2), the test cell, and a switch consisting of the normally open contacts of a Clare HG 1002 mercury relay. This constitutes the controlled circuit which acts to pass constant current through the cell upon command from the control circuit. The batteries

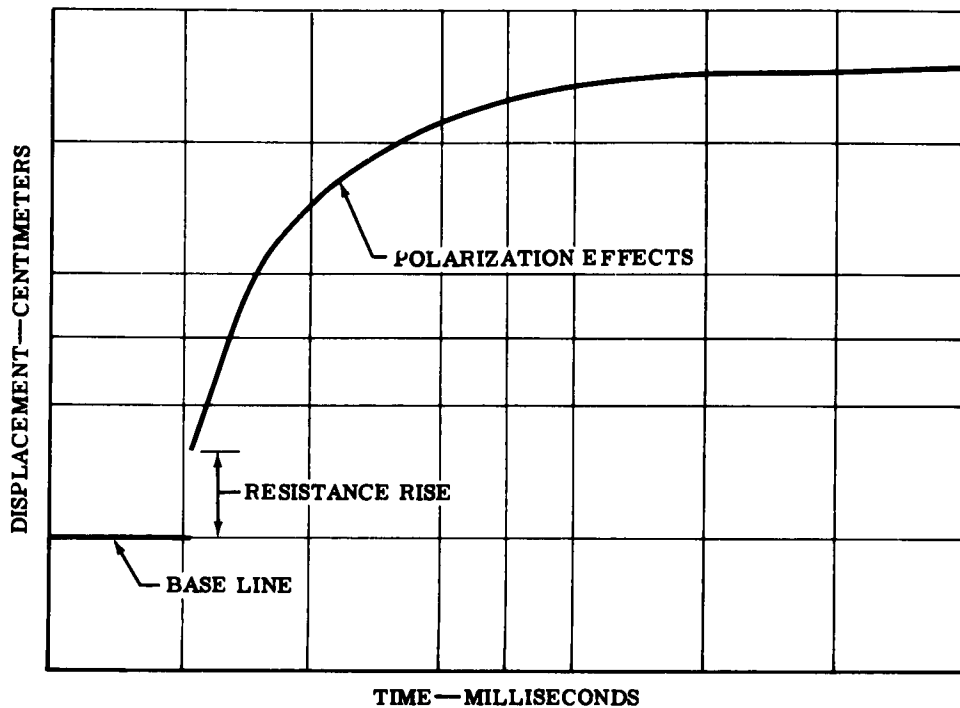


Figure 19. Oscilloscope Trace of Polarization Effect

serve to supply the d-c power to R_1 , R_2 , and the test cell. The limiting resistor (R_1) is much higher in resistance (10K to 100K-ohms) than the test cell (1 to 10 ohms). Under this condition, changes in cell resistance due to polarization have negligible effect upon the circuit current since this change hardly changes the total circuit resistance. The measurement of the constant current (I_k) is accomplished by measuring the voltage drop across the accurately known calibration resistor (R_2) with a potentiometer. The instantaneous voltage drop across the cell is applied to the vertical input of a high gain d-c oscilloscope. The oscilloscope is triggered to sweep when the mercury-wetted contacts of the mercury relay close. The image of the trace is recorded with a Polaroid camera. The magnitude of the voltage-drop (V), indicative of the true resistance, is obtained by multiplying the sensitivity of the oscilloscope (mv/cm) by the appropriate dimension in centimeters taken from the photograph. The internal resistance (R_e) of the cell is obtained by using Ohm's law:

$$R_e = \frac{V}{I_k} \quad (27)$$

The armature and external trigger circuits consist of a power source of two 45-volt batteries in series, a smooth-acting push button switch (S_1), a voltage dropping resistor (R_3), a bypass capacitor (C_1), the mercury relay armature, and a coupling capacitor (C_2). Closing the

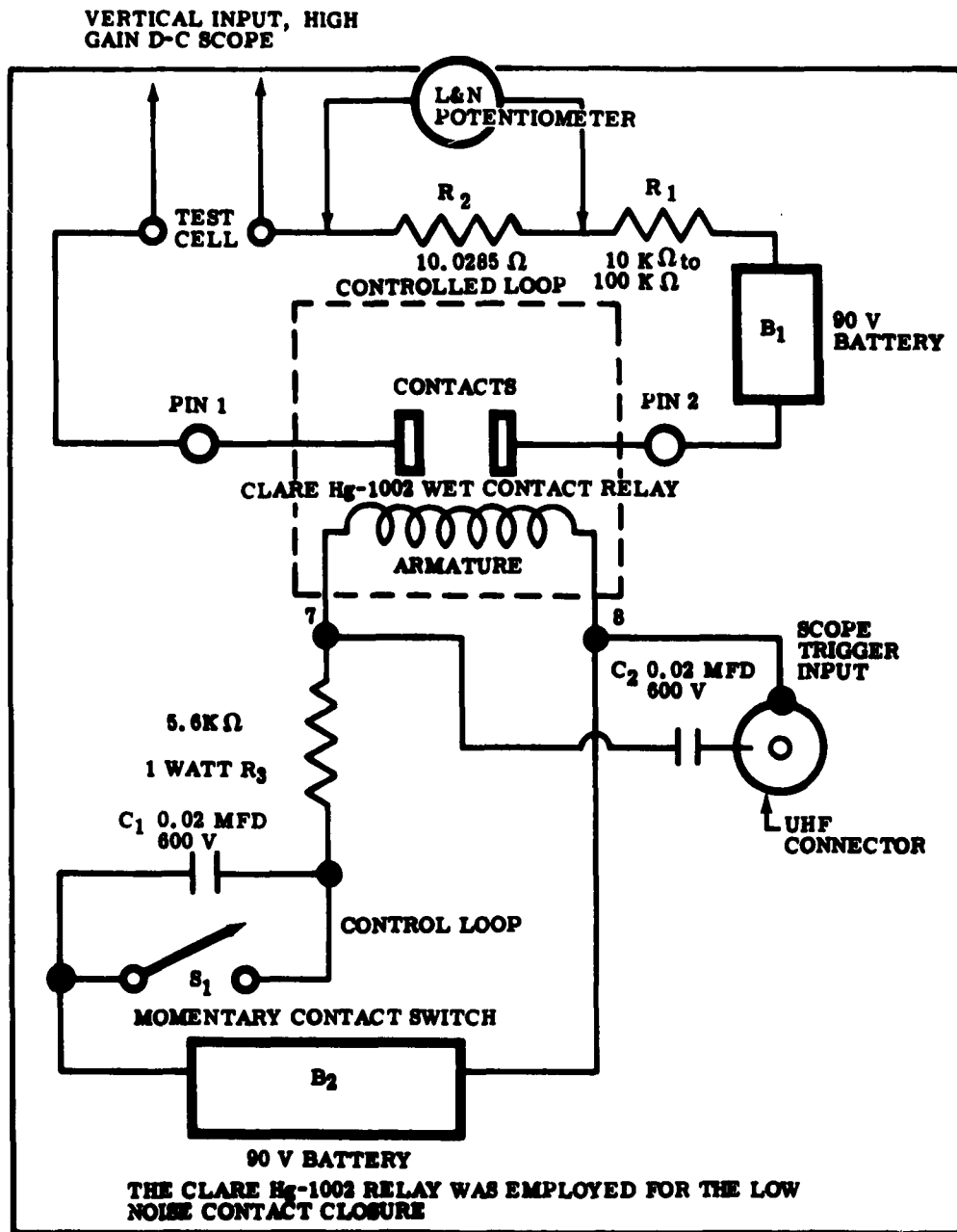


Figure 20. Schematic of Constant Current Conductivity Apparatus

switch (S_1) energizes the armature coil and triggers the oscilloscope. The armature closes the contacts in the constant-current loop. The voltage dropping resistor (R_3) limits the relay coil current to nine milliamperes. Capacitor C_1 suppresses voltage hash when the switch (S_1) is made. Excessive hash could carry over to the controlled circuitry.

Possible refinements to this method include a double pole double throw switch to reverse the current direction in the constant current loop. This reverses the electrode reactions and counteracts electrode changes.

ELECTROLYTE IMPREGNATION AND RETENTION

The degree of saturation of a matrix with an electrolyte depends on the ease of electrolyte penetration in the interstices of the body. The ease of penetration of a porous body by a given electrolyte depends on the permeability of the porous body and on the viscosity of the electrolyte. The retention of the electrolyte within the matrix is essentially dependent on the same parameters, the difference being the reverse or ease of desaturation. Depletion of electrolyte by a different material in contact with the matrix (such as a metal, which might have preferential wetting properties) presents a different variable, affecting electrolyte retention.

Impregnation Test Procedures

It was conceived that maximum penetration of the molten and aqueous electrolytes into electrolyte matrices would necessitate using a vacuum impregnation technique. Quantities of the residual gas present in the specimens prior to impregnation could become trapped inside if positive pressurizing methods were employed. Residual gas is greatly reduced by the vacuum method of impregnation.

The procedure followed in vacuum impregnating the specimens was simply to evacuate the impregnation container with the specimens either immersed in the electrolyte or suspended above until a steady vacuum of approximately 1 mm Hg was attained. The specimens were impregnated by bringing the system to atmospheric pressure while they were immersed in the electrolyte.

The apparatus employed in impregnating small specimens with molten ternary electrolyte is shown in Figure 21. The specimens are placed in a stainless steel wire basket which can be lowered into a 750-cc alumina crucible containing approximately 250-cc of molten electrolyte. The vacuum container is a stainless steel can with a water-cooled cover. A silicone rubber O-ring is secured between the flanges of the tank and cover to provide a vacuum tight seal. The impregnation basket is raised and lowered by a heavy wire rod placed through a small neoprene rubber stopper which is placed in a hole provided in the center of the cover. The vacuum container is placed in a furnace with its top protruding, allowing access to the water-cooled cover. Figure 22 is a similar tank used for impregnation of larger specimens.

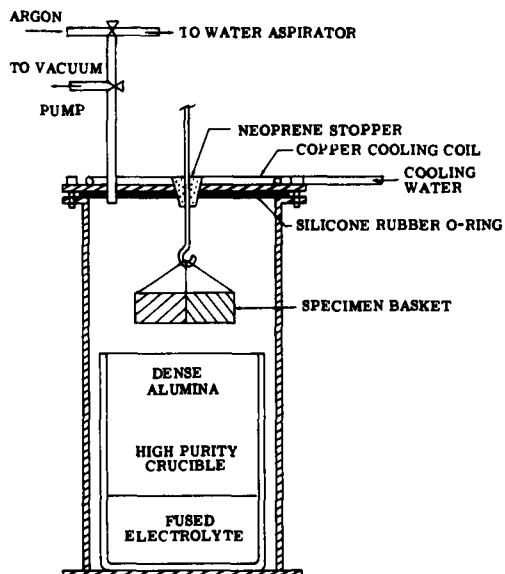


Figure 21. Vacuum Impregnation Tank for Small Specimens

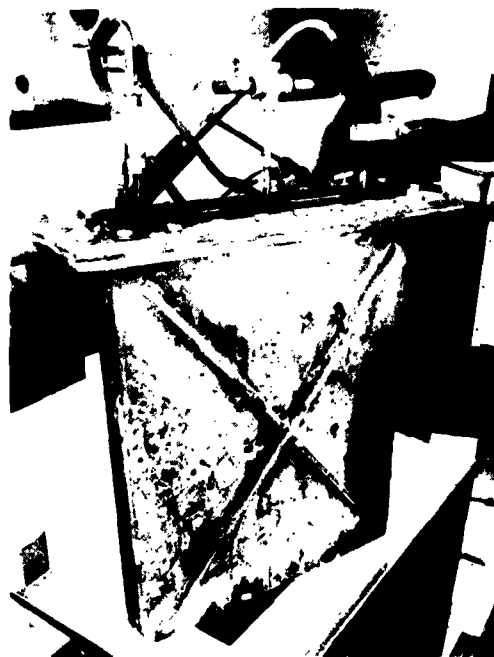


Figure 22. Vacuum Impregnation Tank for Large Specimens

Special precautions were observed in vacuum impregnating with the ternary electrolyte. High purity argon gas was employed in pressurizing the system. The vacuum-pressurizing technique was repeated four times, ending with a positive argon pressure of approximately 4 lb/in.² to ensure complete penetration. Subsequent to this, the basket containing the specimens was withdrawn from the electrolyte just above the surface to allow drainage of excess surface electrolyte. The basket was raised to the inner surface of the cover to cool in an argon atmosphere before the specimens were removed and stored. Gradual attack on the wire basket, discoloring the electrolyte, presents a problem, but was not observed to affect the electrolyte seriously. This should be corrected with newer, Teflon-lined equipment.

Electrolyte Retention

Electrolyte retention is based on the surface tensions of the electrolyte mixture held within the pores of the matrix and the surface tensions of the amalgams present in the cells. This can be strongly affected by the production of mercury vapor in the lower cell half, should overheating take place. A guide to the requisite pore sizes is available from mercury porosimeter tests

which measure the pressures necessary to force mercury through unimpregnated or open pores. It must be remembered that the pressures necessary to force mercury vapors through an impregnated pore would be even higher and may be calculated as follows:

$$p = \frac{-4 \sigma \cos \theta}{D} = \frac{-175}{D} \text{ (Based on wetting angle, } \theta = 130^\circ \text{ at room temperature) } \quad (28)$$

where σ is the surface tension of the liquid, θ is the wetting angle, p is the applied pressure, and D is the diameter of the smallest pore filled at pressure p .

From Equation (28), a pressure differential of 15 psi would cause mercury to pass through an empty pore approximately 15 microns in diameter. A pore of 5-micron diameter would require a pressure of approximately 35 psi to force mercury into it.

V. LIQUID METAL CELLS

This section contains a discussion of the various types of cells that have been studied in this work. A brief description of each cell type is given, along with the purposes and benefits derived from each. Each of the cell configurations serves a basic purpose in the advancement of the liquid metal cell program.

FLAT-TYPE CIRCULAR CELL

This cell (Figures 23, 24, 25, and 26) was evolved from the first concepts of how a liquid metal cell would be configured for space use and offers the advantages of low volume, low reactant weight-to-surface area ratio, and adaptability to stacking. The first cells built utilized a matrix of approximately 46-cm² electrode area. A later design of essentially the same configuration has an electrode area of 81 cm² while holding to the same radial dimension and reducing the cell thickness. The matrix would seat on the ledge of the lower cell half (Figure 23), a dense ceramic gasket would seat on the matrix and the rim of the upper cell half, and an O-ring would form the seal between the dense gasket and lower cell half at the outside of the cell. Figure 24 is a view of a typical sintered matrix and the impervious gasket used in the cell. Figure 25 is a view of the top half of the cell showing white faces which had been flame sprayed with aluminum oxide (originally considered as an insulating material), but the flame sprayed alumina was not used in later cells because of its poor compatibility with the amalgam and the electrolyte. Figure 26 shows the two cell halves as they would be assembled in the press. Detail drawings of these cell halves are shown in Figures 27, 28, and 29. In the view of the bottom side of the cell, tubes No. 13, 2, and 7 will have electrical sensors (see Section VIII, Support Equipment) attached to them to indicate (1) the levelness of the cell, (2) the point at which the mercury level just reaches the matrix, and (3) the point at which the mercury head

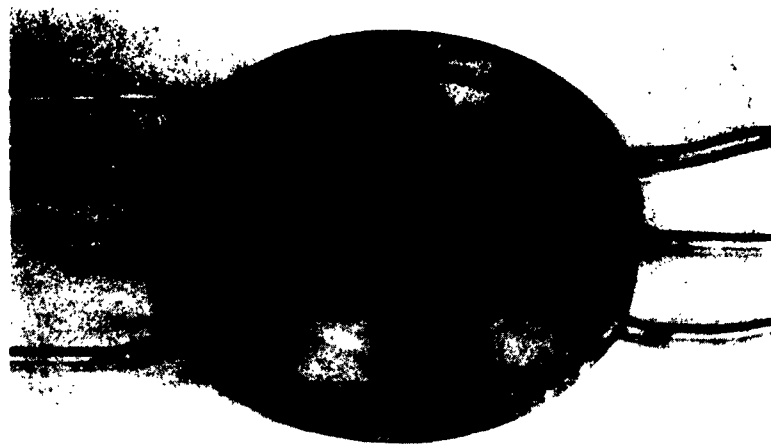


Figure 23. Bottom Half of Circular Cell

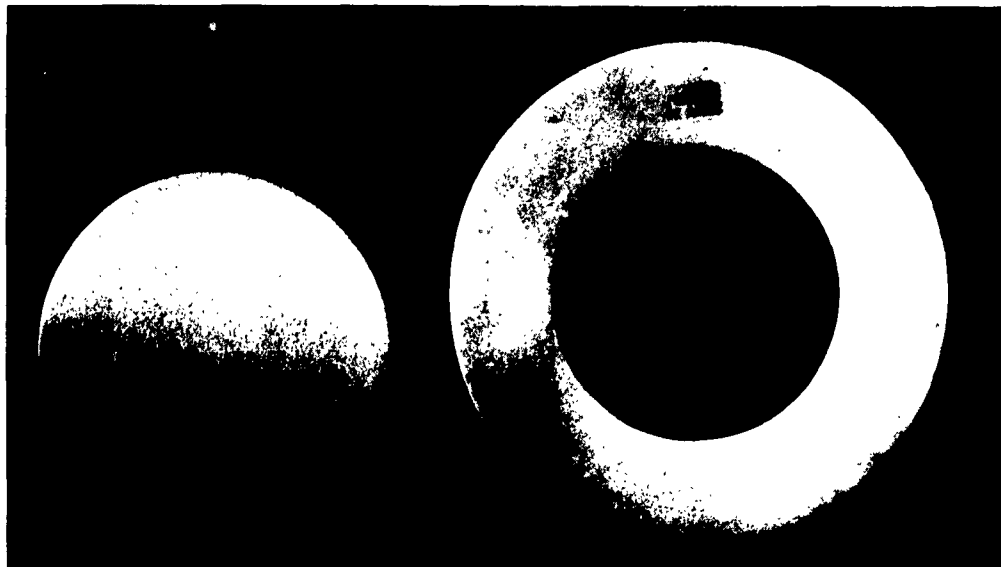


Figure 24. No. 5186 Matrix and A-402 Gasket



Figure 25. Top Half of Circular Cell

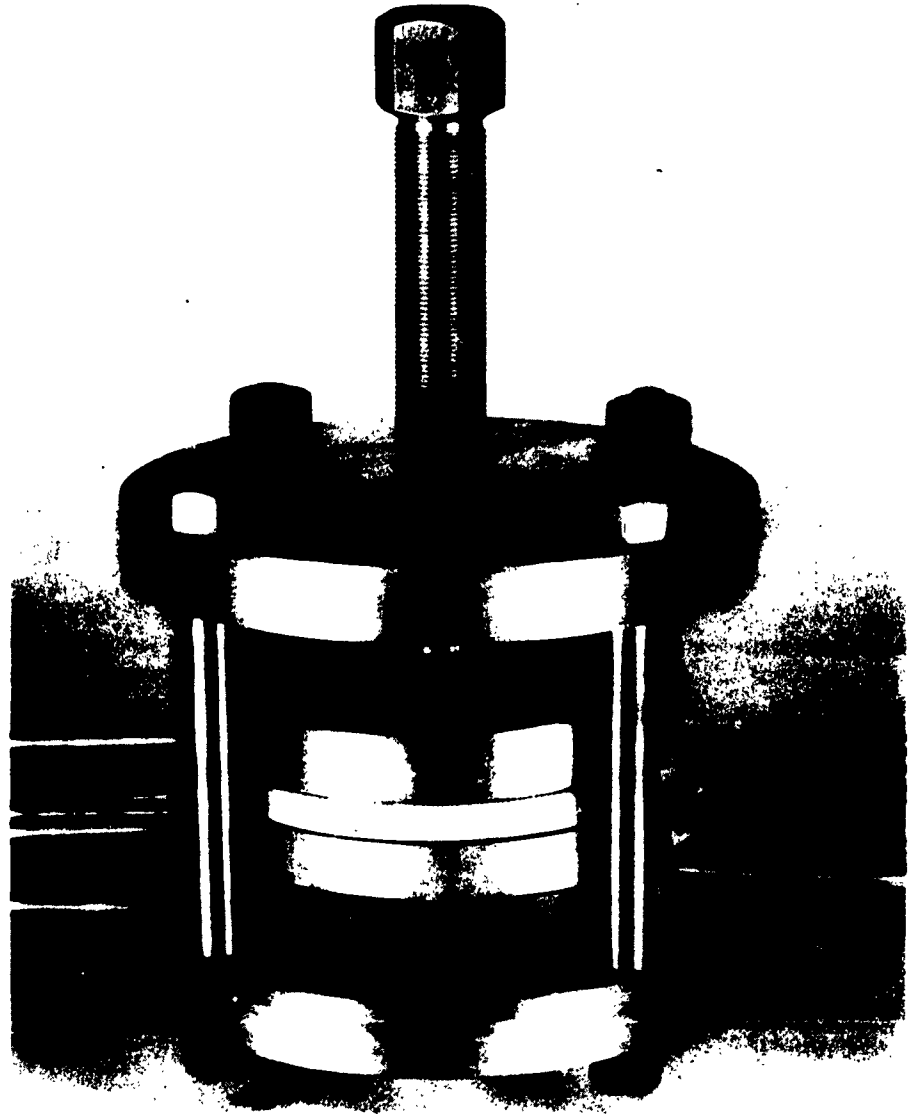


Figure 26. Cell in Press

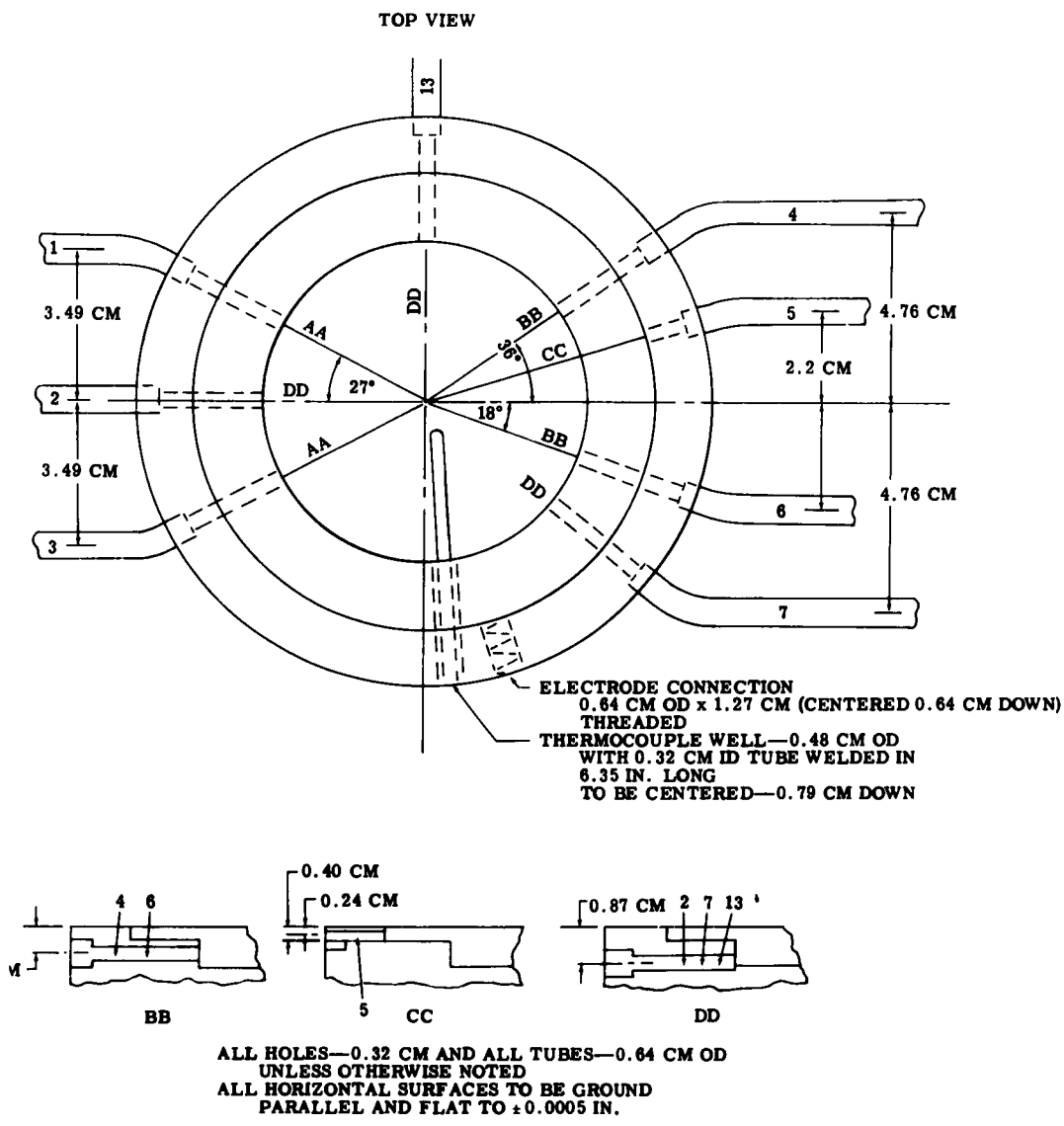


Figure 27. Detail of Bottom Half of Circular Cell

becomes sufficient to breach the seal. Tubes 1 and 3 will feed out approximately an 8 percent (mole) potassium amalgam. Pure mercury will feed the cell through either tube No. 4 or by-pass tube No. 6; tube No. 7 is a drain for the mercury side of the cell; and tube No. 5 will allow electrolyte to seep into the electrolyte annulus to replenish any possible electrolyte losses. The thermocouple well is indicated as extending into the interior of the cell.

With reference to Figure 28, the anode chamber, tube No. 8, is an argon inlet which will allow argon to sweep through the upper half of the cell and clear it of air before and after loading; tubes No. 9 and 11 allow potassium or potassium amalgam to flow into the upper cell half; tube No. 10 could be used to drain the cell if it is desired to change amalgam composition or to shut down the cell for disassembly; tubes No. 12 and 14 are overflows for the potassium side. Figure 29 is a drawing of the proposed intermediate cell (exclusive of piping) to be used in the construction of a basic cell unit. The intermediate cell is merely a combination of a bottom half and a top half built in one piece for a series connection—all piping being as indicated in Figures 27 and 28. Figures 30 through 35 detail the components used in the press.

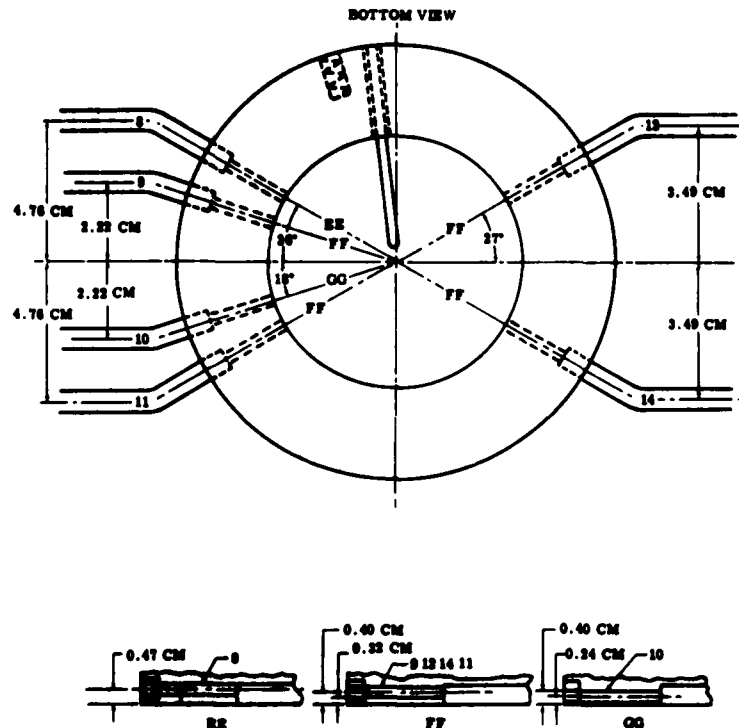


Figure 28. Detail of Top Half of Circular Cell

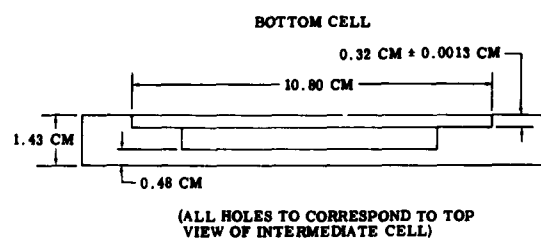
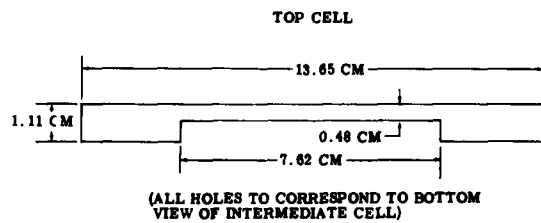
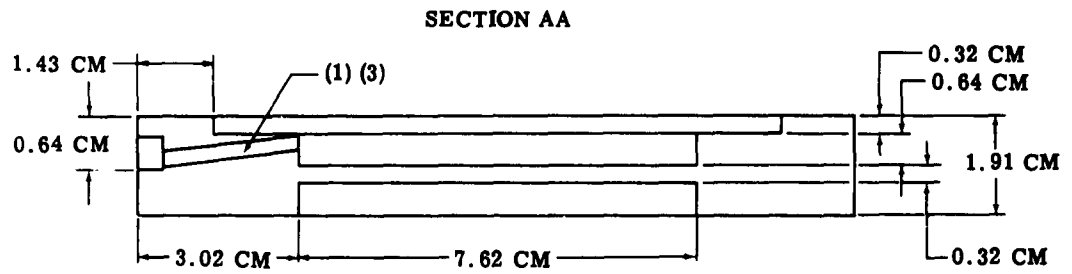


Figure 29. Detail of Cell Profile and Intermediate-Type Cells

It became apparent that a fundamental problem was present in the matrix material being used; and while a large investigative effort was placed in this direction, work on this type of cell halted and further cell investigations were carried on with special purpose configurations listed in the following paragraphs. The circular cell work will be reinstated as the new matrix materials become available.

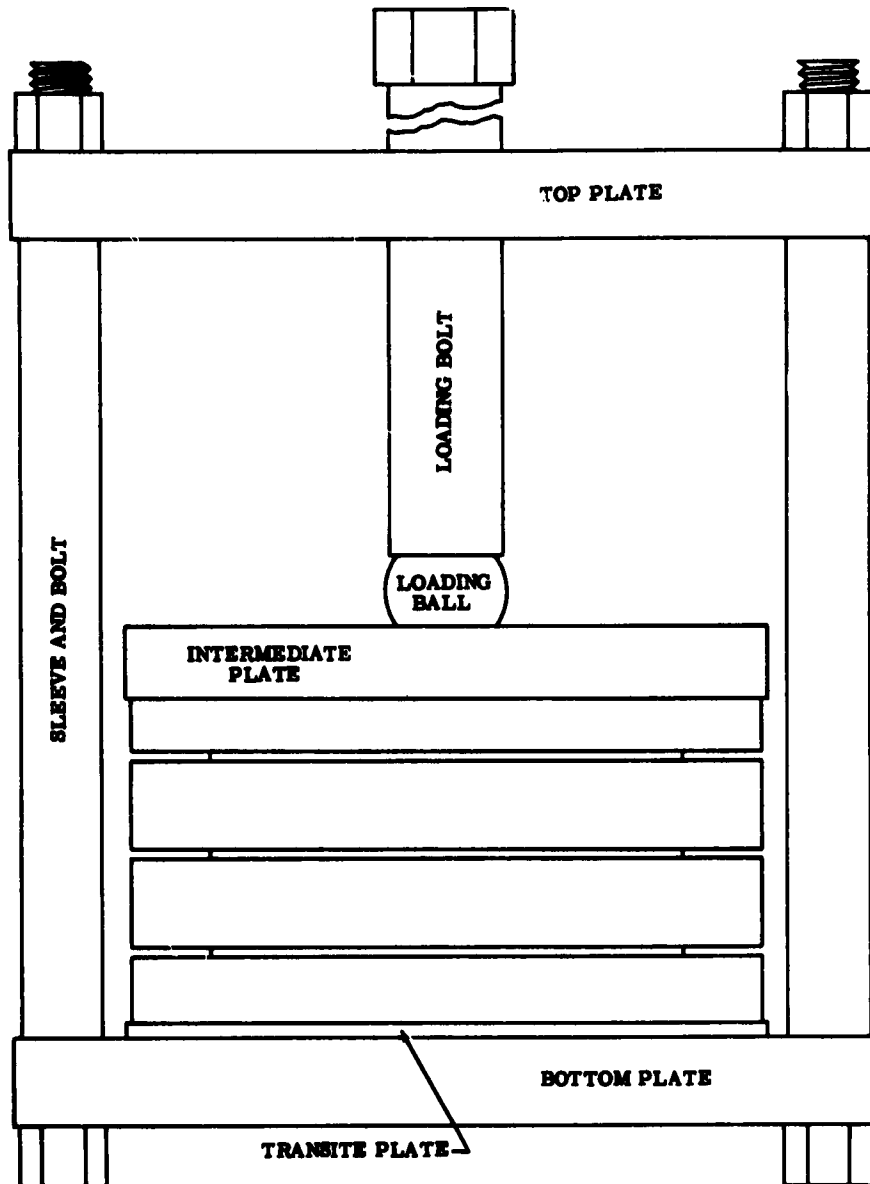


Figure 30. Press Assembled

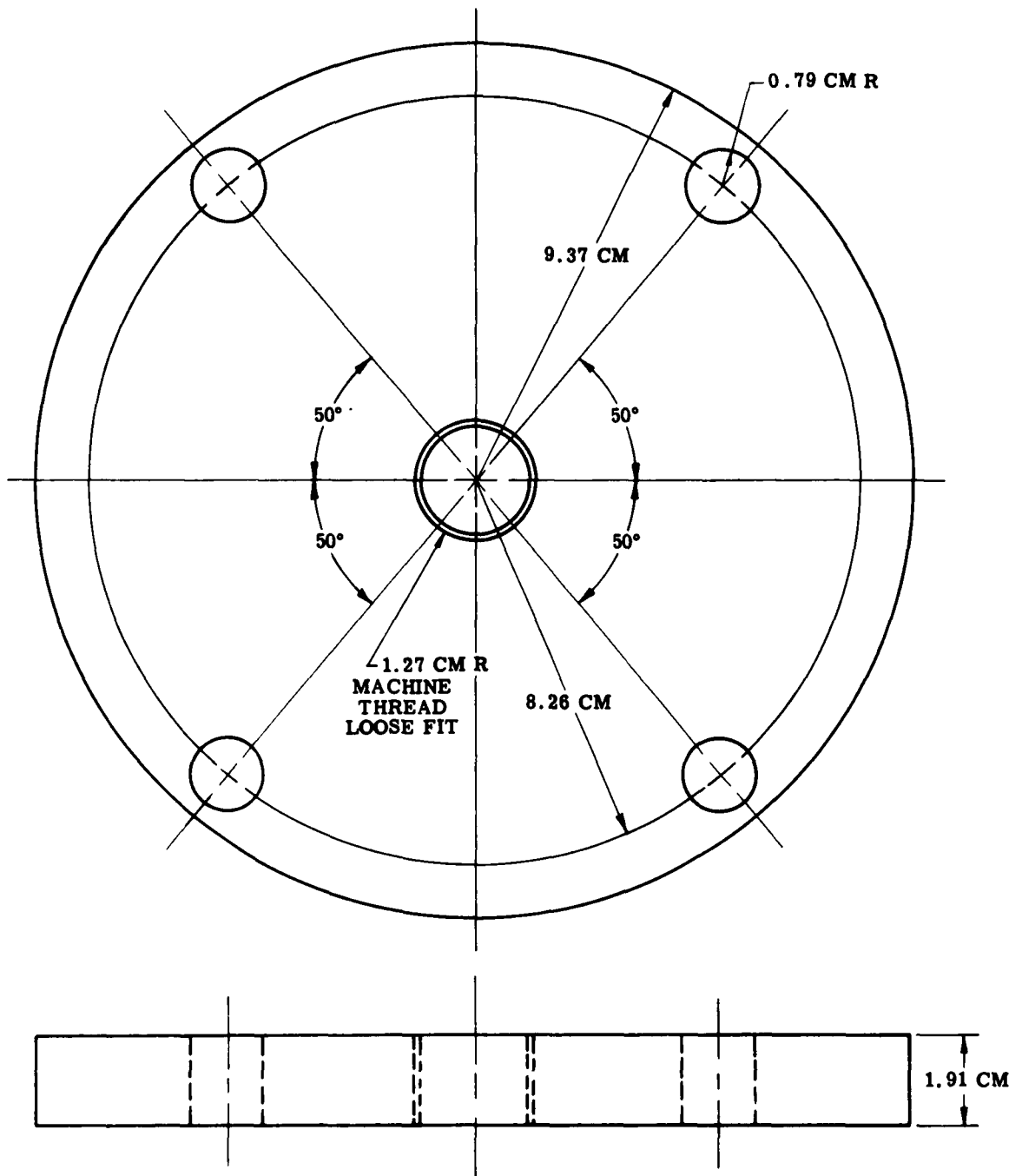


Figure 31. Press—Top Plate

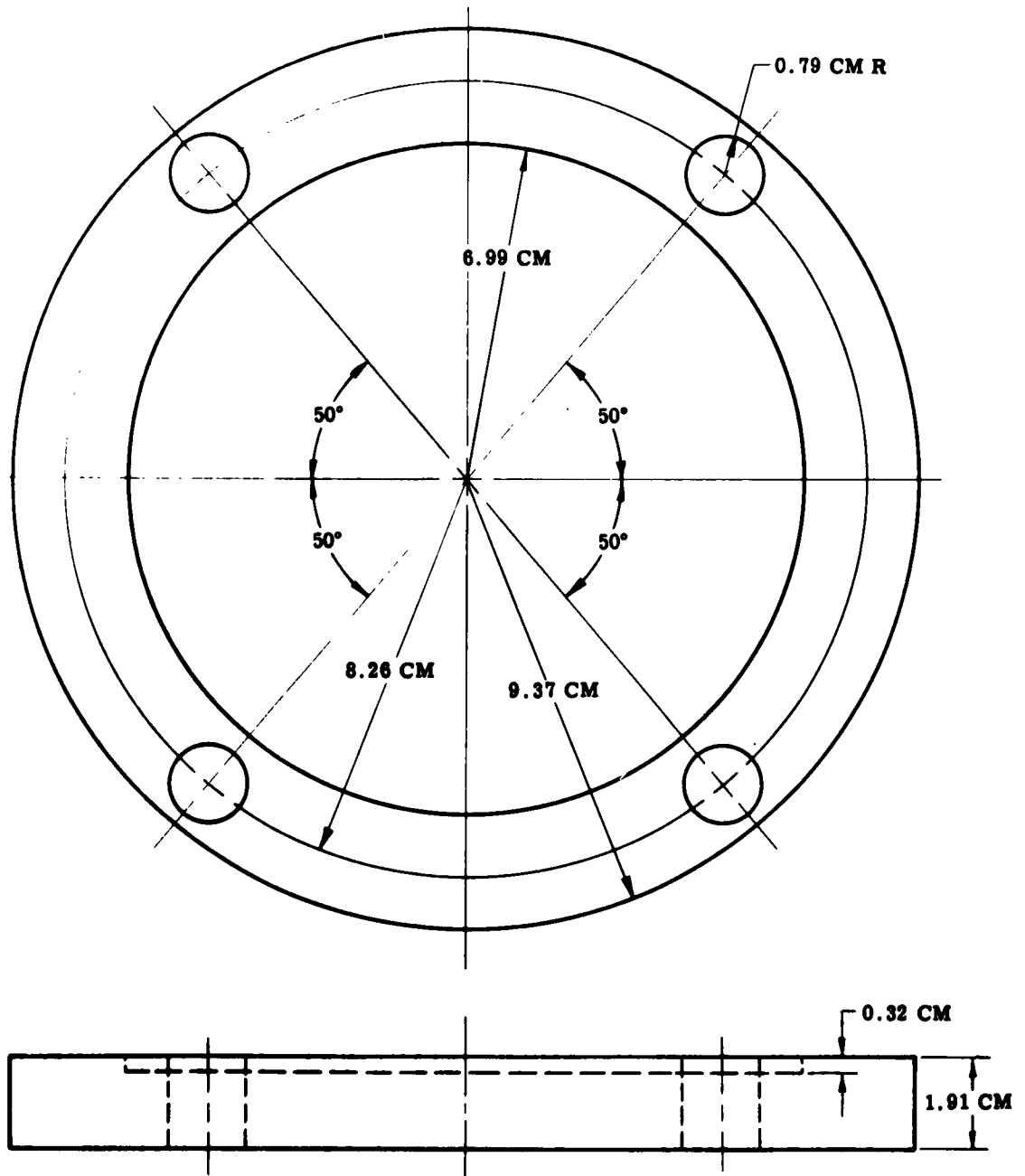


Figure 32. Press—Bottom Plate

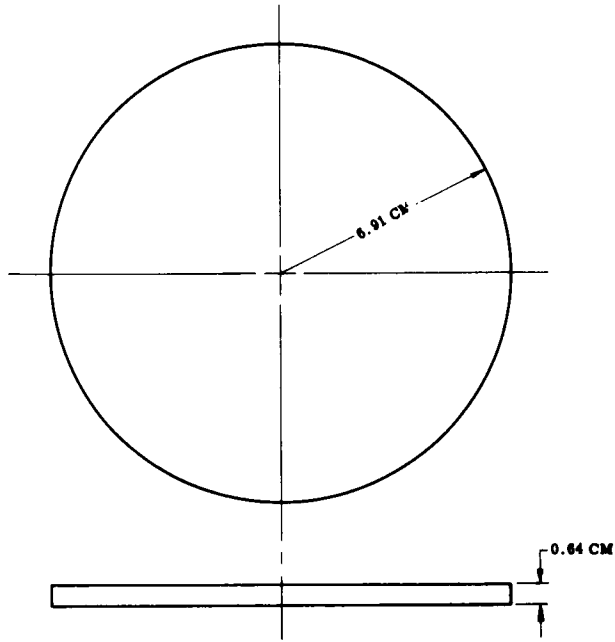


Figure 33. Press—Transite Insulating Plate

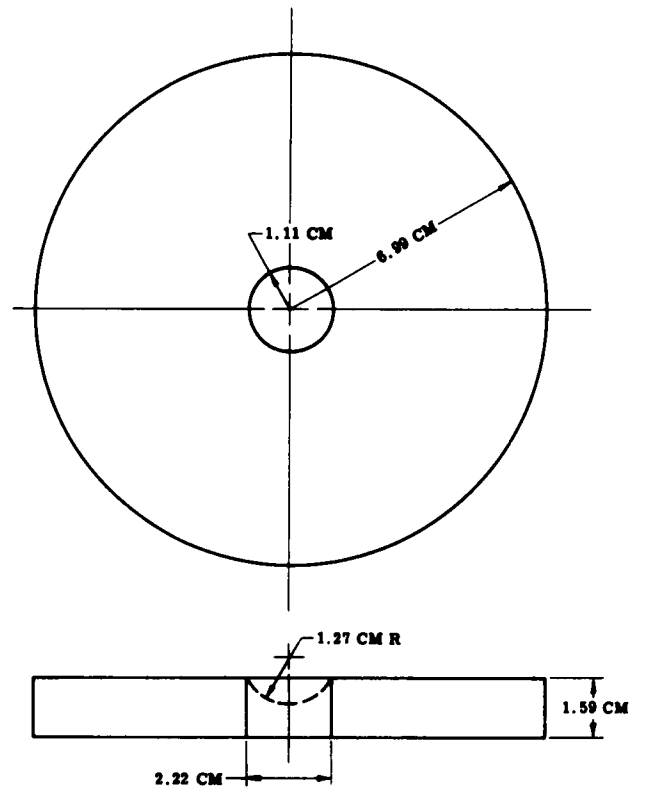


Figure 34. Press—Load Plate

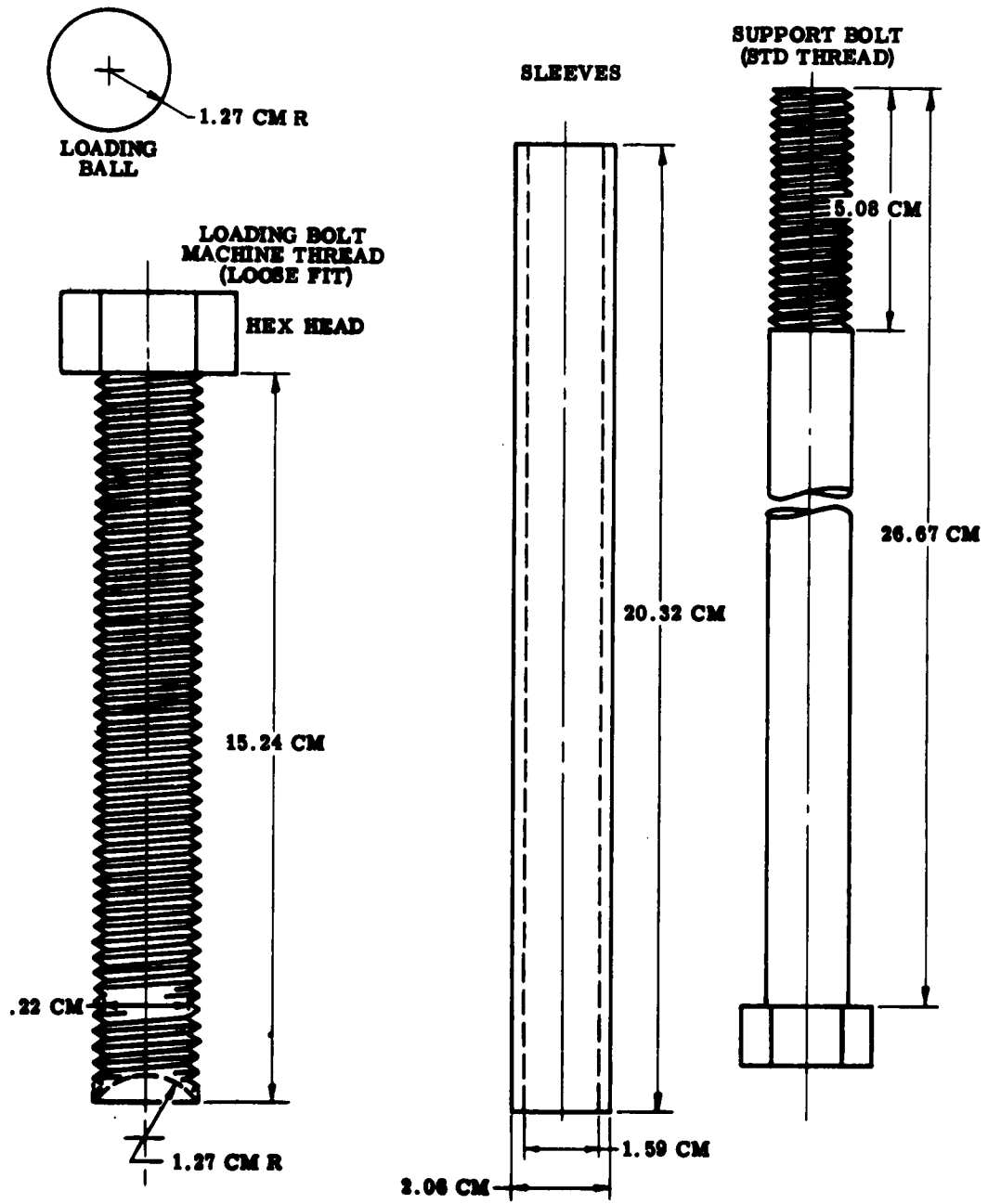


Figure 35. Press—Small Parts

SINGLE CUP CELL—STATIC TYPE

The single cup cell, as shown in Figure 36, is a static-type cell with potassium-amalgam contained in a previously impregnated porous alumina cup which dips into a pool of mercury. The cup material (Table IX) is known to have a short life in the system but, nevertheless, was useful for investigations of short duration (6 hr). The depth of immersion is controlled to avoid subjecting the electrolyte contained in the pores to displacement forces. The seals of ceramic-to-metal, accomplished with silicone or neoprene rubbers, are made possible through the use of cooling coils near the upper reaches of the cell. After operation, when cell emf is low, reversal of current will charge the cell, restoring liquid metals to their original compositions. In effect, this operates as a secondary battery.

The single cup cell offers a convenient, simple means of studying cell performance with an electrolyte-matrix combination for separations of liquid metals while eliminating many of the engineering problems associated with a finalized space design.

DOUBLE CUP CELL

This research-type cell (Figure 37), is similar in construction to the single cup cell, but it uses two porous alumina cups—one containing mercury and the other containing potassium-amalgam. The two cups dip into a pool of electrolyte so that there is a constant capillary replenishment. An electrolyte-resistant, gold foil reference electrode is added so that potentials can be measured between the gold-potassium, gold-mercury, and potassium-mercury electrodes.

In this way the behavior of the individual electrodes may be determined. This cell is virtually immune to internal shorting because:

1. There is no piece of porous ceramic which is common to both liquid metal interfaces
2. A small crack or a pressure differential in either electrode compartment would merely cause liquid metal to seep into the large well at the bottom of the cell, and this would have to fill to some depth before shorting would occur.

This cell configuration does not readily lend itself to use as a power cell because of difficulties involved in feeding reactants, indeterminate current path lengths, etc, but it has yielded cogent information on electrode behavior.

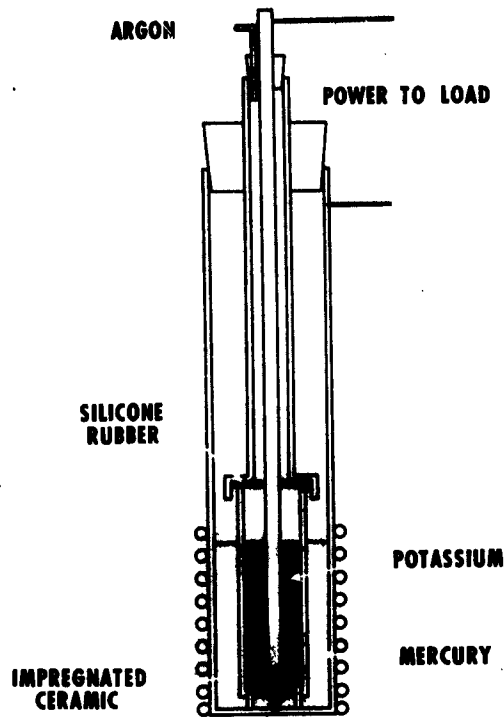


Figure 36. Single Cup Cell—Static Type

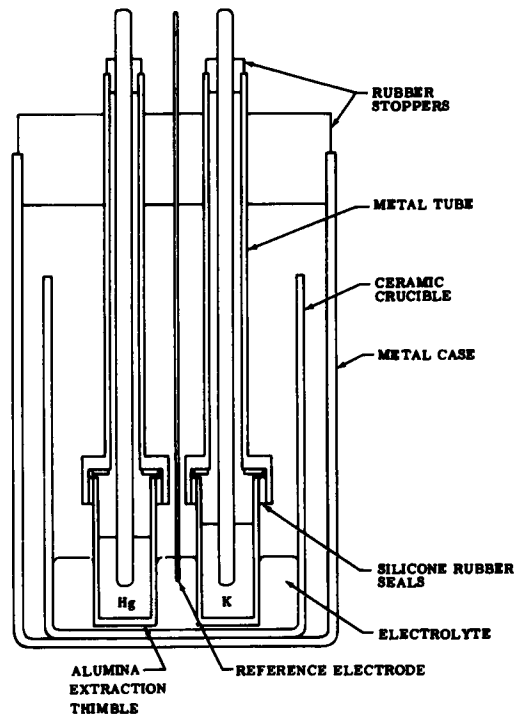


Figure 37. Double Cup Cell

DIFFERENTIAL DENSITY CELL—STATIC TYPE

Figure 38 depicts this cell in a static configuration. The ceramic matrix is eliminated and the inherent densities of the materials are used for separation—e. g. (at cell operating temperature), 12.9 gm/cm^3 for mercury, 2.4 gm/cm^3 for electrolyte, and 0.7 gm/cm^3 for potassium. Thus, the potassium floats on the electrolyte and the electrolyte floats on the mercury. Metal leads are sheathed in ceramic to eliminate electrical shorts. The use of amalgam up to 75 percent (mole) potassium is not precluded, and the mercury electrode may be safely allowed to absorb up to 65 percent (mole) potassium. The chief advantage of this cell is in its lack of a matrix, since this means that the pure electrochemical performance—sans matrix perturbation—can be studied, and it sets the performance goals of a matrix-type cell. Performance might be limited somewhat by the necessity for a thicker electrolyte cross section than would be needed if a matrix were used. Resistivity is the important parameter. Figure 39 is a photograph taken in the laboratory of the single cup, double cup, and static differential density cells in operation.

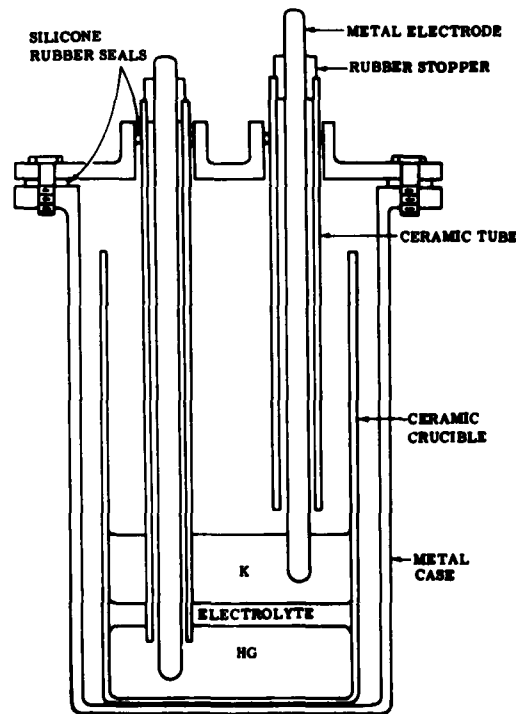


Figure 38. Differential Density Cell—Static Type

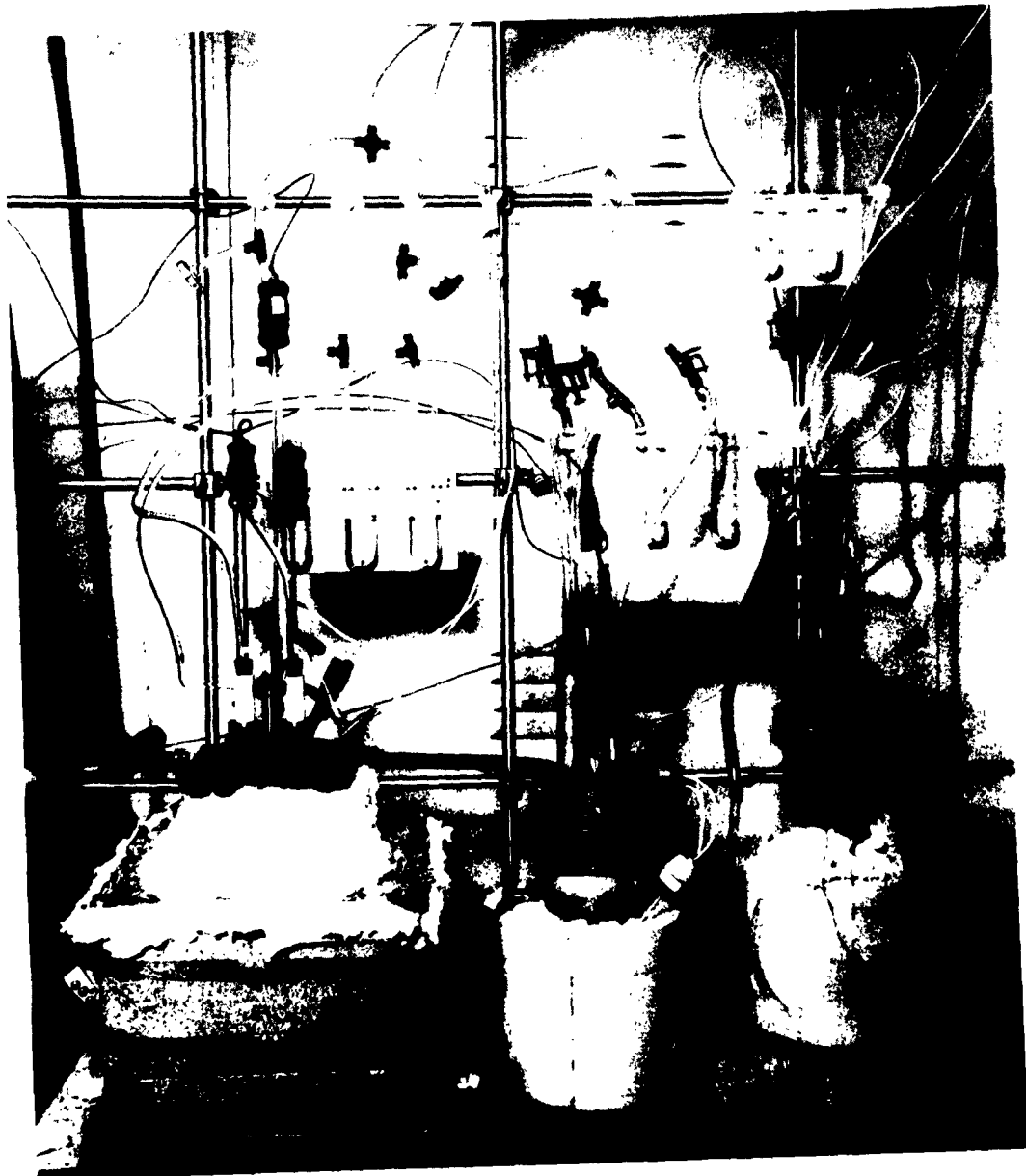


Figure 39. Three Cells in Laboratory Setting

SINGLE CUP CELL—FLOWING TYPE

To show the regenerative capability of the potassium-mercury liquid metal cell system, the single cup cell shown in Figures 40 and 41 was run in the laboratory with periodic additions of potassium to the inside of the cup and mercury flowing through the cell. Both an RA-139 alumina and an M magnesia cup were used on this type of cell. Mercury flow was metered by use of a chemical buret. Open circuit voltage was used to measure the potassium concentration in the mercury; cell voltage demonstrated the operational and regenerative characteristics of the cell.

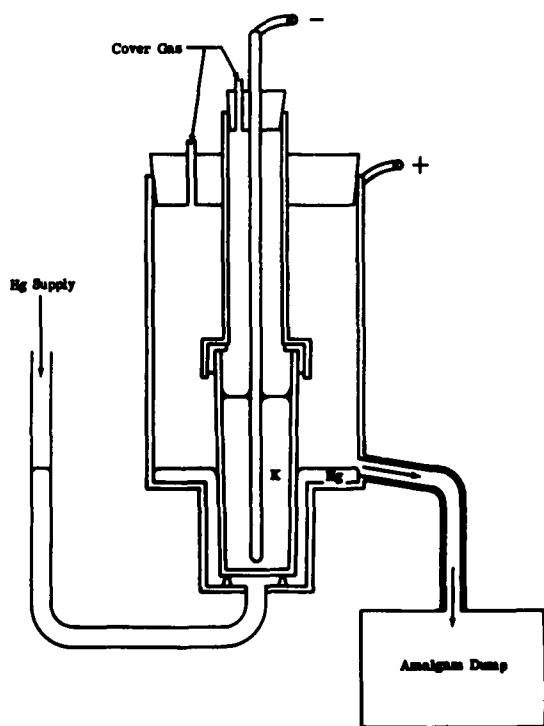


Figure 40. Single Cup Cell—Flowing Type



Figure 41. Flowing Single Cup Cell
in Operation

DIFFERENTIAL DENSITY CELL—FLOWING TYPE

A schematic of the flowing differential density cell is shown in Figure 42. Basically, its principle is the same as that of the static-type cell except for the replenishment of materials. Potassium is added periodically through the potassium feed located to the right of the cell, and a constant, controlled mercury feed comes in at the left. The actual cell is maintained inside the inverted dense alumina cup, and mercury flows underneath the mercury-electrolyte interface, coming in droplets through the port and spreading out on the plate shown in the drawing. A later cell was changed slightly in configuration. A constant mercury level is maintained by leakage to the outside of the inverted cup and flow over the weir shown leading to the amalgam catch tank. The regenerative capability is determined by the ability to maintain a constant voltage by replenishment of reactants at a steady rate while the cell is under some load, accompanied by the ability to vary the cell voltage as a function of feed rate of mercury.

RECTANGULAR CELL

Another approach to the construction of a more advanced type of engineering cell is the rectangular type using a picture frame matrix (Figures 43, 44, and 45). The cell consists of a porous piece of ceramic enclosed on four sides by a dense impervious ceramic frame. The porous portion would be approximately 0.3 cm thick and the impervious frame would be approximately 0.9 cm thick. The overall cell area would be 232 cm². Feed and effluent piping would consist of holes drilled through the metal plates which form the barriers between cells when compressed to either side of the frame. At the same time, the plates would act as the series electrical connection from one cell unit to the next. In this manner the cell stack can be built up to any given voltage.

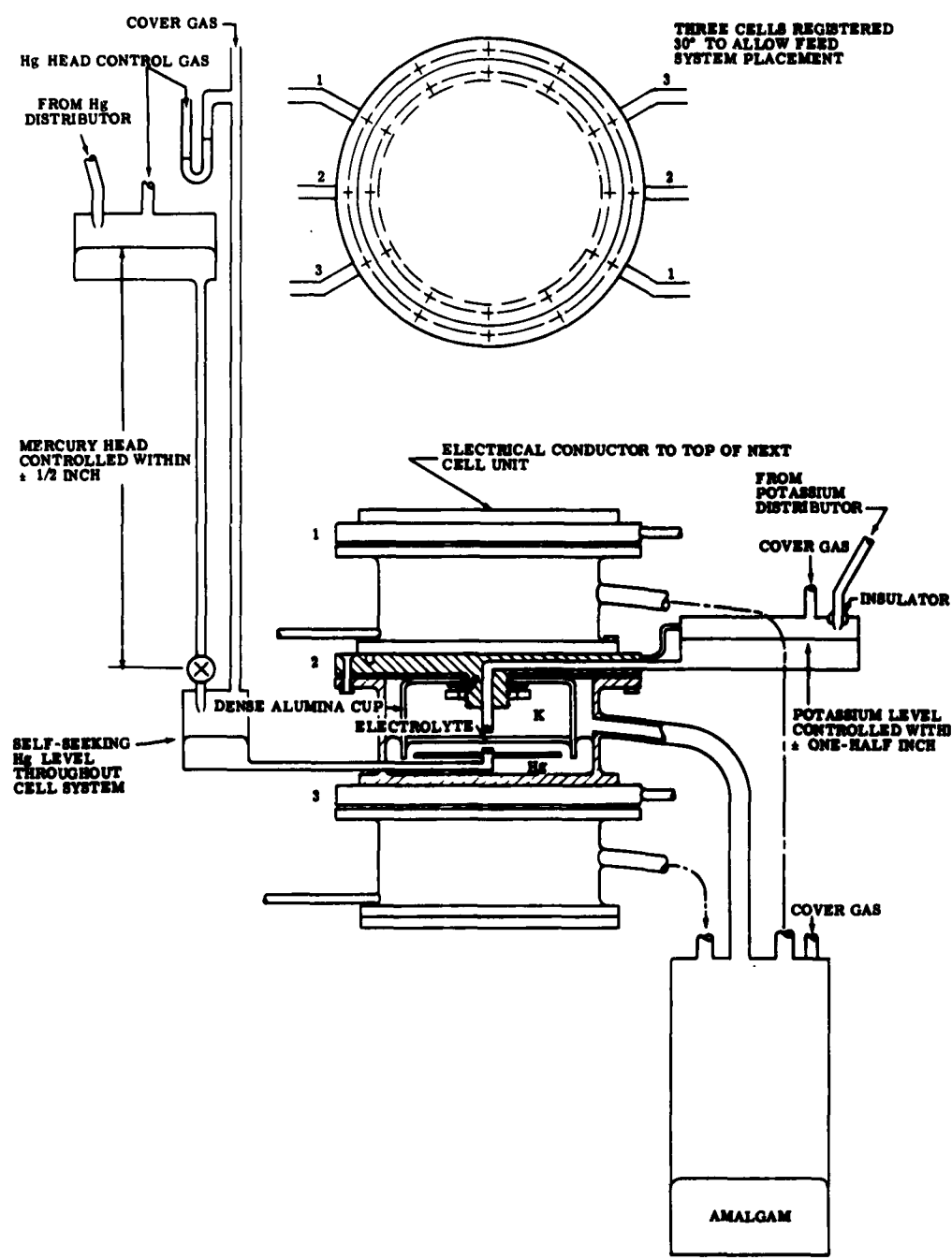


Figure 42. Differential Density Cell—Flowing Type

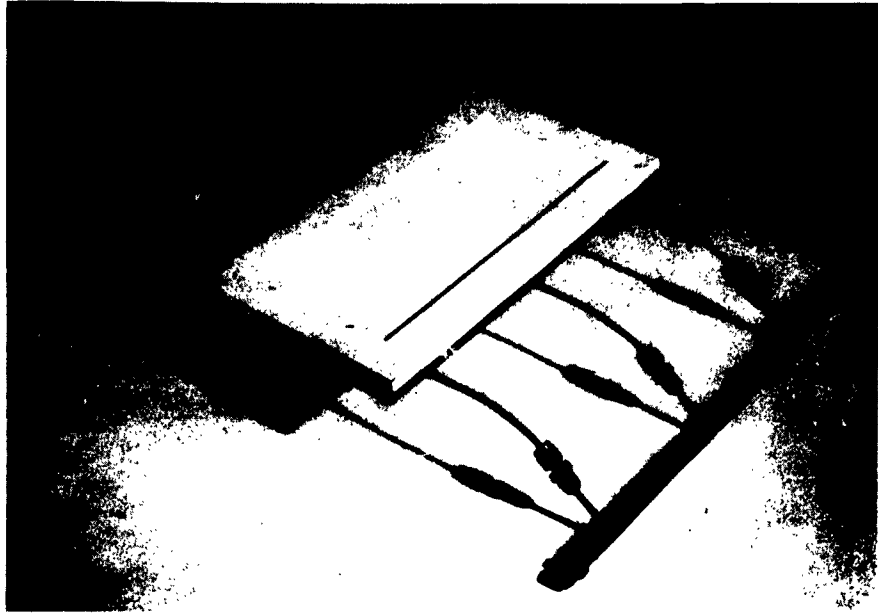


Figure 43. Rectangular Cell with Matrix in Place



Figure 44. Rectangular Cell Outside of Press

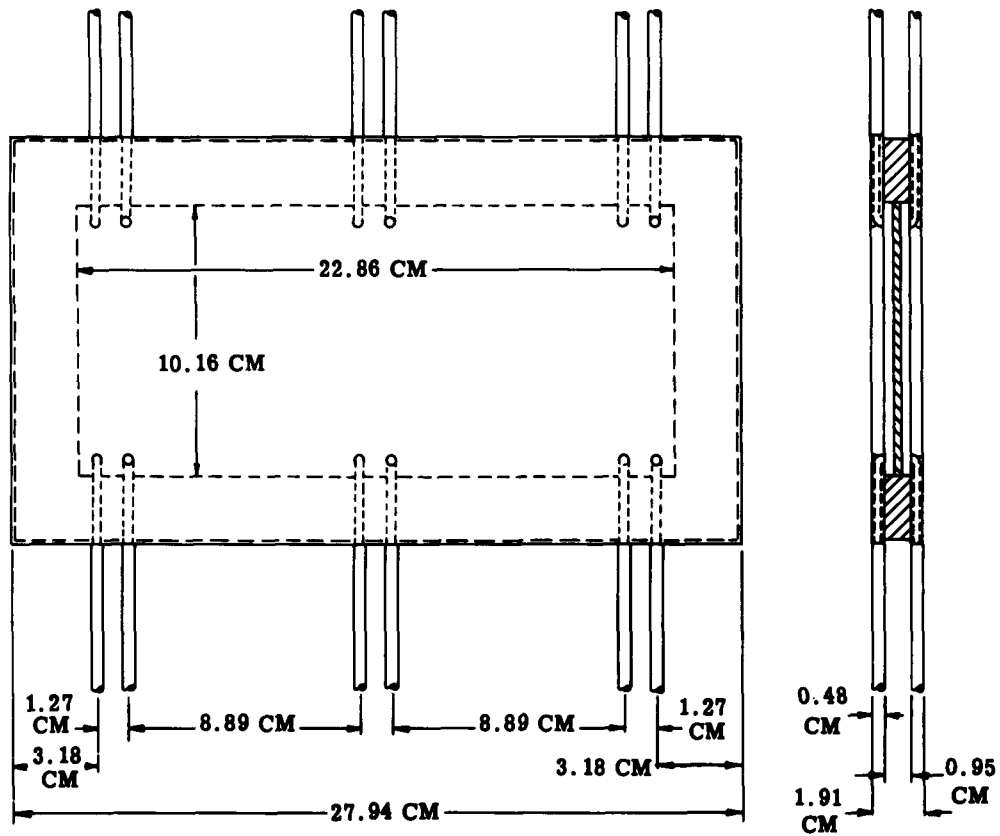


Figure 45. Detail of Rectangular Cell

VI. EXPERIMENTAL RESULTS

Experimental results for the program may be classified into three major categories—conductivities, seals, and cells.

CONDUCTIVITY MEASUREMENTS

Electrolyte conductivity for the basic ternary composition, KOH-KBr-KI, was determined to be $1 \text{ ohm}^{-1} \text{ cm}^{-1}$ at cell operating temperature—573°K. During the course of the program conductivities were studied in several manners. The conductivities or resistivities of operating cells were determined and are reported later in this section. The effective electrode areas of some ceramics were determined by means of their formation factors using an aqueous electrolyte. Then, effective areas were redetermined using the ternary eutectic. Lastly, conductivities were determined for composite matrices utilizing MgO powders of the 6-micron range.

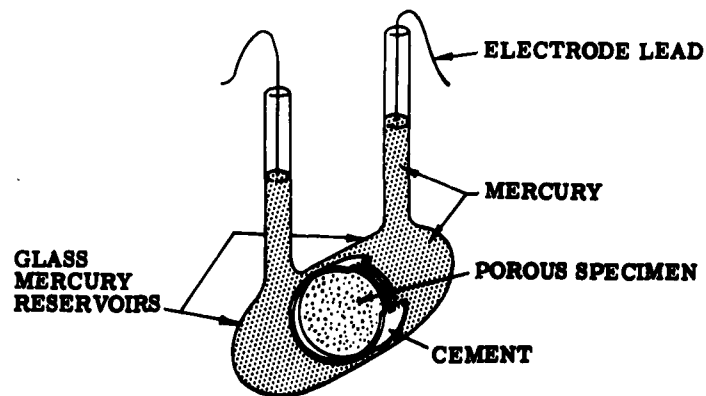
Formation Factor (Effective Electrode Area)

The resistance of the matrix-electrolyte combination is a function of the through pores only—those that are open on both ends. Equation (18), $R_e = \rho (L/A)$, describes the matrix resistance, where A is the area of the matrix. If no matrix were present, A would represent the full electrode area. However, since a matrix is interposed, the true value of A would be the combined area of the through pores that the two liquid metals contact. A means of determining the through pores, representing A , has been worked out in the Allison laboratories. This method involves calculation of the resistance of a cell having a known area and thickness of a normal KCl solution whose conductivity is accurately known. A sample of matrix is then interposed in the cell after having been impregnated under vacuum with the same solution. The resistance is again measured by high frequency a-c methods. Thus, comparing the resistance measured with the known resistance of the pure KCl solution, a ratio may be taken which is called the formation factor.

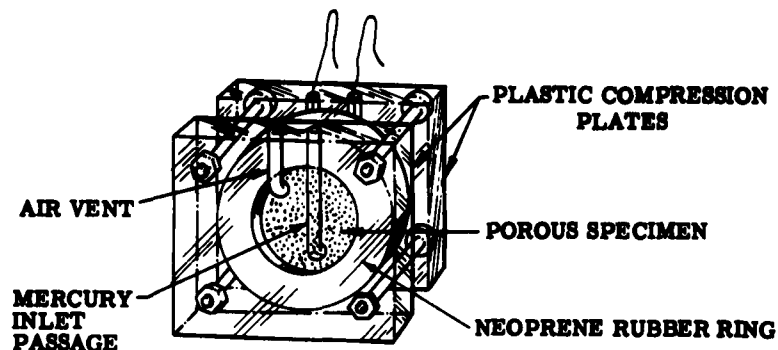
The formation factors for electrolyte matrices were determined with both aqueous solutions and molten ternary electrolyte. Discrepancies which occurred between values determined with aqueous KCl and those observed using molten ternary electrolyte were attributed to insufficient impregnation or retention of the molten electrolyte. The possibility of a reaction between the fused electrolyte and matrix material yielding a higher formation factor than that determined with aqueous KCl was not overlooked. The data obtained in both cases are presented in the following.

Aluminum oxide and magnesium oxide porous matrix specimens were machined to form 0.32-cm thick by 2.22-cm diameter discs and impregnated by a vacuum technique (Section IV) with 0.1 N KCl. The dimensions of the discs were determined and the cell constants calculated for

the individual specimens. Two types of conductivity cells were employed in holding the specimens. Figure 46 shows the two types. The first type consists of two sections of glass cemented around the specimen. The container was first filled with aqueous electrolyte and the specimen vacuum was impregnated. Excess electrolyte was poured off and mercury metal was introduced as electrodes to provide complete specimen contact. The second type of cell consisted of a section of neoprene rubber with a hole cut in the center slightly smaller in diameter than the specimens. The specimens were forced into this hole and then impregnated with aqueous KCl under a vacuum. The rubber section containing the specimen was then clamped, as shown, between two plastic plates. Passages bored in the plastic provided an entrance for mercury and an exit for entrained air. Copper leads placed in the mercury facilitated passing current through the cell. Table XV reveals the values of formation factor obtained.



FORMATION FACTOR CELL—GLASS TYPE



FORMATION FACTOR CELL—PLASTIC TYPE

Figure 46. Aqueous Electrolyte Formation Factor Cells

The formation factors for aluminum oxide materials No. 5186 (24 percent porosity) and LA-831 (45 percent porosity) were calculated from data obtained for the conductivity of the molten ternary electrolyte (60 mole percent KOH, 20 mole percent KBr, and 20 mole percent KI) and from data obtained for the conductivity of the electrolyte matrices of these materials. Table XVI shows a comparison between the formation factors obtained with aqueous KCl and that obtained with the ternary electrolyte.

TABLE XV	
Formation Factors of Various Porous Aluminum Oxides	
<u>Type</u>	<u>(F)</u>
4186	8.85
5139	7.58
5186	10.80
5190	11.30
5213	11.80
LA-830	4.45
LA-831	4.24

TABLE XVI		
Formation Factor Comparison		
<u>Type</u>	<u>Aqueous</u>	<u>KOH-KBr-KI</u>
5186	(F) = 10.8	(F) = 38.0
LA-831	(F) = 4.24	(F) = 9.0

It is believed that degradation of the oxide (Al_2O_3) in varying degrees between the 5186 and the purer LA-831 leads to the differences evidenced between ratios of 5186/LA-831 for aqueous and molten electrolytes.

Electrolyte Matrix Conductivity Measurement

The apparatus shown in Figure 47 is employed in measuring the resistance of consolidated and unconsolidated electrolyte matrices. The consolidated electrolyte matrices tested were 0.32-cm thick, 2.22-cm diameter discs of aluminum oxide impregnated with the 60-20-20 ternary electrolyte. The unconsolidated electrolyte matrices tested were 1.59-cm thick by 1.59-cm diameter pills. The unconsolidated electrolyte matrices or composite electrolyte were 35 percent by weight 70-15-15 ternary electrolyte mixture with six-micron size magnesium oxide powder. The pills are formed by pressing and sintering. This concept was developed by Broers,²⁸ who pressure-formed a rigid matrix using MgO powder in a sodium-lithium-carbonate electrolyte. The unconsolidated electrolyte-matrix has paste-like properties at cell operating temperatures—Broer's work has indicated that conductivities close to those for the pure electrolyte can be obtained. These discs are fabricated in the following manner (all steps are carried out under a dry argon atmosphere except for the cold pressing operation).

1. The required amount of MgO powder is mixed with a concentrated aqueous solution of KOH-KBr-KI in the ratio 70-15-15 mole percent.

2. The mixture is evaporated to near dryness at 393°K.
3. The material is baked at 533°K for 30 minutes.
4. The material is then vacuum dried in a stainless steel container for 16 hours at 623°K.
5. The mass is then cooled and ground to 20-mesh size.

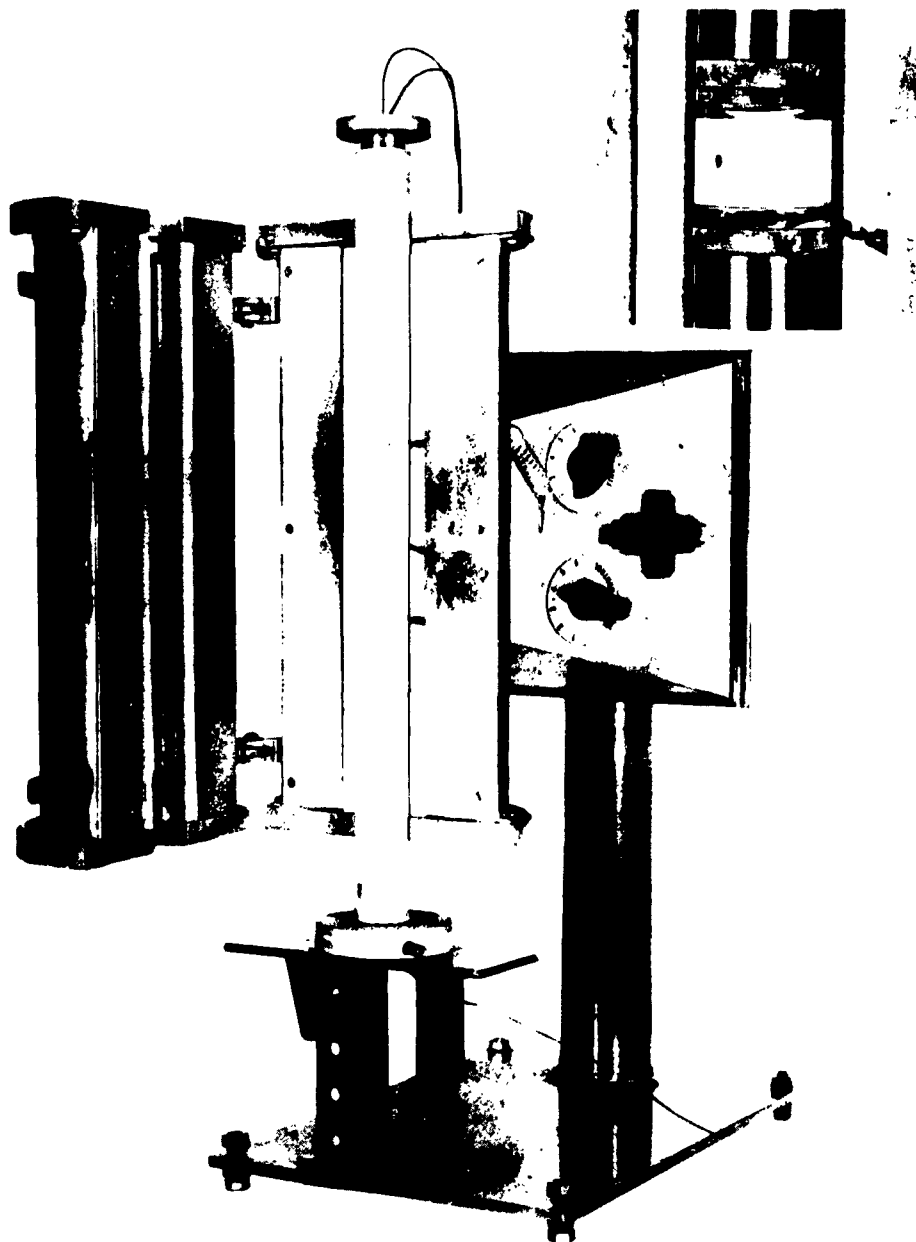


Figure 47. Electrolyte-Matrix Conductivity Apparatus

6. It is sealed in a ceramic ball mill and milled for two to three hours.
7. It is then sent through a 100-mesh screen. At this point the material can be stored in dry, tightly closed bottles.
8. It is then cold pressed to shape in hardened steel dies at 10,000 to 20,000 psi.
9. The material is then final baked in a vacuum at 623°K for two hours.

The result is an electrolyte-matrix disc which is rigid enough to be used in a liquid metal cell. To avoid moisture and carbonate contamination, the finished shapes are stored in tightly closed vessels containing argon until ready for use.

The conductivity apparatus shown in Figure 47 consists of a tube furnace containing two 2.54-cm diameter gold-faced nickel disc electrodes. The electrodes are supported by cylindrical, thin wall steel tubes which are free to slide inside a 2.54-cm ID ceramic combustion tube. The electrode discs butt against ceramic disc inserts, shouldered in steel tubes, which isolate the electrodes electrically from the steel tubes. The electrode leads are heavy copper wire, brazed to the backs of the electrodes, which extend out the top and bottom of the furnace through holes provided in ceramic end caps. The electrolyte matrix temperature is derived from a chromel-alumel thermocouple embedded in the upper electrode. An argon inlet is provided at the bottom of the furnace which permits bottom filling and overflow of argon within the combustion tube.

Prior to placing the matrix specimens in the conductivity apparatus, they are transferred to a glove box under argon where gold leaf is placed on their contact faces. This practice ensures good contact of the specimen with the gold faced electrodes.

A ceramic spacer (shown in Figure 47) is used in the apparatus when testing the composite electrolyte specimens. The spacer, being 1.52-cm high, bears the weight of the upper electrode after initial compression of the 1.59-cm specimen.

The cell constants for the electrolyte specimens were calculated from their dimensions and values for specific conductance versus temperature calculated from resistance measurements. The resulting conductivities for the consolidated matrices were lower than was expected, based upon formation factors determined using aqueous KCl. Insufficient electrolyte impregnation and retention were considered as possible explanations of this result. Also, the possibility of electrolyte segregation and differential freezing were deemed possible explanations. The formation of carbonate layers on the surface because of the presence of CO₂ was considered, but the argon atmosphere rendered this condition unlikely.

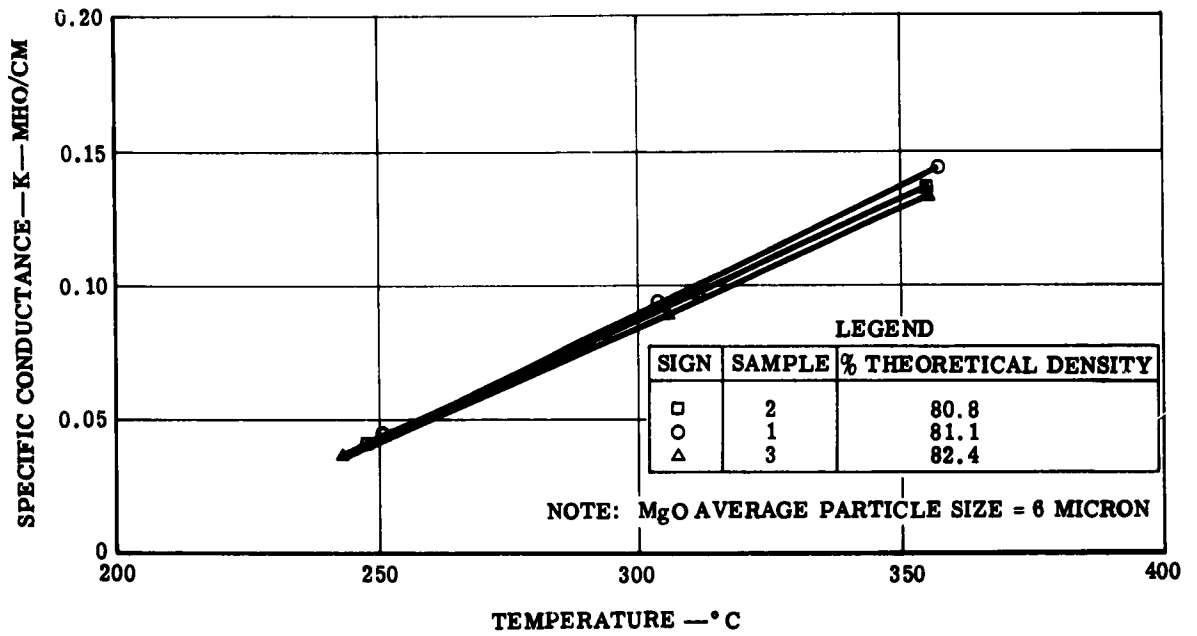


Figure 48. Conductance of 31/69 Percent Composite Matrix

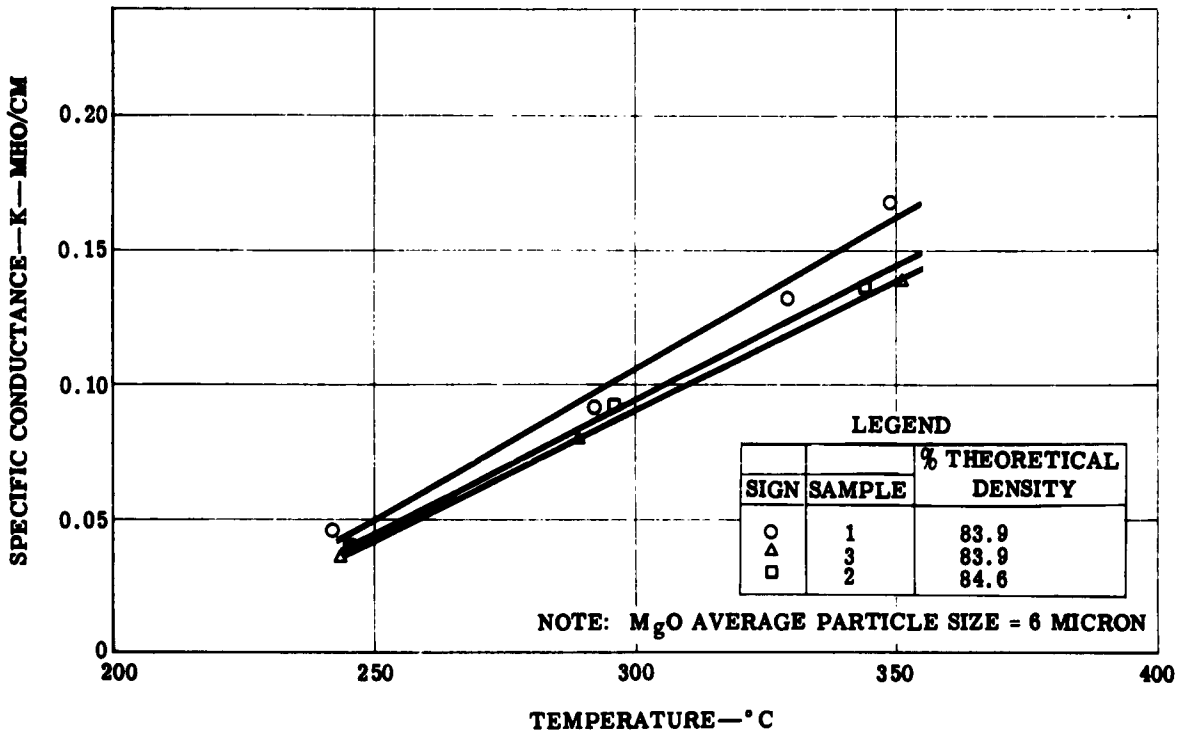


Figure 49. Conductance of 33/67 Percent Composite Matrix

Samples prepared for conductivity measurements contained 31, 33, and 35 percent by weight of the electrolyte and 69, 67, and 65 percent MgO, respectively. Theoretical densities of the mixes varied as shown in Figures 48, 49, 50, and 51. The compressive yield strength of the 33 percent electrolyte-67 percent MgO samples was measured and determined to be 10.6 psi. A comparison of both a-c and d-c methods is indicated in Figure 50.

Work has been completed on specimens made with MgO powders in the six-micron range of particle size. Compressive yield strength measurements for the specimens show a decrease in strength with increasing theoretical density (a function of electrolyte saturation). Theoretical densities obtained in the pressing and sintering operation were controlled to yield values from 80 to 94 percent of theoretical values. It can be concluded from the results shown in Figures 48, 49, 50, and 51 that increasing the theoretical density (i. e., electrolyte saturation) results in higher conductivities. The 93.3 percent theoretical density (35/65 specimen) demonstrated the highest conductivity—0.137 mho/cm at 573°K. This is equivalent to a resistivity of 7.25 ohm-cm.

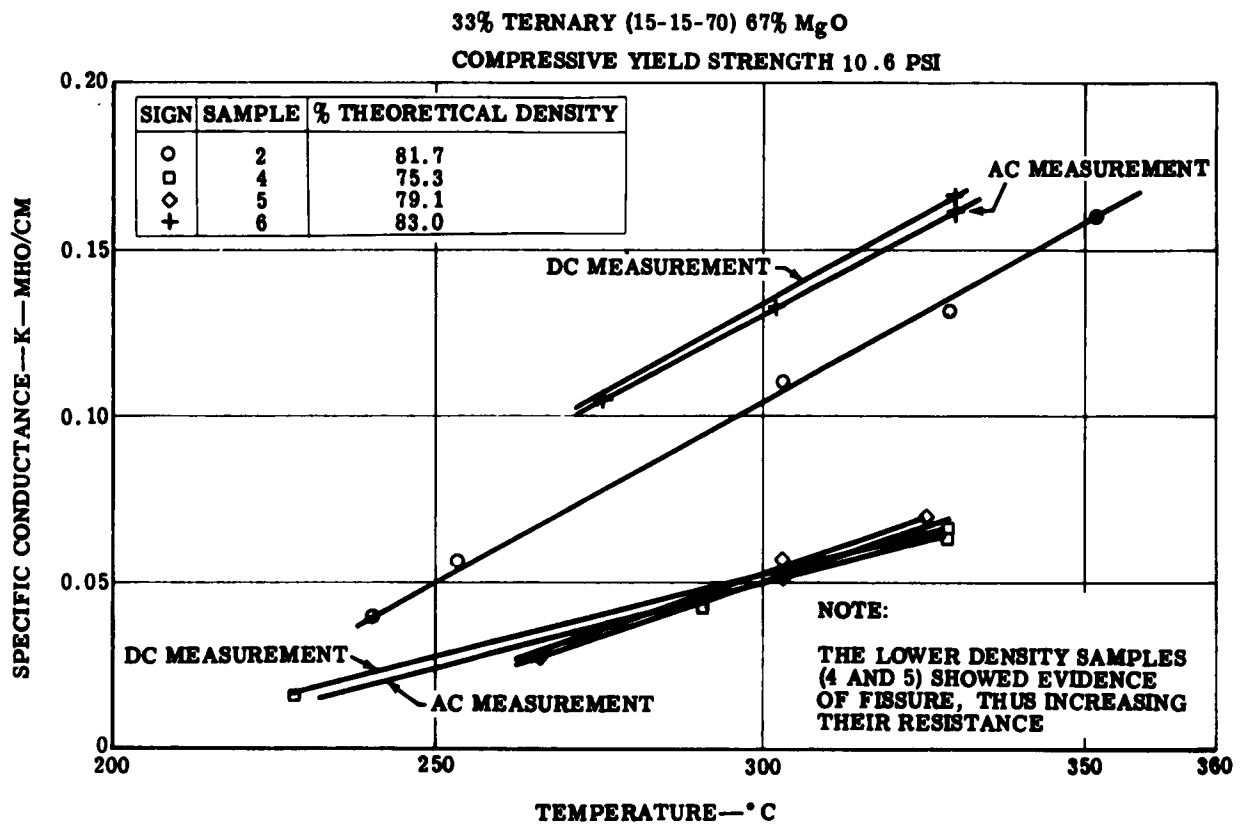


Figure 50. Conductance of 33/67 Percent Composite Matrix

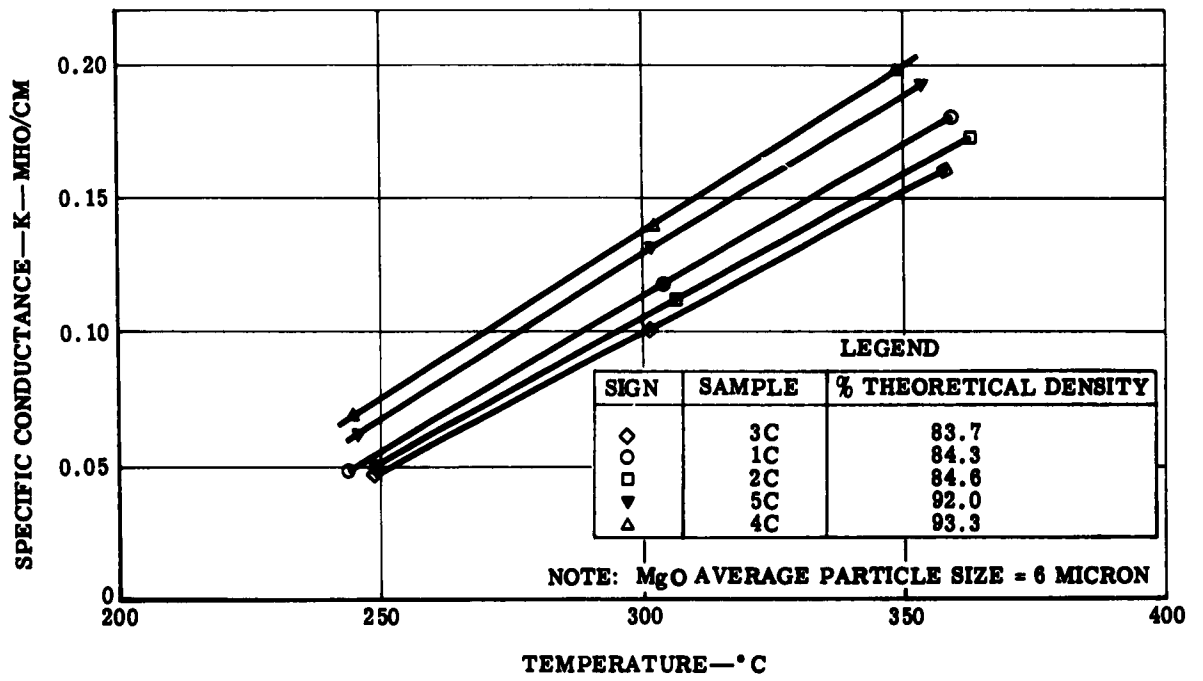


Figure 51. Conductance of 35/65 Percent Composite Matrix

SEAL STUDIES

From the standpoint of design and the end goal of the program—a stack of liquid metal cells, many cells high—a compressive-type seal would appear to be ideal. Resilient materials for gasketing are essentially eliminated because of operating conditions or compatibility problems. Chemical seals—ceramic to metal—are not attractive because they depend on glassy (high silica) phases for bonding—i. e. enamels. Satisfactory, binderless bonds of porous to dense ceramics are presently beyond the state of the art. Therefore, a compressive-type seal (metal-dense ceramic gasket-porous ceramic matrix-metal) would appear to be the straightforward approach.

Considerable work will be necessary to accomplish this goal. Since the properties of ceramics are so dependent on manufacturing procedures (see Section III), it became apparent that the mechanical strengths of the most promising materials needed to be investigated in detail, and that a further detailed investigation of surface finishes necessary to produce a reliable seal needed to be made. In order to develop the techniques required and obtain preliminary planning data with which to start testing seals, the following work was carried out during the program.

1. The compressive strengths of two porous magnesia matrix materials and one magnesia and one alumina dense gasket material were measured. The porous pieces were tested at cell operating temperature (approximately 548°K) both impregnated and unimpregnated. The dense pieces were tested without electrolyte at 548°K.
2. The surface finish and flatness required to effect a seal against a low potassium amalgam were determined.

Compressive Strengths of Selected Ceramics

A view of the laboratory setup for measuring the mechanical properties of the ceramics is shown in Figure 52. In the center is the hydraulic press which, acting through a hardened steel ram, exerts the load on the sample held within the furnace. The furnace contains a nickel-plated pot (with argon feed for inert atmosphere) which has a flexible nickel foil cover, thus allowing the application of force to samples which have been impregnated with electrolyte contained in the pot. A side arm (not shown) on the ram actuates a linear potentiometer to indicate the strain of the sample. At the right of Figure 52 is an x-y recorder which indicated stress-strain relationships. A Blackhawk electric hydraulic pump was used to drive the hydraulic press.

Ceramic samples were $1.9 \times 1.9 \times 0.5$ cm in dimension. The loading ram had an area of 1.265 cm^2 and the hydraulic press had an area of 71.2 cm^2 . Thus, the sample stress was 56.3 times the pressure output of the hydraulic pump. Unimpregnated samples were brought to temperature, positioned on a hardened steel block, and loaded to the yield point. Impregnated samples were impregnated according to standard vacuum techniques (Section IV), held



Figure 52. Seal Testing Equipment

under the electrolyte in the closed inerted pot for 16 hours, and then tested while still in the inert atmosphere. Results are shown in Tables XVII through XX.

TABLE XVII			
Measured Compressive Strengths of Morganite Porous Magnesia*			
Unimpregnated		Impregnated	
<u>Sample No.</u>	<u>Stress</u> <u>(kg/cm²)</u>	<u>Sample No.</u>	<u>Stress</u> <u>(kg/cm²)</u>
5	426	25	323
6	473	26	512
7	493	27	583
11	473	28	670
12	434	29	434
Average	460		504

*Morganite is an extremely high purity magnesia of 44% apparent porosity

The variation within the impregnated samples runs somewhat higher than that within the unimpregnated samples due to the greater difficulty of manipulation and placing of samples inside the covered pot. There is no significant difference between the wet and dry strengths as measured.

TABLE XVIII			
Measured Compressive Strengths of LM-833 Porous Magnesia			
Unimpregnated		Impregnated	
<u>Sample No.</u>	<u>Stress (kg/cm²)</u>	<u>Sample No.</u>	<u>Stress (kg/cm²)</u>
8	1537	30	Poorly loaded
9	1450	31	1300
10	1439	32	1281
13	1320	33	1419
14	<u>1340</u>	34	<u>985</u>
Average	1417		1246

Again, there is no significant difference between wet and dry strengths, which speaks well of magnesia as a possible matrix material.

TABLE XIX	
Measured Compressive Strengths of M-208 Impervious Alumina	
<u>Sample No.</u>	<u>Stress (kg/cm²)</u>
15	6345
16	5045
17	4887
21	4335
22	<u>4847</u>
Average	5092

TABLE XX	
Measured Compressive Strengths of A-402 Impervious Alumina	
<u>Sample No.</u>	<u>Stress (kg/cm²)</u>
20	12,808 (cracked)
23	14,424 (cracked)
24	<u>15,685 (cracked)</u>
Average	14,306

The A-402 material did not fail by compression but, rather, by cracking—probably induced by bending of the steel supporting block at these extremely high loads.

These determinations proved the testing procedures to be satisfactory for the purpose of determining a maximum stress which could be safely applied in sealing a liquid metal cell.

Seal Experiment

As mentioned earlier, the anticipated compression seal consists of the interfaces metal-dense ceramic gasket-porous ceramic matrix-metal. The porous ceramic-metal interface should be the most difficult seal to attain because the porous nature of the matrix material in itself would show a high surface roughness. Accordingly, an LA-830 disc (determined to be similar in properties to the LM-833) was ground parallel and smooth and then hand finished to the smoothest surface possible by this method. Profilometer measurement indicated that this surface was equivalent to 1000 RMS. Two steel replicas of upper cell halves (Figure 28) of 10.0-cm OD × 8.26-cm ID were hand lapped to an RMS finish of 8. Total loading area was determined (with allowance for radii) to be 22.6 cm². Reference to Table XVIII indicates that 1050 kg/cm² would be a reasonable loading stress for purposes of the sealing test.

The apparatus was assembled inside the furnace shown in Figure 52 and brought to cell operating temperature. A load of 1050 kg/cm² was applied to the matrix and the cell halves were loaded with a 3 mole percent potassium amalgam. A static head of 100 mm Hg (including inert gas cover) was applied and the cell was allowed to stand for 50 hours. A leveling device was used to determine that no drop in level of amalgam within the standpipes occurred, which indicated that there was no leakage from the cell. A buzzer circuit was applied to the cell halves which would indicate the occurrence of an internal crack by establishing electrical continuity. A visual check was made at 15-minute intervals to determine whether any leakage occurred. A seal was maintained for the 50-hour period. The required specifications for surface finishes can now be established.

RESULTS OF CELL WORK

A summary of cell assembly test results is presented in Table XXI. This represents data from all the cells which were built as a part of this program. In some cases where performance existed at several levels, typical data for each level are shown.

The cells are listed in chronological order and some brief review of the program is appropriate. Work started with the circular cell with an alumina matrix. It was hoped that state of the manufacturing art might make possible the use of the rectangular cell, but attempts at manufacture of a framed piece proved inadequate, though progress was made. When it became apparent that the resistance of the electrolyte impregnated alumina trended upward, single cup cells were run to confirm this phenomenon and eliminate design of the circular cell as a possi-

TABLE XXI
Single Cell Performance

Run No.	Type of Cell	Date	Details	Life (hr)	Load (hr)	Electrode Area (cm ²)	Electrolyte-Matrix Thickness (cm)	EMF, V _o (volt)	Cell Voltage, V _c (volt)	Current (amp)	Current Density (ma/cm ²)	Current Density at Max Power (ma/cm ²)	Power Density (watt/cm ²)	Power Density Extrapolated to Max Power (watt/cm ²)	Internal Resistance (ohm)	Resistivity (ohm-cm)	Reason for Stopping Test
1	C	2/82	Floating Matrix-No. 5186 Alumina	24	0.5	46	0.31	1.10	--	--	--	--	--	--	--	--	Attack on insulation, resulting in internal short and leak
2	C	2/82	No. 5186 Alumina	48	0	46	0.48	1.20	--	--	--	--	--	--	--	--	Tube block, causing seal leak
3	C	2/82	No. 5186 Alumina	120	3	46	0.64	1.50	--	Minimal	--	--	--	--	--	--	High resistance
4	C	3/82	No. 5186 Alumina	--	--	--	--	--	0.52	3.0	65	70	0.0338	0.0343	0.153	47	Bad seal, high resistance
5	SC-ST	3/82	RA-139	--	--	28	~0.15	--	--	--	--	--	--	--	--	--	Overfill and short
6	SC-ST	3/82	RA-139	--	--	28	~0.15	0.4-0.8	--	--	--	--	--	--	--	--	Internal short
7	SC-ST	3/82	RA-139	4	Int	26	~0.15	1.05	0.70	3.4	1.30	194	0.0915	0.1028	0.103	18	Internal short
8	SC-ST	3/82	RA-139	4	Int	26	~0.15	1.19	0.60	2.2	85	95	0.0508	0.0508	0.268	46	Internal short
9	SC-ST	3/82	RA-139	1	Int	16	~0.15	1.04	0.82	1.4	88	207	0.0719	0.1076	0.157	17	Cracked cup
10	SC-ST	3/82	RA-139	72	24	33.5	~0.15	1.15	0.49	2.05	87	76	0.0425	0.0437	0.322	50	Cracked cup
11	DD-ST	4/82	12-min discharge 3-min OC 12-min charge 3-min OC	545	Cycling	11.5	1.5	0.83	0.48	1.0	87	104	0.0420	0.0437	0.350	2.7	Experiment complete
12	C	4/82	LA-830	96	2.5	46	0.15	1.49	0.64	2.6	56	49	0.0360	0.0368	0.327	100	Cracked matrix
13	C	4/82	LA-830	1	0.1	46	0.24	0.52	0.42	0.6	13	34	0.0054	0.0088	0.167	32	Seal failure
14	SC-ST	5/82	RA-139 (60% K)	360	Cycling	20.4	~0.15	0.80	0.56	3.1	150	199	0.0840	0.0895	0.110	15	Cracked matrix
15	DC	5/82	(60% K) LA-831 discs sintered to impervious tubes	550	Cycling	1.26	--	0.99	0.77	0.035	28	57	0.0214	0.0256	0.286	*	Change in electrical resistance
16	DC	6/82	(60% K) RA-139 cups	360	Cycling	25.6	~0.15	1.04	0.06	0.368	24	28	0.0144	0.0145	2.563	*	Experiment complete
17	DD-ST	6/82	35-min discharge 4-min OC	430	Cycling	45	0.635	1.00	0.80	4.0	89	222	0.0710	0.1110	0.050	3.5	Cell joined
18	SC-FT	7/82	RA-139 "M"	--	--	--	--	0.71	0.25	10.2	237	175	0.0570	0.0610	0.045	3.2	Resistance increase
19	SC-FT	7/82	RA-139 "M"	24	8	28	~0.15	0.91	0.35	2.0	71	58	0.0249	0.0263	0.280	52	Internal short
20	DD-FT	9/82	"M"	24	8	26	~0.30	1.05	0.54	2.0	77	78	0.0415	0.0408	0.260	34	Restricted vent upset cell
21	DD-FT	9/82	"M"	24	2.5	81	0.64	1.035	0.97	2.5	31	247	0.0299	0.1264	0.026	3.3	Mixing of reactants upon attempt to change Hg collection pot
22	DD-FT	10/82	"M"	48	25.0	81	0.25	0.53	0.40	7.0	86	181	0.0345	0.0481	0.018	5.8	Mixing of reactants upon attempt to change Hg collection pot
				72	5.5	81	0.125	--	0.53	8.6	109	--	0.0576	--	--	--	

Abbreviations

- Int—Intermittent
- C—Circular
- SC-ST—Single Cup, Static Type
- DD-ST—Differential Density, Static Type
- DC—Double Cup
- SC-FT—Single Cup, Flow Type
- DD-FT—Differential Density, Flow Type
- OC—Open Circuit

*Not determined due to uncertainty of path length

ble fault. Double cup cells were run to eliminate intramatrix shorts and ensure electrolyte saturation of the matrix cups. By this time the problem areas were understood and determined to be in the area of matrix materials, and development of a matrix-type cell was set aside until these materials problems could be resolved. The differential density cell then served to continue the investigation of the electrochemical characteristics of the system while eliminating the problems of matrix perturbation.

Detailed Comments on Cell Runs

Cells 1, 2, and 3

Three circular cells were assembled and tested at an operating temperature of 598°K to determine the voltage stability of the cell design. Instability would indicate leakage between cell halves or possible reactions taking place as was indicated under the discussion of the electrolyte and amalgams. The first cell tested was of the floating matrix type. The cell was heated and charged, and during its early hours of operation there were no indications of instability. Using a 90 percent (mole) potassium amalgam versus pure mercury, the cell developed an emf of 1.1 volts, but after several hours of operation, a self-discharging mode was indicated in which the cell voltage started to fall off gradually. Upon standing over night, the emf had dropped to 0.2 volt. Flushing the lower chamber with fresh mercury and recharging the upper compartment with fresh amalgam restored the open circuit voltage to approximately 0.6 volt. Within a short time thereafter, the cell leaked and completely shorted. Examination of the cell indicated that the flame-sprayed alumina (which had been used at that time for insulation) had been grossly attacked by the electrolyte, exposing the underlying metal and allowing the matrix more than the specified 0.01-cm movement. This condition was corrected with a gasket of the A-402 impervious alumina with proved durability in molten electrolytes.

The other two cells assembled were used to test the compression-type seal using matrices of 0.48 cm and 0.64 cm. In these cases the external seal was on the matrix with no contact between the cell rims. Cell 2, when loaded with a 90 percent (mole) potassium amalgam, established a stable emf of 1.2 volts but failed on the second day when an exit tube clogged and the seal was breached. Cell 3, with a 0.64-cm matrix resulted in low power output. Voltage stability was good, but the cell indicated a high initial internal resistance.

The resistance of the 0.64-cm cell, initially 3.1 ohms, later increased to the 30-ohm range, and still later dropped to 12 ohms. Just before failure, the resistance again increased to the 30-ohm range. A cell using a No. 5186 matrix of these dimensions (assuming an effective electrode area of 8-10 percent) should yield a matrix resistance of about 0.14 ohms, plus contact or other internal resistances. When disassembled and examined, the cell matrix showed areas through the cross section that were filled with a gray, metallic appearing material (Figure 53). Microscopic examination indicated that this gray material consisted of potassium-mercury amalgam. The maximum power output of the cell was 0.03 watt.

Cell 4

Cell 4, of the new matrix configuration, was then assembled using the No. 5186 material. This matrix had a thickness of 0.48 cm around the rim, but the thickness of the area separating the electrode compartments was 0.15 cm. This cell was put into operation immediately after the installation of the vacuum impregnated matrix. With an open circuit voltage of 0.98 volt, 3 amperes were delivered for a short time at a cell voltage of 0.52 volt for a power output of nearly 1.6 watts using a 90 percent (mole) potassium amalgam versus pure mercury. These conditions yielded almost maximum power density. The seal was breached at this point and, by the time the cell press was tightened down to eliminate the leak, a tenfold change in cell resistance from the initial 0.153 ohm took place. The cell continued to operate at low power densities for the next four days. On the fifth day, a higher power output of approximately 0.35 watt was obtained, and on the sixth day the cell shorted out. Disassembly of the cell and examination of the matrix again showed potassium-mercury amalgam permeating the cross section of the matrix. The calculated matrix resistance for a cell of this type should be 0.03 ohm. As indicated previously, the cell resistance (matrix resistance plus any contact resistance or IR drops from cell to the voltage take-off leads) was calculated as 0.153 ohm during the early stages of operation, 1.5 ohms during the middle stages, and 1.2 ohms just before failure.

Cells 15 and 16

Figure 54 is a plot of voltage vs time for the double cup cell containing RA-139 type ceramic (silica binder). The cycle consisted of 12 minutes discharge, three minutes open circuit, 12 minutes charge, followed by three minutes of open circuit. Changes in open circuit voltage within any given half-cycle corresponded to calculated coulombic changes in electrode composition. After 65 hours of cycling, however, a change (gradual decrease) in open circuit voltage indicated somewhat less than 100 percent coulombic efficiency. This may or may not be partially due to polarization effects, but part of the loss must be due to the noncoulombic transfer of potassium due to its partial solubility in the electrolyte.



Figure 53. Shorted Matrix

Figure 55 is a voltage-current plot for the same double cup cell showing curves for two different open circuit values. Average resistance was about 0.9 ohm—a high value due to the longer cell path involved in the two cells used in this configuration. Straightness of the lines, however, indicates a lack of polarization at these current densities. RA-139 cups were used for these cells in spite of the silica binders because of the unavailability of LA materials in the cup configuration.

During operation of the double cup cell—sintered discs and 60 percent-20 percent-20 percent (mole) KOH-KBr-KI electrolyte—a situation occurred where cell resistance would increase sharply. Raising the cell temperature brought resistance down again. This phenomenon occurred in either the charge or discharge half-cycle. It was determined that a freezing of electrolyte between the electrodes caused this increase, as shown in Figure 56. This phenomenon was not noticed again after switching to a 70 percent-15 percent-15 percent electrolyte.

An electrolyte-resistant gold electrode was inserted in the double cup cell to act as a reference electrode—polarization and resistance were measured using high speed a-c methods. A photograph from the oscilloscope screen is shown in Figure 57. The distance between horizontal lines is a measure of the IR_e drop across the cell and corresponds perfectly with that reported in Table XXI. The slight slope of the line indicates a small polarization.

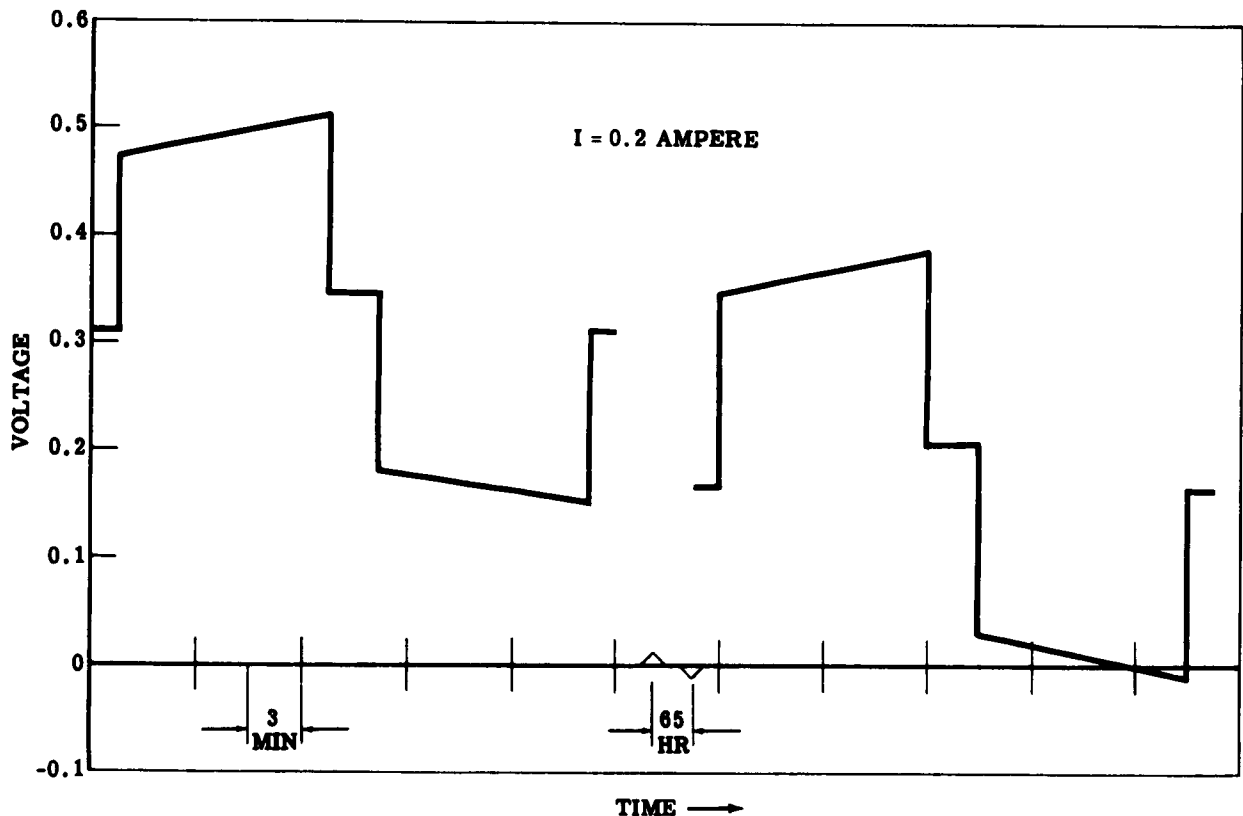


Figure 54. Voltage-Time Curve for Double Cup Cell

An example of the value of this type of cell is shown in Figure 58, which is a potential diagram taken of the double cup, sintered disc cell before the freeze-up occurred. At the left, an open circuit gold-potassium potential of 1.91 volts was read while, at the right, the open circuit gold-mercury potential was 0.92 volt for a net V_O of 0.99 volt.

Under load, the Au-K and Au-Hg potentials are again measured and the changes attributed to the voltage drop across the two electrolyte interfaces. These voltage drops are added (algebraically) to the gold-potassium potential to give a new reference voltage at the Hg electrode. When the gold-Hg potential is added at this level, the difference shown on the diagram as V_c results. This is the cell terminal voltage. The difference $V_O - V_c$ is equal to the sum of the two electrode voltage drops by construction. The separate electrode resistances may be determined in a manner similar to that for the total internal resistance by dividing the two voltage drops by the cell current. For this case the cell is symmetrical with the resistances computed, or $R_K = 3.4$ ohms and $R_{Hg} = 3.3$ ohms.

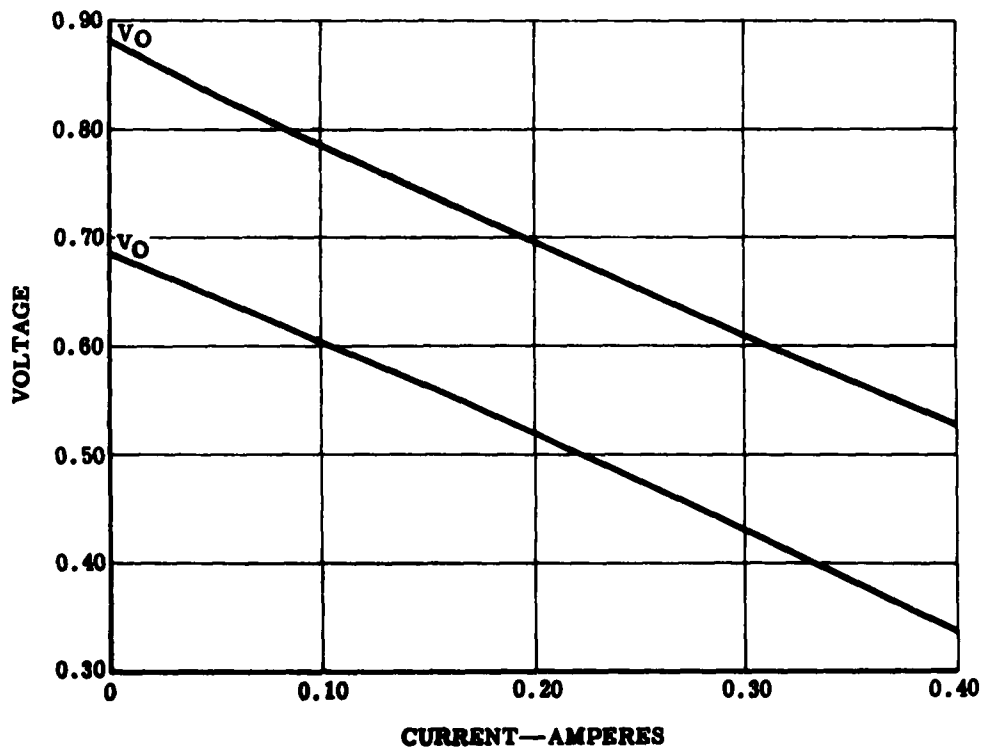


Figure 55. Voltage-Current Curve for Double Cup Cell



Figure 56. Freezing of Electrolyte in Double Cup Cell

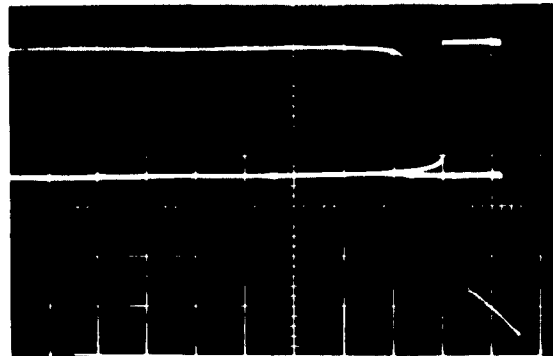


Figure 57. Resistance Measurement with Cathode Ray Oscilloscope

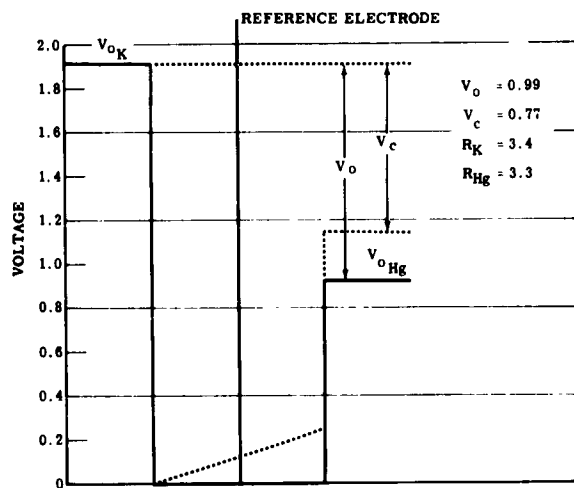


Figure 58. Single Electrode Measurements in Double Cup Cell with Sintered Discs

Figure 59 is a similar plot made shortly before freezing occurred. Here, the drop across the potassium electrode was nearly double ($R_K = 8.4$ ohms) the drop across the mercury electrode ($R_{Hg} = 4.5$ ohms). In this case the dotted line shows a break at the gold electrode reference position on the diagram. The sum of the voltage drops is again equal to the cell internal voltage drop, but the difference in slope is indicative of the difference in resistance. This difference was shown to be caused by electrode freezing at the potassium side. It is hoped to expand the studies made with this cell configuration so that fundamental data may be obtained.

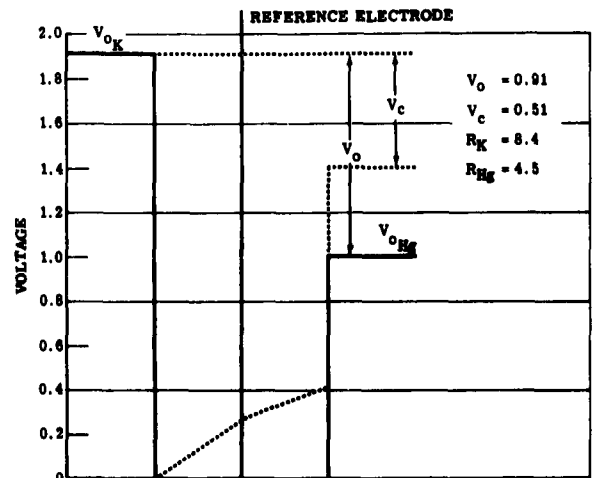


Figure 59. Single Electrode Measurements in Double Cup Cell with Sintered Discs

Cell 11

Figure 60 is a voltage-time plot for the differential density cell (Cell 11). The half-cycle again was a 12-minute, three-minute interval. Again, a slight inefficiency was observed over a five-cycle period with the open circuit voltage falling from 0.84 to 0.83 volt.

Figure 61 is a plot of the voltage-current characteristics of (differential density) Cell 11. At the lower current density, again, no indication of polarization was seen.

Cell 17

Figure 62 is a voltage-time curve for Cell 17, a differential density cell. In this case, current densities were higher and some polarization was seen in the recovery to open circuit after discharge. The slow climb back to open circuit values indicates what may be a concentration polarization in the Hg layer. Recovery after charge was normal. It should be noted, too, that this cell had a longer period for each cycle.

Cell 18

To show the regenerative capability of the potassium-mercury liquid metal cell system, the single cup cell shown in Figure 40 was run in the laboratory with periodic additions of potassium to the inside of the cup and mercury flowing through the cell. Mercury flow was metered by use of a chemical buret. Open circuit voltage was used to measure the potassium concentration in the mercury—cell voltage demonstrated the operational and regenerative characteristics of the cell.

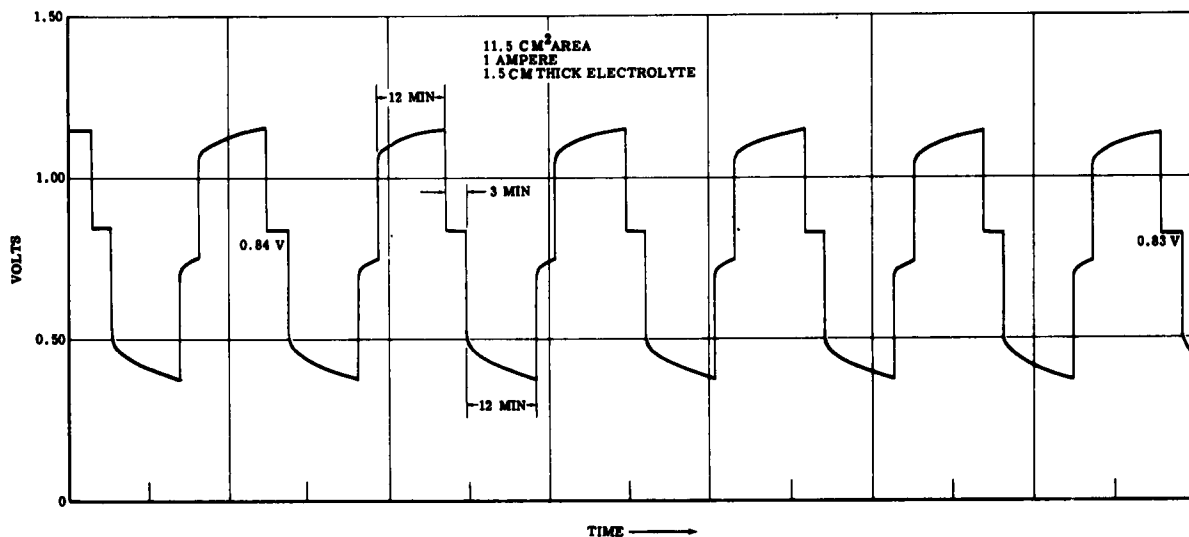


Figure 60. Voltage-Time Curve for (Differential Density) Cell 11

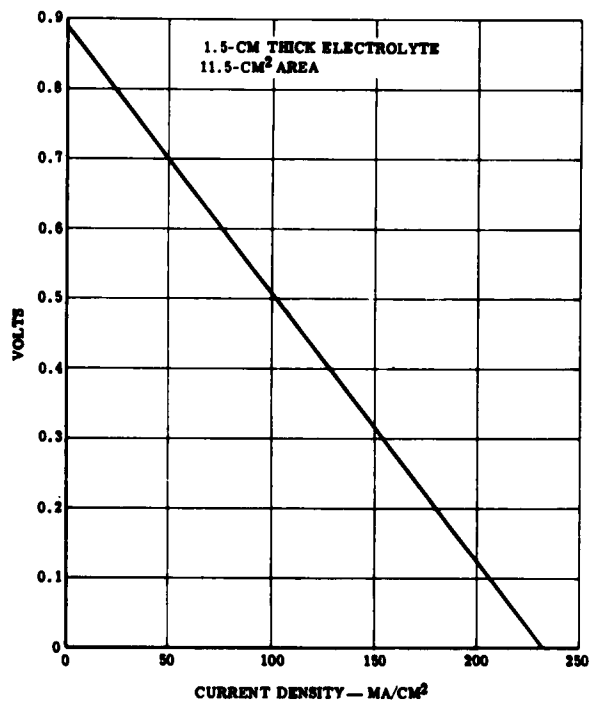


Figure 61. Voltage-Current Curve for (Differential Density) Cell 11

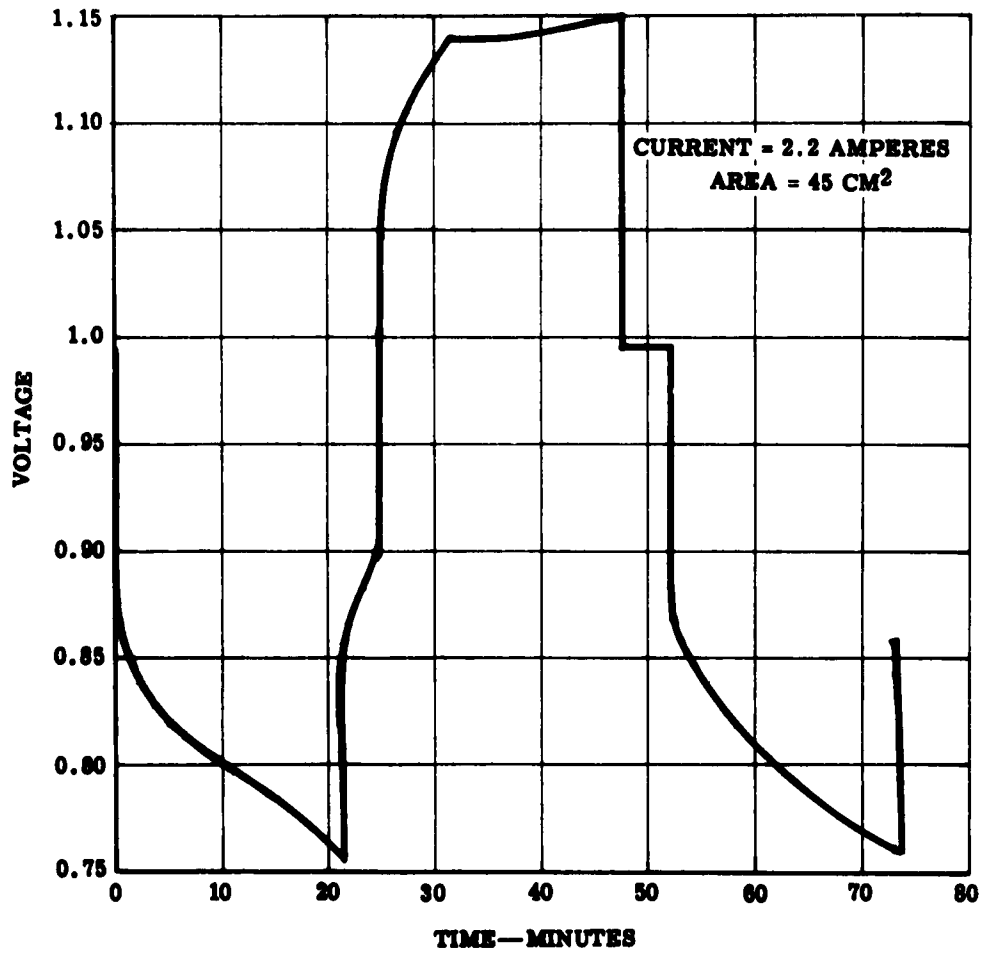


Figure 62. Voltage-Time Curve for (Differential Density) Cell 17

The experiment showed that a matrix-type liquid metal cell could be regenerated on the cathode side. Throughout various phases of the test, the cell emf was changed by discharge and regeneration from 1.165 volts to 0.78 volts and back to 1.065 volts. During one 27-minute period, the cell was held at a constant emf of 0.91 volt. An equivalent static cell running under the same load would have ended with an emf of 0.38 volt, corresponding to a potassium mole fraction of 0.22.

Proof of the regenerative principle can be shown by two methods. First, it should be demonstrated that the cell emf can be recovered by adding fresh mercury to the cathode after the cell has been degraded using a long-term electrical load. Second, it should be demonstrated that there is a mercury flow which will support the cell at near-constant electrical performance.

In the configuration used for this test (Figure 40), the mercury storage volume was reduced by decreasing the diameter of the steel tubing around the cup matrix. A constant level weir held the cathode metal-electrolyte area constant. The mercury supply was introduced at the bottom-center to give a maximum flush of the amalgam from the matrix surface. The less dense amalgam was washed to the top and dumped to a lower level container.

The dimensions for the cell were:

- Inside diameter of large cylinder—7.0 cm
- Inside diameter of small cylinder—3.6 cm
- Weir-controlled Hg level—approximately 0.32 cm (variable with liquid meniscus during buildup prior to dumping)
- Submerged depth of extraction thimble—3.2 cm
- Bottom clearance of extraction thimble—0.32 cm
- Matrix cup—RA-139 alumina extraction thimble—2.54-cm OD, 1.5-mm wall, and 6.98-cm length

Mercury flow was controlled manually by a 50-cm³ buret located above the cell cathode metal level. The mercury supply flowed to the high temperature regions of the cell and was heated prior to entry. The mass flow value was computed from a volumetric-time reading at atmospheric conditions.

Potassium storage was not adequate to support this device for high coulombic loads. Therefore, potassium was loaded at intervals determined by the theoretical consumption based on the integration of current in ampere-minutes.

No provision was made to analyze the cell products—i. e., the amalgam dumped to the lower reservoir. This value may be estimated from flow data.

A pure resistance electrical load was used to ensure that the true cell performance was matched to the regenerative flow rate. Any degradation of cell performance due to a change in internal resistance would be reflected as a lowering of current and terminal voltage for a constant external load resistance. This condition can be explained in terms of a static or nonregenerative cell and the effect eliminated from the analysis of the regenerative performance.

To describe the configuration further, the following computations are given:

- The inside cup volume was measured to the 6.35-cm point using mercury. This volume was found to be 20.2 cm³; therefore, the maximum potassium load was

$$M_{K_i} = (20.2)(0.78) = 15.8 \text{ gm}$$

- The outside annular volume was broken down into three layers—that below the cup, that surrounding the cup, and that in the upper overflow region. This was done for convenience in later analysis work. The total volume was the sum of these three, respectively.

$$\begin{aligned} \text{Vol Hg} &= \text{Vol}_1 + \text{Vol}_2 + \text{Vol}_3 \\ &= 3.27 + 13.2 + 10.6 \\ &= 27.1 \text{ cm}^3 \end{aligned}$$

The cell was loaded and the temperature raised to the operating condition. The initial cell emf was 2.05 volts, which is typical of this type of cell. This value was reduced to 1.14 volts by 9.4 amp-min electrical load and later regenerated to 1.17 volts by the flow of 46.9 gm of mercury. The cell was left on open circuit for the night, and was found to be at 1.165 volts the next morning.

Prior to the regenerative tests, the cell was given a discharge load of 108 amp-min. The first attempt to supply mercury became the trial test on the control of the equipment, and therefore, mercury flow was not steady in the early running. Later control was adequate to demonstrate the regenerative principle.

The raw data taken during the test were:

1. Open circuit voltage — V_o
2. Cell terminal voltage— V_c
3. Cell potential— V_o^* —taken at the instant of open circuit switching to establish a true internal resistance without polarization effects

4. Current— I —read from an ammeter just prior to open circuit switching
5. Current duration time— Δt_I —taken from the time recordings
6. Volume of mercury supply— $\Delta \text{Vol}_{\text{Hg}}$ —measured by a buret
7. Time increment for mercury supply
8. Reference temperature— T_K —taken at the potassium pool

It was proposed to obtain parameters for comparison to demonstrate that the test equipment was regenerated to a degree satisfactory for future systems requirements. Therefore, a theoretical regenerative flow value was developed as a goal for actual flow requirements.

The following simple model was used to obtain a theoretical flow value. A pool of mercury at equilibrium has a potassium concentration, x , to be maintained at a constant value by a mercury supply, $\left(\frac{dM}{dt}\right)_{\text{Hg}}$. It is assumed that the fresh mercury is well distributed into the pool and that the amalgam which is dumped has a potassium concentration equal to that of the pool. For a given flow of potassium into this pool (proportional to the current), there is an ideal flow of mercury which will cause equilibrium. This is:

$$\left(\frac{dM}{dt}\right)_{\text{Hg}} = (200.6) (60) \frac{I}{nF} \left(\frac{1}{x} - 1\right)$$

where

$$\frac{I}{nF} = \left(\frac{dM_K}{dt}\right)_{\text{ion}}, \text{ which is the ionic flow of potassium through the electrolyte and}$$

$$\left(\frac{1}{x} - 1\right) = \text{gm Hg per gm-ion of K per minute.}$$

The flow is converted to mass units per minute by the use of the atomic weight of Hg, which is 200.6, and a time conversion of 60 sec/min. This parameter will reflect the requirement to attain equilibrium at a given time during the run even though equilibrium may not have been established at that time. It merely shows the flow requirement as a function of the current and the concentration at a given time. The actual mercury flow was obtained by the incremental ratio of the mercury supply and the time increment to give the values of $\left(\frac{\Delta M}{\Delta t}\right)_{\text{Hg}}$.

Another comparison, which was made to show extended life of the cell as a result of regeneration, was that of the actual concentration, x_{act} , to an equivalent static cell concentration, x_s . The actual concentration was obtained by readout from the curve of emf vs concentration, Figure 63. The equivalent static cell concentration was obtained as described in the following paragraphs.

Assume that the cell configuration is such that an increase in volume of the amalgam due to the potassium ion flow is not relieved by an instantaneous efflux but is retained in the pool. Then the concentration will be based on an accumulation of potassium in a constant quantity of Hg. This is computed by

$$x_s = \frac{\Sigma \Delta M_K}{\Sigma \Delta M_K + M_{Hg}}$$

where M_K and M_{Hg} are the molar quantities of potassium and mercury, respectively.

The quantity of mercury for this cell was found from the initial value based on volume as

$$M_{Hg} = \frac{Vol_{Hg} d_{Hg}}{200.6} = \frac{(27.1)(12.8)}{200.6}$$

$$= 1.73 \text{ gm-atom}$$

The sum of the potassium transfer was given by

$$\Sigma \Delta M_K = \frac{\Sigma(I \Delta t_I)}{nF}$$

$$= 6.22(10)^{-4} \Sigma(I \Delta t_I)$$

where $\Sigma(I \Delta t_I)$ is given in ampere-minutes and M_K in gm-atoms.

An important parameter used to follow the condition of the cell was that of the internal resistance, R_e . This value was computed from

$$R_e = \frac{V_{\delta}^* - V_c}{I}$$

The total mercury supply was also tabulated. Although no provision was made to analyze the product in the amalgam tank, it is of interest to note the average concentration for the duration of the test was determined to be 0.0447 mole fraction potassium.

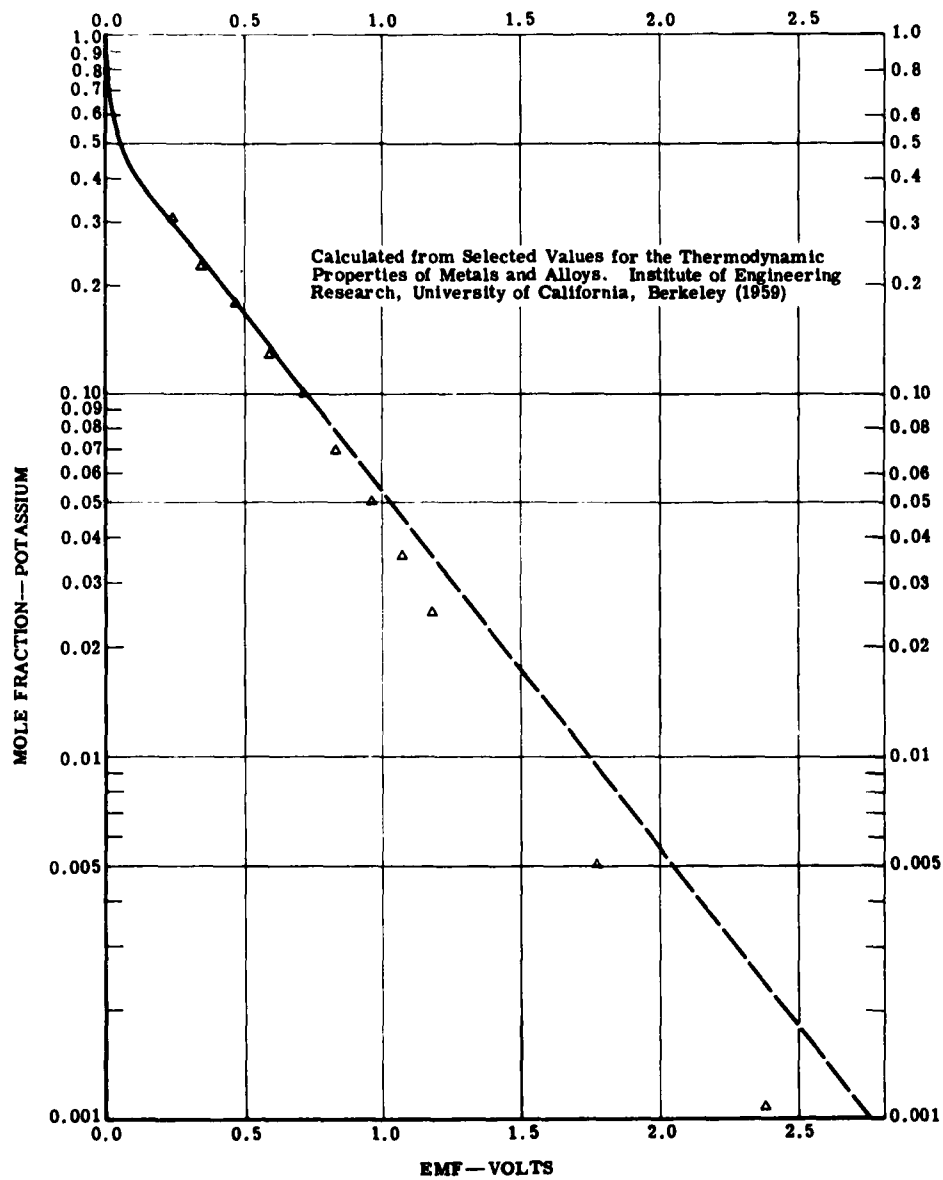


Figure 63. EMF vs Concentration of K and Hg

Cell power, W , and voltage ratio, η_c , were tabulated to show relative performance of the cell. It was noted that the cell was run beyond the maximum power point ($\eta_c = 0.5$) to gain high current, which was of primary importance in the regenerative run. These two parameters have not been plotted in graphical form.

Two plots of the various parameters with time have been made. Figure 64 was developed to show the comparison between actual mercury flow and ideal mercury flow. Cell potential and current were plotted for immediate reference, since ideal flow is a function of each.

Figure 65 is a plot of the cell performance parameters—voltages, current, internal resistance, and concentration. The theoretical static cell concentration was plotted for comparison purposes.

Figure 65 is a plot of the actual mercury flow, $\left(\frac{\Delta M}{\Delta t}\right)_{\text{Hg}}$, an ideal flow, $\left(\frac{dM}{dt}\right)_{\text{Hg}}$, and the two parameters—cell potential and current—which make up the ideal flow value. Two discontinuities appear in the curves where the cell was opened to introduce potassium. The curve of the actual flow was plotted in the increment form, $\frac{\Delta M}{\Delta t}$, for the time period measured. This represented a true average flow, although the observed characteristic of the metering valve was that of a decreasing flow after each adjustment to a new flow value.

A short period is shown as an estimated process (dashed lines) during the unattended time. Current- and voltage-dependent parameters were computed for an average value during this period.

Recovery of the cell potential by mercury supply was begun after 95 minutes. The regenerative supply flow was, in general, greater than the theoretical requirement. This caused an increase in cell potential during the period up to 155 minutes. The slope of the theoretical flow curve, $\frac{dM}{dt}$, became nearly zero as the actual flow approached the same value at 110 min., 125 min, and 140 min.

Another regenerative run was accomplished between 210 and 257 min after a 31-min discharge. An immediate change in the slope of cell potential resulted from the first mercury supply at 210 min, and an absolute recovery began at 216 min as the Hg flow was increased to a value greater than the ideal flow. A constant flow was maintained for 27 min after the 230-min point. It will be noted that the ideal value was higher than this flow while the cell potential remained nearly constant. The change in the ideal flow for this period was directly related to the decreasing current.

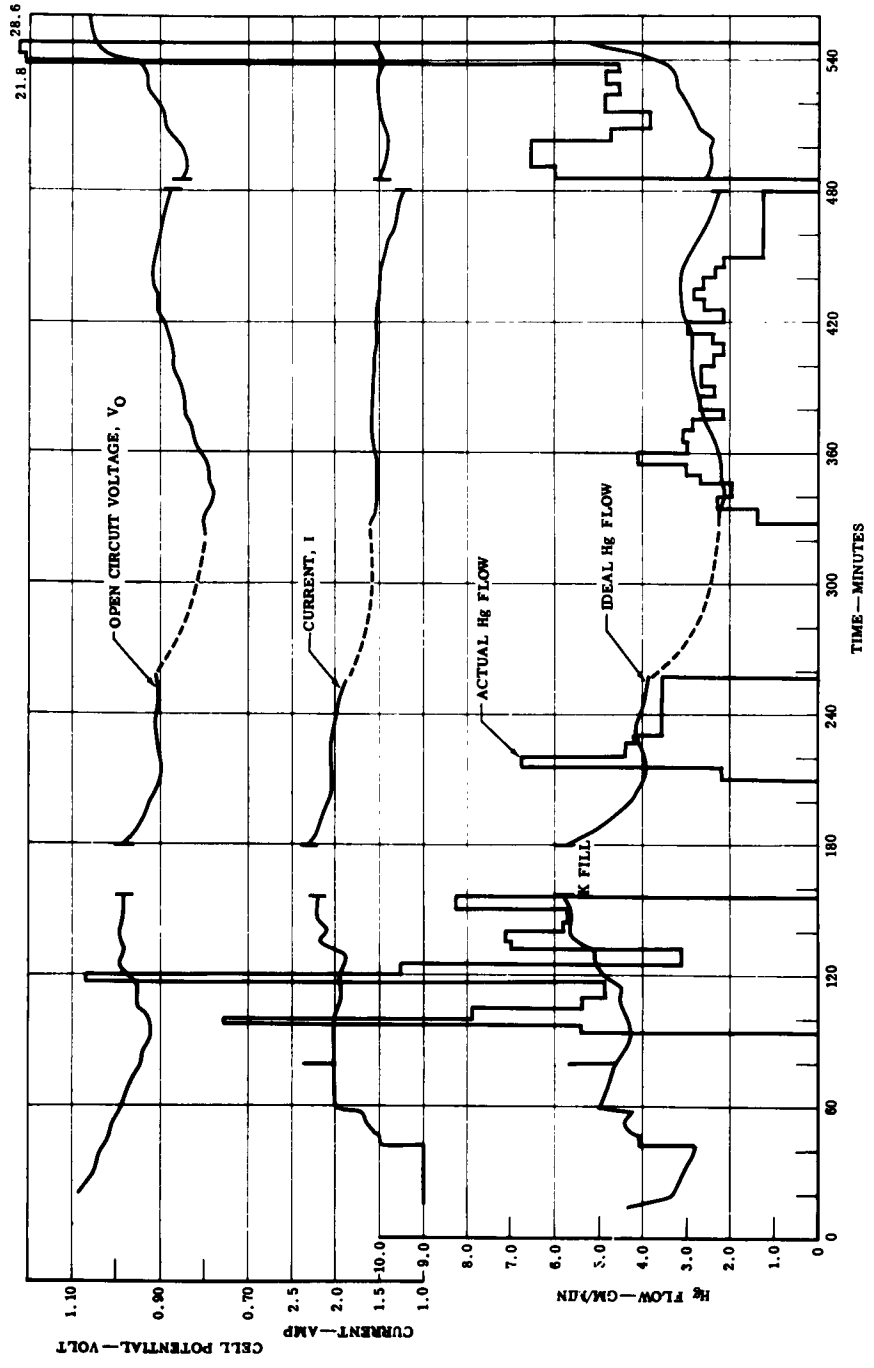


Figure 64. Operating Characteristics of Flowing Single Cup Cell (18)

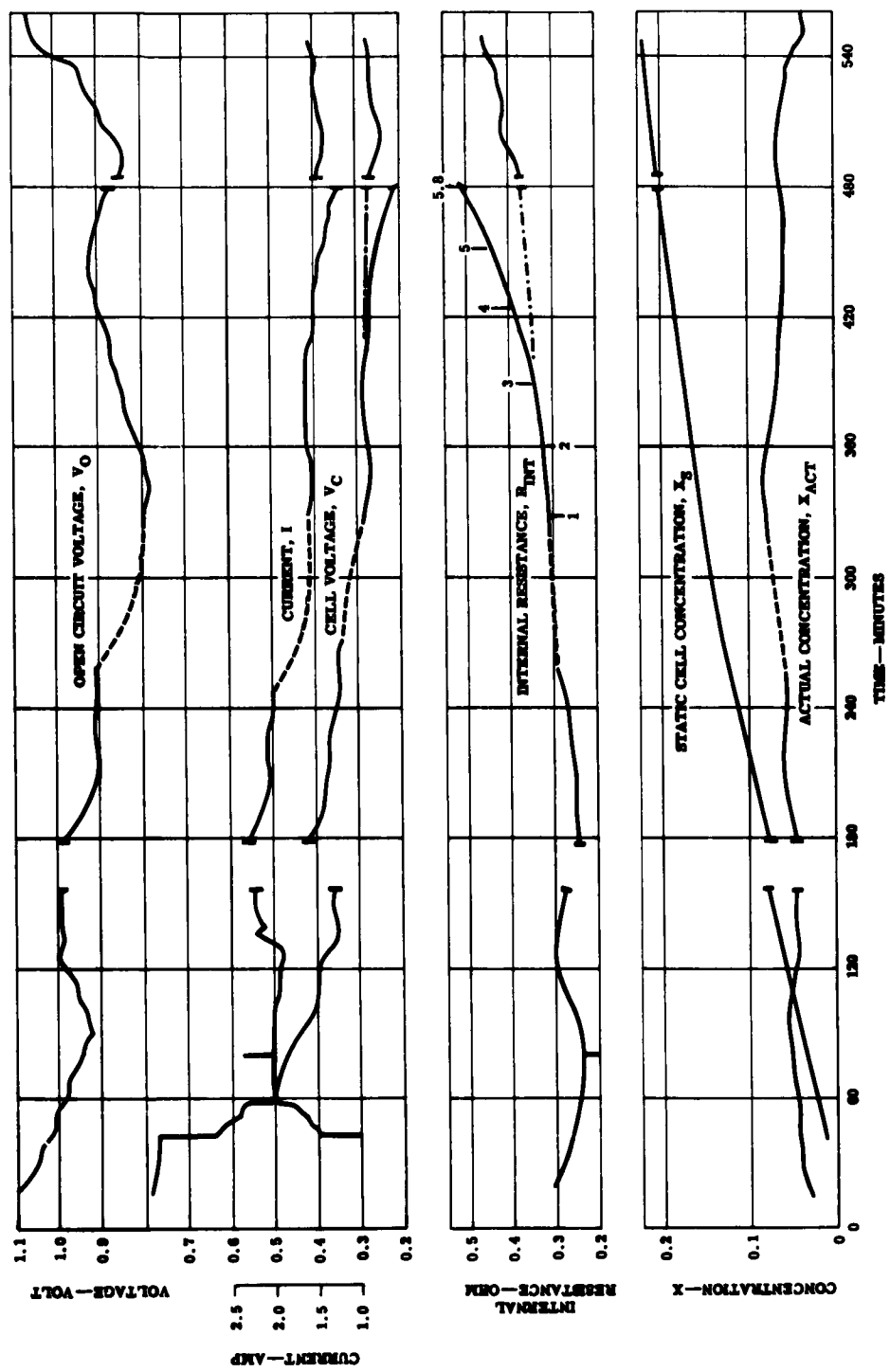


Figure 65. Operating Characteristics of Flowing Single Cup Cell (18)

During the period 328 min to 480 min, an attempt was made to adjust flow for the maintenance of constant cell performance. Two factors limited this phase of the experiment. First, the flow regulation valve became difficult to adjust. Second, the cell internal resistance started to increase at a greater rate. A flow rate lower than the ideal was required to maintain equilibrium, and that the cell potential was increased during this time.

The last period of the test, just prior to shutdown, was used to determine the maximum recovery of cell potential that could be obtained after an 8-hr operation. The first 53 min were devoted to a moderate recovery flow rate which gave an increase in the cell potential from 0.855 to 0.935 volt. During the last 9 min, a very high flushing flow was used. A final recovered reading was taken to show that the open circuit voltage was recovered to 1.065. This is shown in Figure 64 by a rise to a limit after the 547-min point where the flow was shut off.

The estimated cell concentration, x_g , when operating as a static cell configuration, is shown in Figure 65.

These values, when compared with the actual concentration, x_{act} , show that cell performance would be greatly degraded without the use of regeneration.

Some question was raised by the early comparison where x_g was lower than x_{act} . This may be explained, in part, by the following argument. It was questionable as to how much of the total mercury pool could be used in the computation. The upper layer (10.6 cm³) was likened to a flow path and may not enter into the reactions near the electrolyte interface. Also, early potassium flow into the pool would cause a change in volume which would remove mercury from the cell before diffusion could cause ideal pool mixing. Therefore, the actual concentration, x_{act} , value would be increased by the reduced mercury inventory within the pool. Suffice it to say that the comparison was conservative over the later times of the run and certainly showed that the cell was supported by regeneration.

Although regeneration by a resupply of the liquid metals was entirely reflected in the cell potential, some expectation of increased performance was justified. In this case, the cell voltage and current dropped off during the run and was recovered only slightly with the large increase in cell potential near the end of the test. Reference to the change in internal resistance should clarify the phenomenon.

The internal resistance in Figure 65 increases steadily throughout the test. This was expected, since data derived from many static tests of the alumina extraction thimble matrix showed the same characteristic.

A lack of sufficient potassium supply caused a high resistance to occur during this test between the 400-min and 480-min points. This was best seen by the sudden drop in internal resistance

after a fresh load of potassium was introduced. A check of the estimated potassium consumption versus the accumulated potassium load showed that the cell became starved of potassium prior to the last load. That is, the amount loaded was 19.1 gm while that consumed was 17.1 gm, or a net of two grams in the cell.

Since the inside volume adjacent to the mercury was 10.1 cm^3 , the amount of potassium retained in the cup should be 7.8 gm. The curve of internal resistance, Figure 65, has been labeled with the number of grams of deficiency—i. e., the difference between the required 7.8 gm and the estimated inventory.

The effect on internal resistance became noticeable after a 3-gm deficiency. This was experienced in previous cells. The mercury contact area was apparently the governing factor in cell performance, while the potassium wetted the matrix wall above the actual level and continued to function.

The loss of potassium-wetted area caused an internal resistance change to 0.522 ohm at 480 min with a deficiency of 5.8 gm, or an estimated inventory of 2 gm as stated previously. A connecting linear curve was constructed to show the probable resistance and voltage, had this deficiency been averted.

It is concluded from this experiment that:

1. The cathode metal of a liquid metal cell may be regenerated to support cell performance.
2. Flow control and matrix material must be improved to obtain good long-term performance.
3. The vertical flow configuration of this cell offers advantages in that the less dense amalgam is easily carried away from the cell.

Cell 19

This cell was a single cup cell of the flowing type similar to Cell 18. The one difference was in the cup used for the matrix. Cell 18 used an alumina cup and exhibited a steep increase in internal resistance. Cell 19 used a porous magnesia cup (Magnesia M, Table X) and showed no change in internal resistance over the life span of the cell. Corresponding data are plotted in Figures 66 and 67.

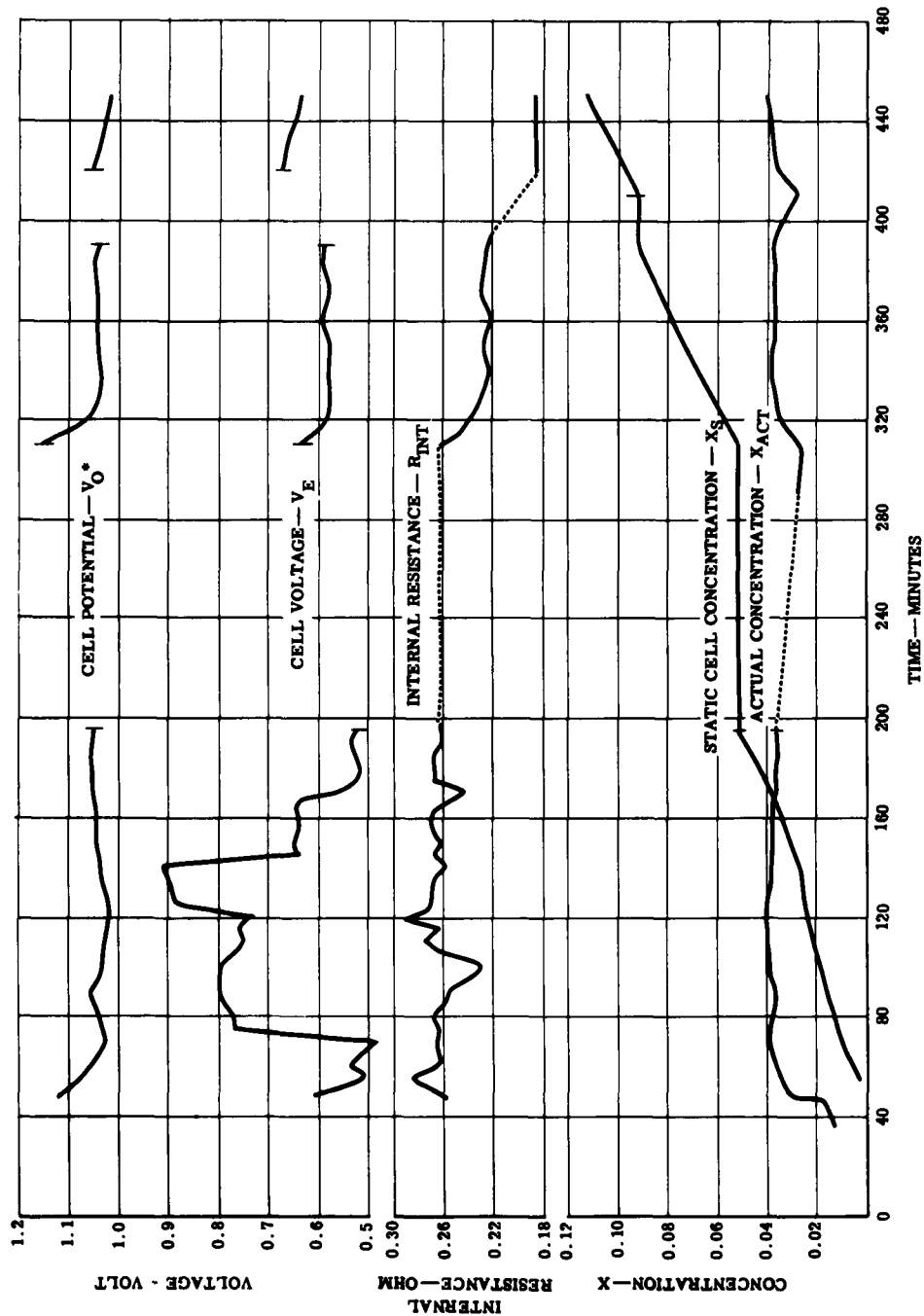


Figure 66. Operating Characteristics of Flowing Single Cup Cell-MgO Matrix (19)

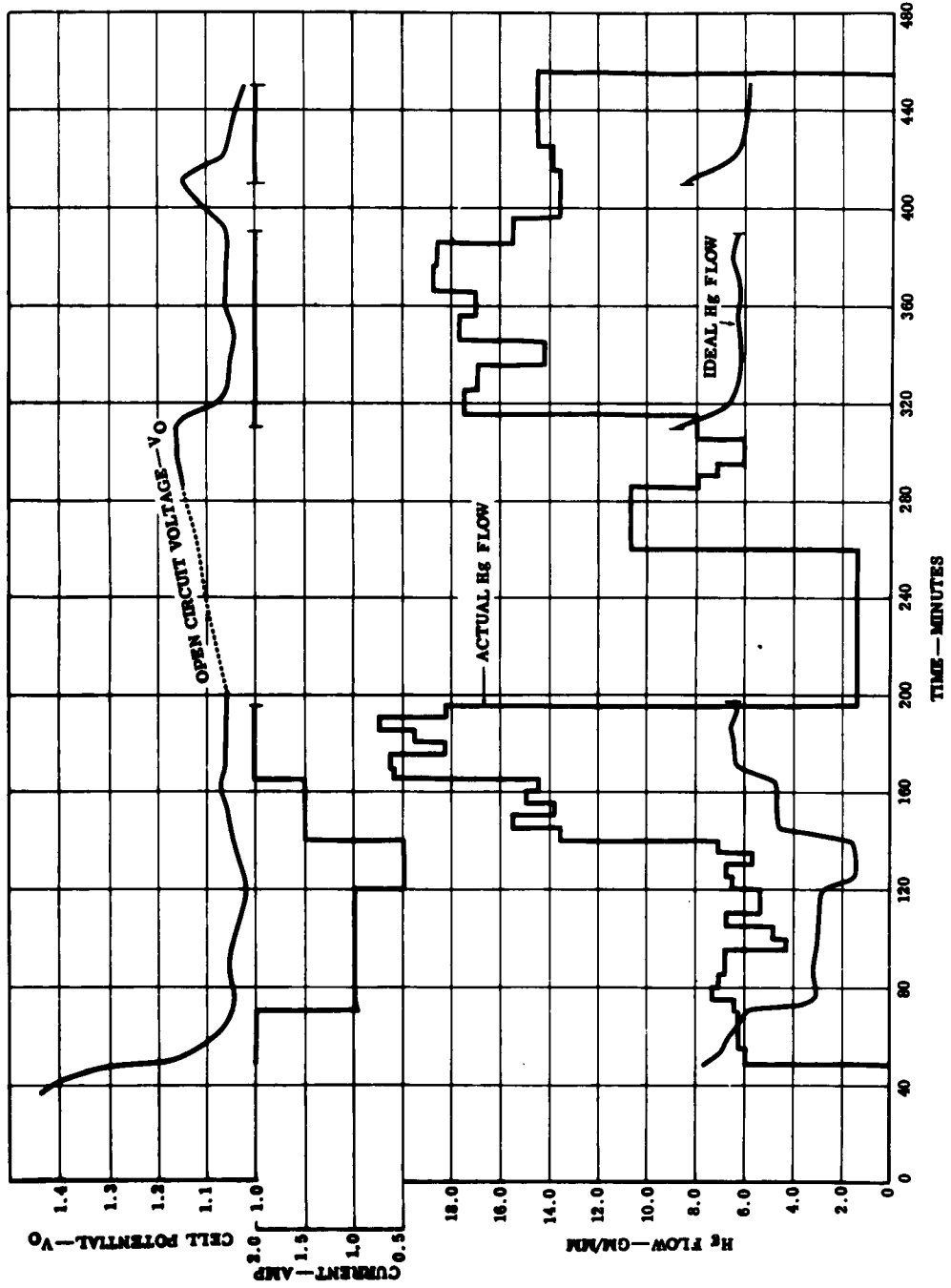


Figure 67. Operating Characteristics of Flowing Single Cup Cell-MgO Matrix (19)

Cell 21

A schematic of the flowing differential density cell is shown in Figure 42. Figure 68 is a view of the cell as set up in the laboratory. Figure 69 is a plot of the operating characteristics of the flowing-type differential density cell. The cell was operational for 25 hr, during which time various attempts were made to support the cell at high electrical performance with mercury flow. Cell performance was maintained at a power density greater than 50 w/ft^2 for an accumulated time of 65 min. Steady-state operation appeared to be established near 7 amp and 0.4 volt—for a power density of 32 w/ft^2 for 10 hr. Power operation at values greater than 20 w/ft^2 was accomplished for a period of 17 hr and 51 min.

Poor flow distribution within the cell caused the inability to hold the cell potential at the design emf of 0.8 volt. A flow of $1 \text{ cm}^3/\text{min}$ of mercury for 2.5 hr did bring the cell potential back to 0.77 volt during the latter part of the test. Subsequent cell performance (at 23 hr and 18 min of test time) was 9.7 amp and 0.58 volt, which is a power density of 64.6 w/ft^2 . The performance dropped to 20 w/ft^2 after 1.5 hr of operation.

Cell 22

A differential density cell of the same configuration as Cell 21 was run with one major change—the flow characteristics were improved to some extent by the insertion of a mercury heat tank in the mercury flow line. It was believed that the introduction of cold mercury into the previous cell was a partial cause of the poor hydrodynamic flow. It was felt that the introduction of hot mercury prevented the cell cool-down caused by higher mercury flow rates and improved potassium diffusion inside the mercury electrode. In addition, the large mercury heating tank served as a surge tank which allowed the mercury to pulse occasionally as effluent amalgam poured over the weir. This cell was operated for nearly six hours at power densities above 50 watts/ft^2 and cell voltages above 0.5 volt. Voltage and current traces were very steady and are summarized in Table XXII.

At the start of the test the internal resistance of the cell had dropped to 0.014 ohm, which corresponds to an apparent electrolyte thickness of 0.32 cm. Figure 70 shows the cell prior to operation.

Although the mercury flow was held at around $4 \text{ cm}^3/\text{min}$, this flow had no effect on cell operation until high flows were caused by a dump over the weir. Within a one-minute period after a dump, the performance of the cell would recover from the values near 50 watts/ft^2 up to values as high as 60 watts/ft^2 . This cyclic performance showed a period of about 15 minutes. Operation continued for a period of nearly six hours before cell failure. Failure was caused by a sudden surge of pressure in the cell during an amalgam transfer manipulation. The amalgam transfer was being attempted in order that more storage room would be available for continued operation of the cell.

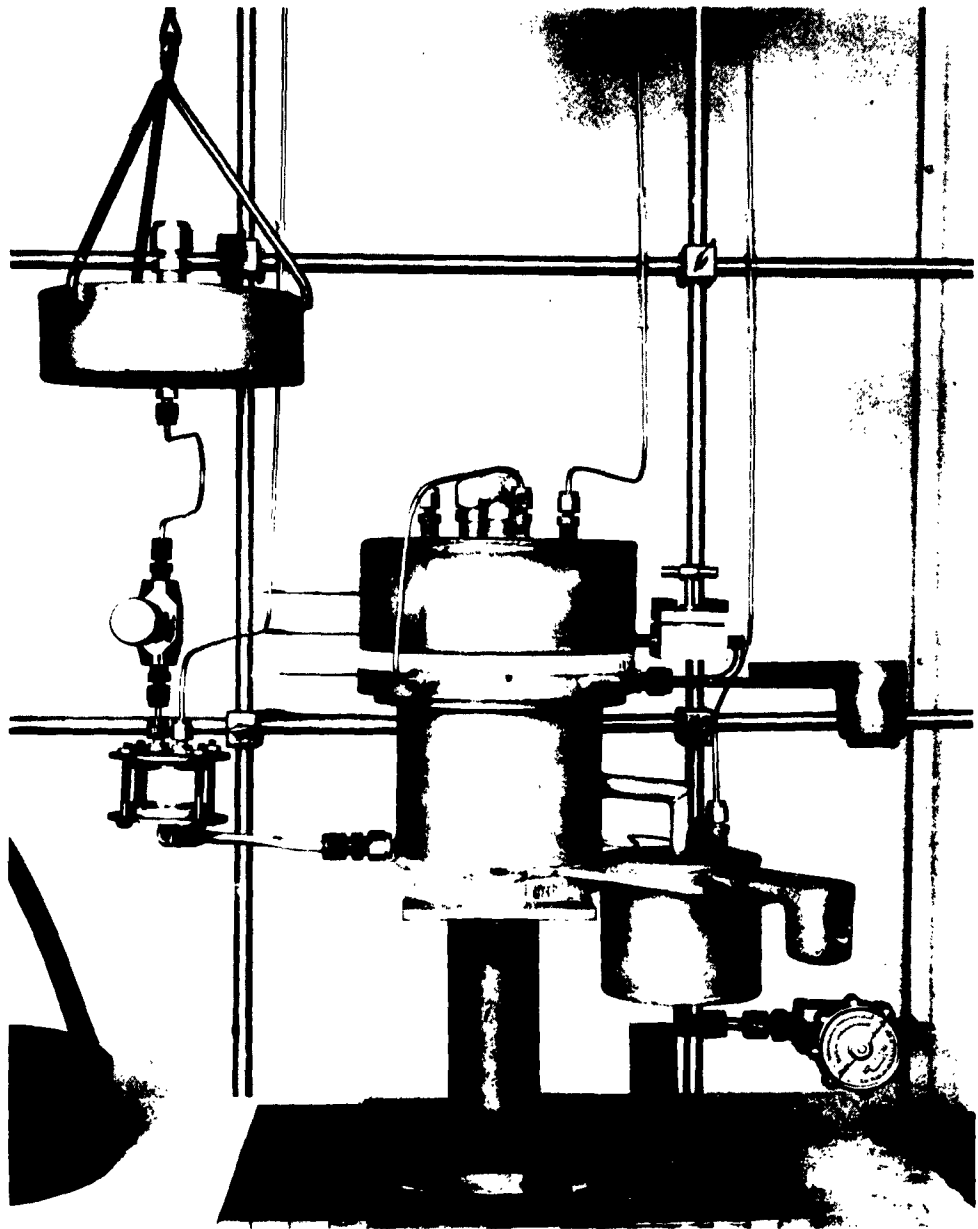


Figure 68. Flowing Differential Density Cell

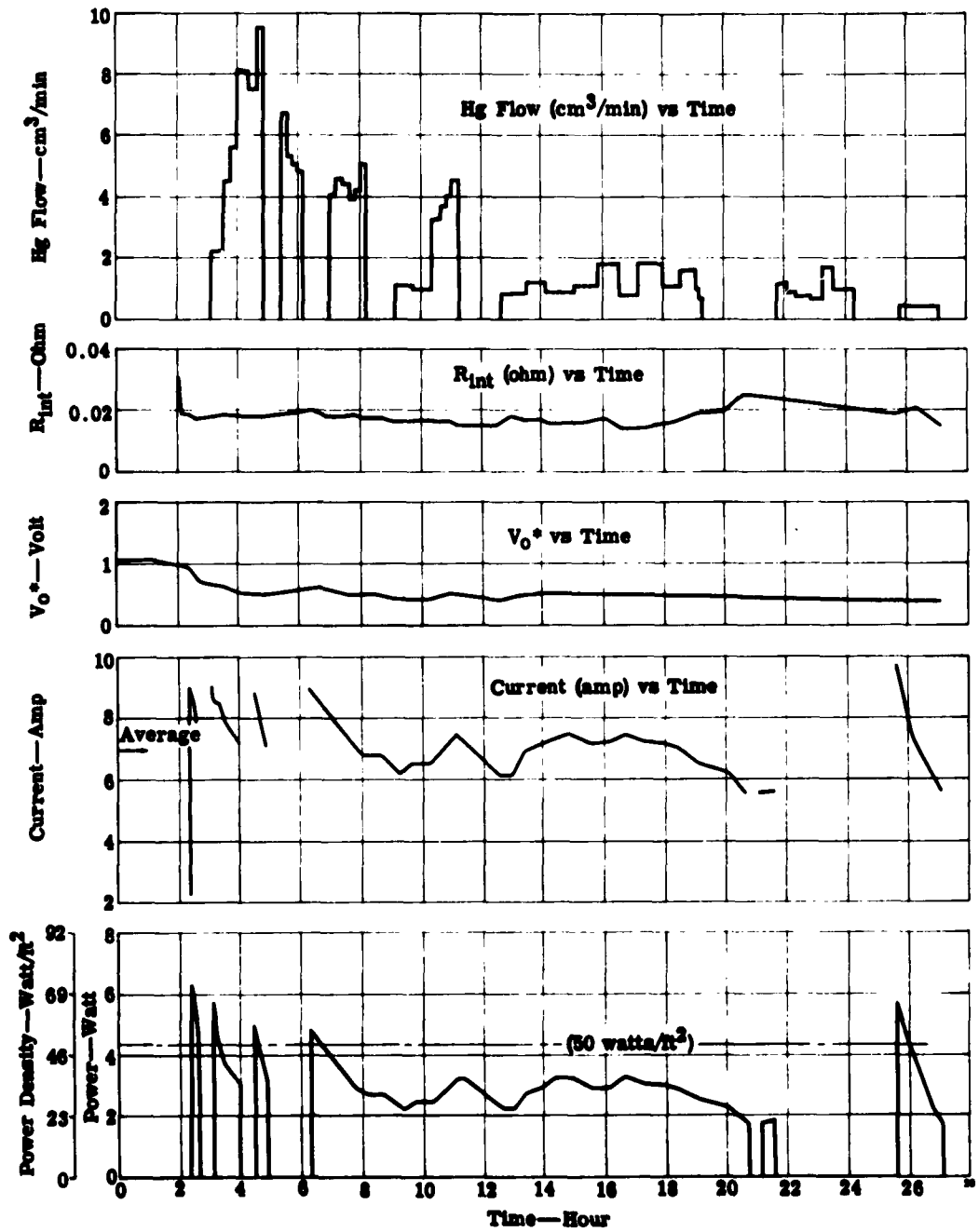


Figure 69. Operating Characteristics of Differential Density Cell (21)

TABLE XXII

Performance of Cell 22

<u>Time</u>	<u>Current (amp)</u>	<u>Cell Voltage</u>	<u>Power Density (w/cm²)</u>	<u>Power Density (w/ft²)</u>
1:45 pm	9.8	0.54	0.0653	60.7
2:00	8.6	0.53	0.0563	52.4
3:00	9.1	0.56	0.0629	58.5
4:00	8.9	0.54	0.0593	55.1
5:00	8.9	0.54	0.0593	55.1
6:00	9.0	0.55	0.0611	56.8
7:00	8.9	0.54	0.0593	55.1
7:15	8.8	0.53	0.0576	53.6

Regeneration of the cathode material of a liquid metal cell can be accomplished without any direct effect on the static performance of the cell. This is shown by the ability to control the cell potential on all configurations tested.



Figure 70. Differential Density Cell (22) Prior to Operation

VII. PROBLEM AREAS AND SOLUTIONS

In a development project of this type, many potential problem areas can be anticipated after a preliminary consideration of goals, state of the art, theory, past experience, etc. Other problem areas can be elucidated only in a step wise manner after laboratory work at a particular level of development. The following paragraphs will list:

1. Generalized problem areas anticipated at various levels of development—from inception to the ultimate multicell stack suitable for space purposes
2. Particular problem areas anticipated or discovered during this first level of the development process, with specific solutions either proposed or already accomplished

GENERALIZED PROBLEM AREAS

First Level—Selection and advancement of materials for construction and sealing of single cells. Make laboratory runs and evaluate for next problem area.

Second Level—Engineering of multicell stack to perfect seals, feed system, purification trains, etc. Make laboratory runs and evaluate for next problem area.

Third Level—Extension of material life spans and optimization of performance levels through detailed studies of flow, matrix, electrolyte properties, etc. Make laboratory runs and evaluate for next problem area.

Fourth Level—Matching of stack performance with support equipment (regenerator, pumps, radiators, etc). Make laboratory runs and evaluate for next problem area.

Fifth Level—Final adaption of system to space use (remote startup, resistance to g-forces, vibration, etc; behavior in zero g field). Carry out laboratory runs, in-field testing, and evaluation.

Work is well into the first level of problem areas and is commencing at the second level.

PARTICULAR PROBLEM AREAS AT THE FIRST LEVEL AND THEIR SOLUTIONS (PROPOSED OR ACCOMPLISHED)

Selection of Materials for Cell Construction

Ferritic stainless steels have been shown to be satisfactory for cell construction at present stages of cell life. Some slight attack was shown by the action of electrolyte, and the attack

became serious in the presence of air (this was a problem only when a seal leak was present). No need for improvement is seen until possibly the third level.

Matrix

Matrix problems are more resistant to simple solution than any other problems at this point. It should be emphasized that matrix problems are closely interrelated to the choice of electrolyte and, consequently, could be vastly reduced in scope by a program leading to adoption of a new electrolyte system, or an oxide ceramic material with a compatible binder.

Corrosive Attack on Ceramics

It was indicated in Section III that porous alumina was chosen for a matrix material because of its availability and reported resistance under some conditions to fused hydroxides. Gross attack was ruled out in preliminary compatibility tests at Allison. However, the experimental results indicated an increase in cell resistance when an alumina matrix was used. A partial solution was effected by a change to the newer LA materials (higher porosity, nonsilica bound), but matrix life was nevertheless tenuous at best.

Even though the initial compatibility tests indicated no gross attack, the change in electrical resistance and/or resistivity across the matrix-electrolyte barrier indicated that more subtle changes were taking place. Accordingly, Allison consulted with Purdue University for a detailed physical analysis of alumina specimens which had been subjected to electrolyte impregnation. This analysis consisted generally of water leaching the electrolyte from the pores of the alumina, drying, encapsulation in an epoxy resin, polishing, and microscopic examination. Results are shown in Figures 71, 72, and 73.

Figure 71 is a view of the microstructure of a piece of LA-type alumina prior to impregnation. The dark areas represent the epoxy resin, and the light areas represent the alumina. Figure 72 is a similar piece of alumina which has been impregnated under alternating pressure and vacuum and then held for examination. The photomicrograph shows evidence of attack on the binding posts between the alumina particles with attack on the particle itself. Figure 73 is a view of a sample which had been impregnated, held for 24 hours, and then run in a cell for 16 hours. Attack on the basic particles seemed to have advanced. It is unfortunate that water was used during the process because of previous reports¹⁴ that water would cause disintegration of hydroxide-impregnated ceramics.

Accordingly, the test was rerun at Allison, eliminating the water leach and substituting the removal of electrolyte by a methanol treatment, which evidenced less visually apparent physical attack on the ceramic. Samples of LA-830 alumina and LM-833 magnesia were dried and impregnated in a previously vacuum-treated molten electrolyte. Specimens were held in the



Figure 71. Microstructure of Alumina Disc Prior to Impregnation



Figure 72. Microstructure of Alumina Disc After Impregnation



Figure 73. Microstructure of Alumina Disc After 40 Hours

electrolyte under vacuum according to the following time schedule. One sample of each material was removed (1) immediately after impregnation, (2) after one day exposure, (3) after three days exposure, (4) after seven days exposure, and (5) after fourteen days exposure. An initial unimpregnated sample was used as a control. After removal from the electrolyte solution, the electrolyte was removed from the porous ceramic with the previously mentioned methanol leach. When no further change in pH was indicated, samples were impregnated with a dyed epoxy resin (indicated by the dark areas in Figures 74 through 79). After encapsulation, samples were sectioned and polished and the microstructures were examined. The alumina samples from this test are shown in Figures 74, 75, and 76, and the magnesia samples in Figure 77, 78, and 79. Figures 74 and 77 indicate the unimpregnated samples and show the ceramic particles as large, white areas, with the dark epoxy resin filling in the porous part of the specimen.



Figure 74. Alumina Unexposed to Electrolyte



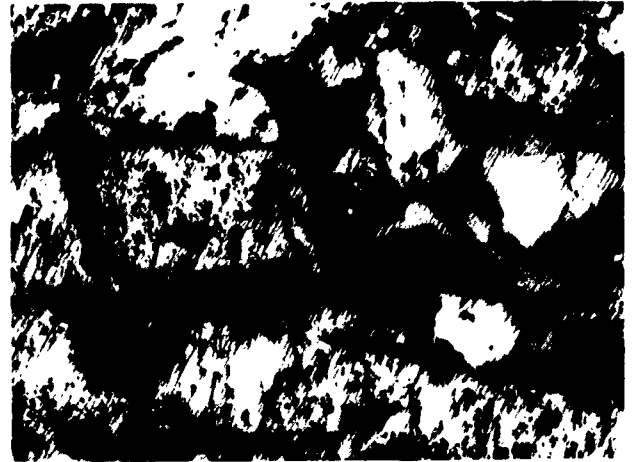
Figure 75. Alumina Immediately After Impregnation



Figure 76. Alumina After 14 Days Exposure to Electrolyte



**Figure 77. Magnesia Unexposed
to Electrolyte**



**Figure 78. Magnesia Immediately
After Impregnation**

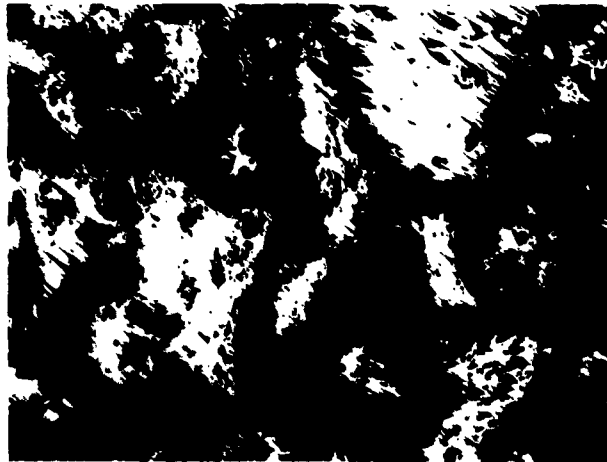


**Figure 79. Magnesia After 14 Days
Exposure to Electrolyte**

The difference in appearance of the individual particles when compared with those which were unexposed indicates definite corrosive attack by the electrolyte. The very dark areas within the ceramic particles are principally the result of loss of material by pull-out during the polishing operation. Very little pull-out occurred when the unexposed specimens were polished. An attempt was made to eliminate the pull-out with only limited success, indicating a weakening of

either particle strength or interparticle binding. The hardness of the particles and the interparticle strength appear to have been greatly reduced as a result of exposure to the electrolyte. The existence of this deterioration was substantiated by the degree of pull-out which occurred during polishing and the lowered resistance to deformation by simple scratching techniques. A point to be stressed is that the reduction of the interparticle strength in the case of magnesia may be the result of attack on the binder only. The alumina samples reputedly contained no binder and, therefore, attack would seem to occur on the basic particle itself. The results obtained at Purdue University, therefore, seem to be confirmed in the case of alumina samples.

The attack on the alumina could result in the formation of potassium aluminate which might affect the electrical resistance by closing the pores of the matrix with insoluble debris from the attack, or by affecting the electrolyte melting point, ionic mobility, etc. It is also possible that the increase in the electrolyte-matrix resistance is not due to corrosive attack but, rather, is a result of depletion of electrolyte within the pores. No reaction similar to the aluminate formation is known for magnesia compounds, which would tend to strengthen the belief that attack on the magnesia samples is centered on the binder. Solution of this problem might lie in the adoption (and availability) of other ceramic systems or in the adoption of an electrolyte system of the proper melting point in which the use of suspect KOH has been eliminated. Corrosive attack on the basic ceramic oxide powder is very important in the program, with respect to either a sintered ceramic matrix or the composite paste matrix.

Further work in this area (Allison sponsored) shows the following results. High purity MgO and Al₂O₃ were held in vacuum-dried electrolyte for periods of 96 hours. At the end of this time no magnesium was found in the electrolyte within the limits of detection. In fact, it was shown that if the electrolyte is extremely dry, even the Al₂O₃ is not dissolved. This work is continuing for longer time periods.

Internal Short Circuiting Through the Matrix Pores

A number of possible mechanisms exist whereby internal short circuiting might occur, but all are easily solved.

1. Direct shorting due to differential pressures was taken care of by control and balance of pressure heads.
2. Penetration of pores by mercury vapor could be prevented by close control of cathode temperatures.
3. Solution of potassium metal in the electrolyte (discussed in item 4) could bring potassium in contact with mercury at the electrolyte-mercury interface with subsequent amalgam formation and "treeing" through.

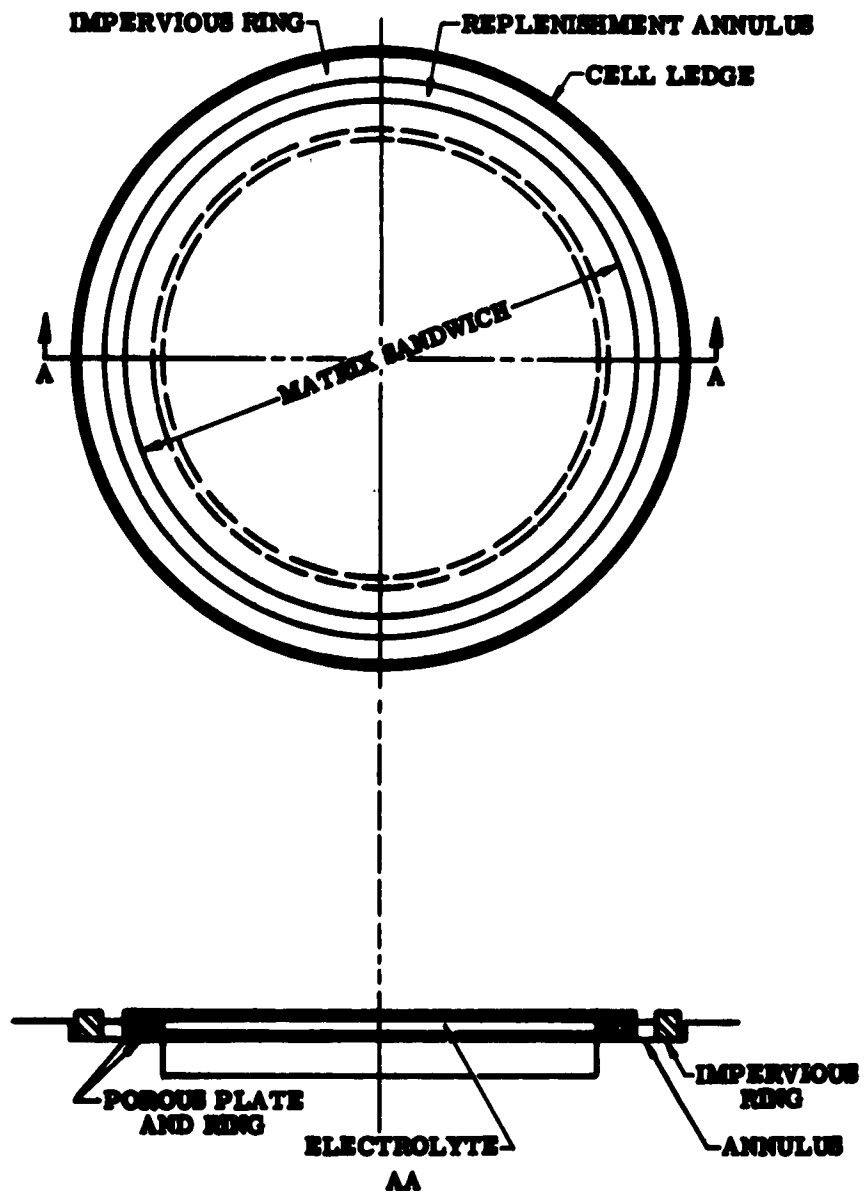


Figure 80. Sandwich Matrix Design

4. Preferential wetting of pores by high potassium amalgams—Both (3) and (4) are solved by use of a sandwich-type matrix as shown in Figure 80. In this case, penetration of a porous plate would not bring the two metal-electrolyte interfaces into shorting proximity. Figure 81 shows the occurrence of metal penetration into a matrix cup (single cup cell) which does not have the benefit of a sandwich effect. After internal shorting, the cup was removed from the cell and immediately placed under kerosene. The cup was thus protected from reaction due to oxygen or moisture. On placement of a drop of water on an area which indicated amalgam penetration by its gray color, bubbles were evolved (hydrogen—due to the decomposition of potassium within the amalgam), and, finally, only tiny droplets of pure mercury remained. These are plainly visible in the photograph.

Stress Failure

Stress-caused failure of the matrix should not cause particular concern, since this can be negated by mechanical design and control of pressure heads. Initial cracking problems on cell heat-up (due to differences in thermal expansion of cell and matrix) encountered during the first quarter were solved by hot clamping of the cell after temperature equilibrium had been established. The end aim, however, should be a cold clamping capability.

Electrolyte

Besides the always continuing desire for an electrolyte of increased ionic conductivity, the only dissatisfaction with the present electrolyte system (70 percent KOH-15 percent KBr-15 percent KI-mole) is its use of KOH. The presence of KOH in the electrolyte was considered as a possible trouble source due to its corrosiveness, but rates of attack were unknown. Yet, the few known potassium cation mixtures which were not unfavorable from a thermodynamic standpoint and which had melting points in the proper range were based on the presence of KOH. During the course of work, electrolyte composition was shifted from a 60 percent-20 percent-20 percent to a 70 percent-15 percent-15 percent mixture to approach more closely the determined eutectic point. Conductivity of the latter composition lies in the range of 1.0 to 1.2 $\text{ohm}^{-1} \text{cm}^{-1}$ for temperatures of 573 to 598°K. Solution to corrosiveness can lie in one of four directions:

1. Choice of a more compatible ceramic material
2. Selection of monocationic system, deleting KOH as a constituent
3. Selection of an exotic electrolyte system—e. g. , tetra-alkyl quaternary ions, synthetic polymers, etc

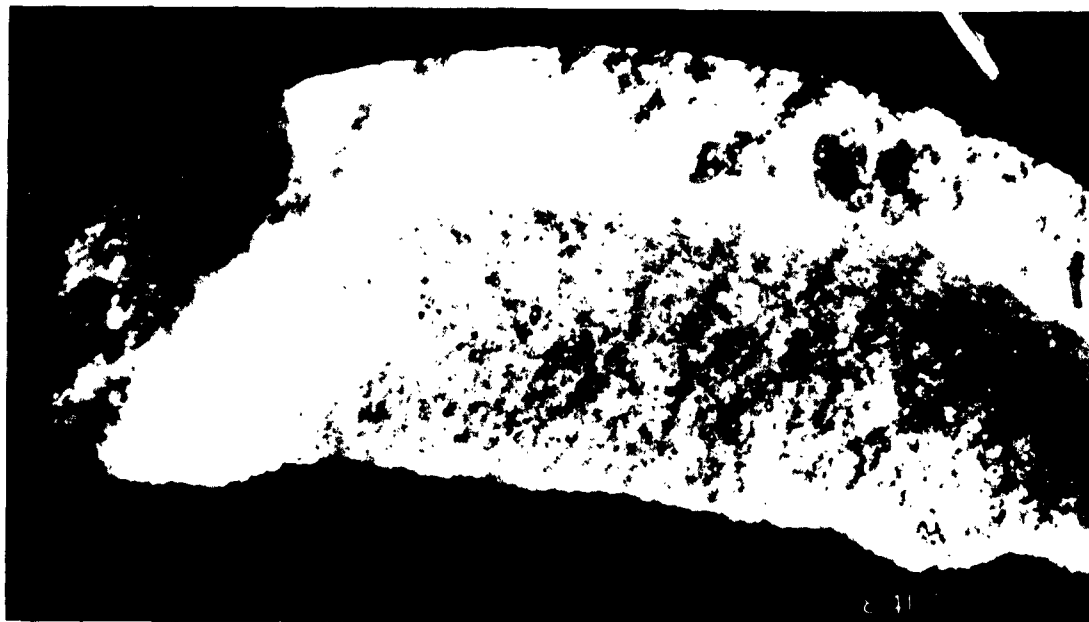


Figure 81. Porous Cup Showing Evidence of Metal Penetration

4. Selection of a higher melting point system with cell operation under pressurized conditions to retard boiling of mercury at the higher temperature

A second facet to the electrolyte problem is the small solubility of potassium metal in the electrolyte (approximately 5 percent, mole), leading to some coulombic inefficiency and self-discharge. Coulombic inefficiency and self-discharge are readily overlooked in a flowing metal cell since replenishment is constantly taking place. Elimination of KOH from the electrolyte system should also solve the solubility problem.

Impurities

Another problem area is the need for pure materials. It is known that plugging of flow lines, or difficulty in future regeneration of reaction products can be caused by impurities in the liquid metals (particularly dissolved oxides of potassium). Figure 82 represents another effect—that of reducible organic materials in the cell (in this case, potassium which has not been thoroughly cleansed of the oil in which it was shipped). The photographs show the absorption of electrically conductive carbon into the matrix cup, with resultant internal short circuiting. The stack design (Figure 83) indicates provisions made for further in-line purification of high-purity starting materials.

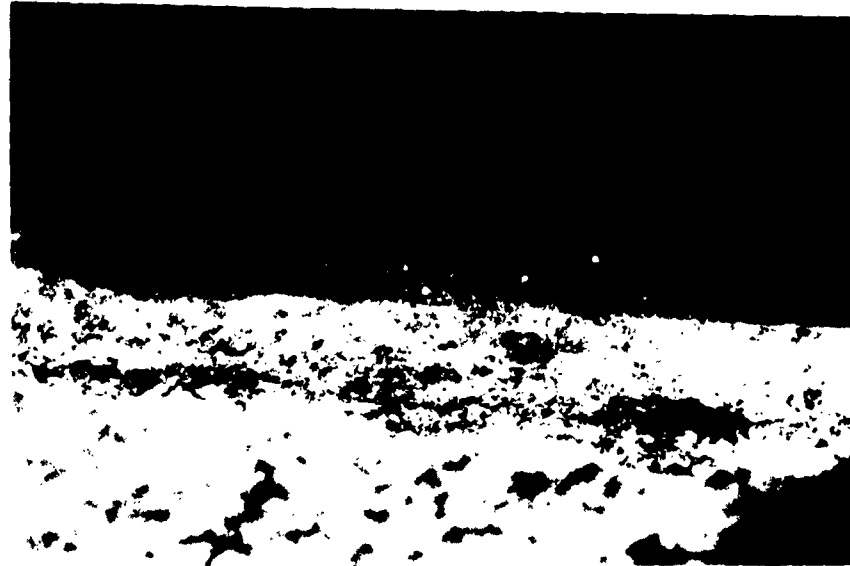


Figure 82. Effect of Impure Materials on Cell Life

Seals

Another problem area of highest priority is the lack of a reliable seal for the flat-type circular cell. Much progress has been made in this area, but operating time of these cells to date is low. The situation arises from the necessity of sealing a porous, frangible ceramic matrix between two metal cell halves. The ideal solution would probably involve a unitized piece of ceramic—porous in the center, impervious at the rim, and completely free of thermal stresses.

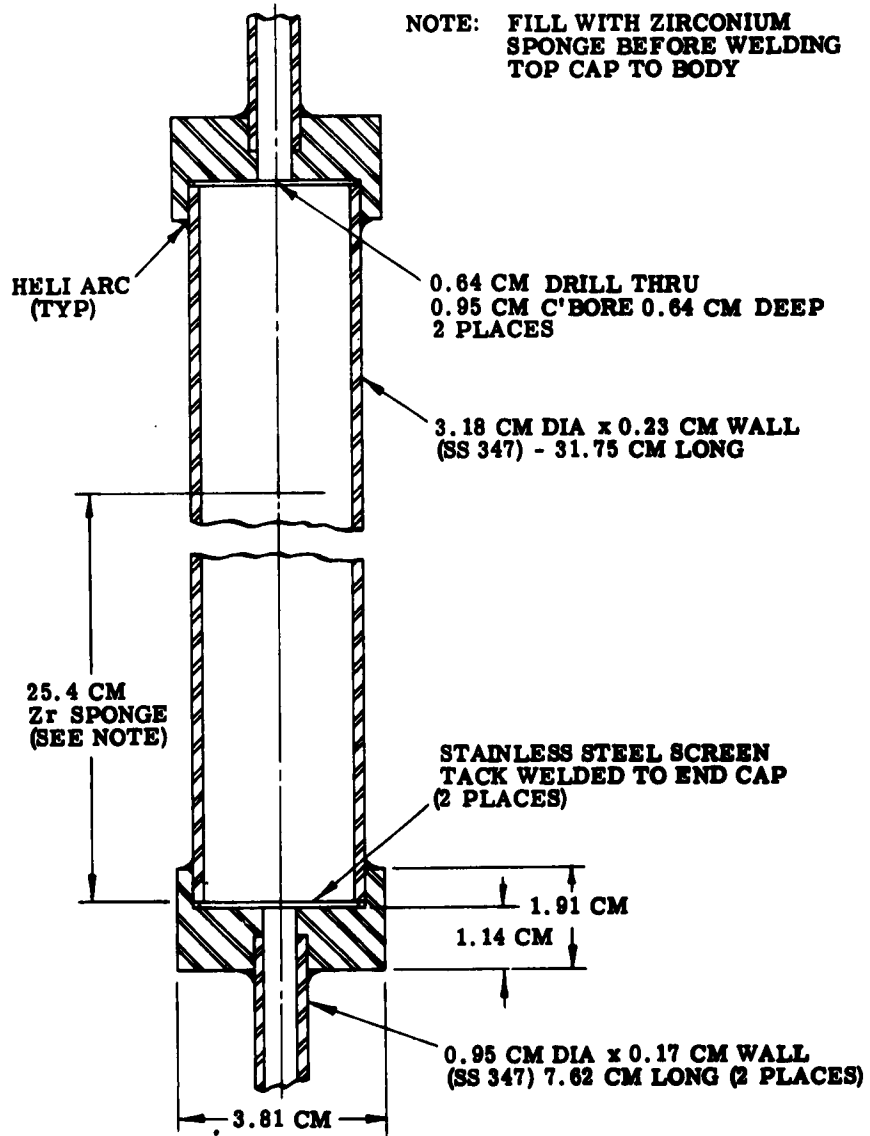


Figure 83. Hot Trap Detail

This solution involves extension of the state of the art—interim solutions would involve finer surface finishes on sealing gaskets and possible adaptation of alkali-resistant silicone rubbers.

Resistances

Resistivity values of the pure electrolyte material as measured in differential density cells have not confirmed those resistivities measured on the conductivity apparatus. Therefore, it is concluded that certain experiments must be carried out to determine the mechanism which causes the cell to perform at different resistivity values than predicted.

RECOMMENDATIONS

It is strongly recommended that the following problem areas be studied at the earliest opportunity.

1. Development of materials to combat corrosiveness of present molten electrolyte—ceramic, resilient and rigid seals, metal piping, etc
2. Maintenance of structural integrity and thermal shock resistance of ceramic matrices under cell operating and launch conditions
3. Development of purification and handling techniques for electrolyte and reactants in the liquid metal cells, including in-line purification
4. Development of rigid analytical techniques for determining true concentration of water and potassium hydroxide, and study of breakdown reactions of potassium hydroxide in the system
5. Development of a reliable cell seal to function under operating conditions without loss of liquid metal or mercury vapor, and adaptation of sealing procedures to multicell units
6. Optimization of cell design to obtain the best stack performance—flow of liquid metals, diffusion, heat utilization and dissipation
7. Optimization of ceramic matrix properties (porosity, pore size, tortuosity) for maximum conductivity and retention
8. Elucidation of electrode kinetics of K-Hg cell—polarization, diffusion, contact resistances, and the effect of various impurities on these parameters

VIII. SUPPORT EQUIPMENT

This work is primarily concerned with the basic electrochemical cell. The eventual configuration will be in a closed-loop system with the liquid metal regenerator. Yet, a very strong need exists for auxiliary support equipment to make possible the running of a "half-loop" stack of cells to fill the need for controlled head, electrically interrupted feed, measurement of flow rates, etc. This section discusses the devices which were constructed for these purposes.

MERCURY FEED

The potassium-mercury liquid metal cell will operate at approximately 0.5 volt per cell. This means that in a one-g system requiring (likely a minimum) 3.5 volts, seven series-connected cells would be needed per unit. In a 28-volt system the number of cells could reach 56. Feeding these cells from a common header or tank would introduce two major problems: (1) the cells would not be connected in electrical series, but would be paralleled out by conduction of the liquid metal, and (2) large hydrostatic forces might be placed on the ceramic matrix separating liquid metals in the bottom-most cells. Each cell could be fed from an individual feed tank, but this would be highly impractical. Therefore, the device shown in Figure 84 has been devised. The mercury is contained in the large stainless steel tank shown in an elevated position. It flows through a shutoff valve into the first lucite cylinder (left) in Figure 84. Figure 85 is a detail of this cylinder or weir. The pipe from the feed tank enters at (1) and the mercury falls dropwise into the larger chamber. It flows out of the weir into the cell through (2), meanwhile building up a head which can rise no higher than the bypass to the next consecutive weir (3). Hole (4) is a provision for pressurization with argon gas, and (5) is an alternate hole for a different feed mode.

Figure 86 is a detail of the next consecutive weir. The overflow from line (3) of the previous weir enters at (6). No. (7) feeds the cell at that particular level, and (8) is the bypass to the next consecutive weir. This mode of feeding could be continued through any number of weirs, and many means are open for further compacting or reduction in space that a large number of weirs would require.

The weir at the right of Figure 84 is the end of the line, or overflow weir. The excess from this cylinder flows through the electromagnetic pump (shown at the far right in the picture) and is recirculated back into the feed tank. Thus, the hydrostatic head which is allowed to build up in any weir is strictly limited, and a whole system of weirs might be built in which the hydrostatic heads applied to any cell matrix would be of the same value. Further, the dropwise manner of feed into any cylinder prevents the continuity of any electrical path through the liquid metals. This portion of the feed system has been tested with mercury flowing and has shown its practicability. Figure 87 is a close-up view of the mercury weirs for a three-cell stack in operation. Due to the slowness of the lens, the feeding metal appears to be flowing in stream-wise fashion (second from left), but this is not the case. Figure 88 is a view of the exit end of

a simulated (plastic matrix) three-cell stack while mercury is flowing through it. By using graduated cylinders for collection vessels, it was found that even flow rates through all three cells could be achieved while electrical discontinuity was maintained.

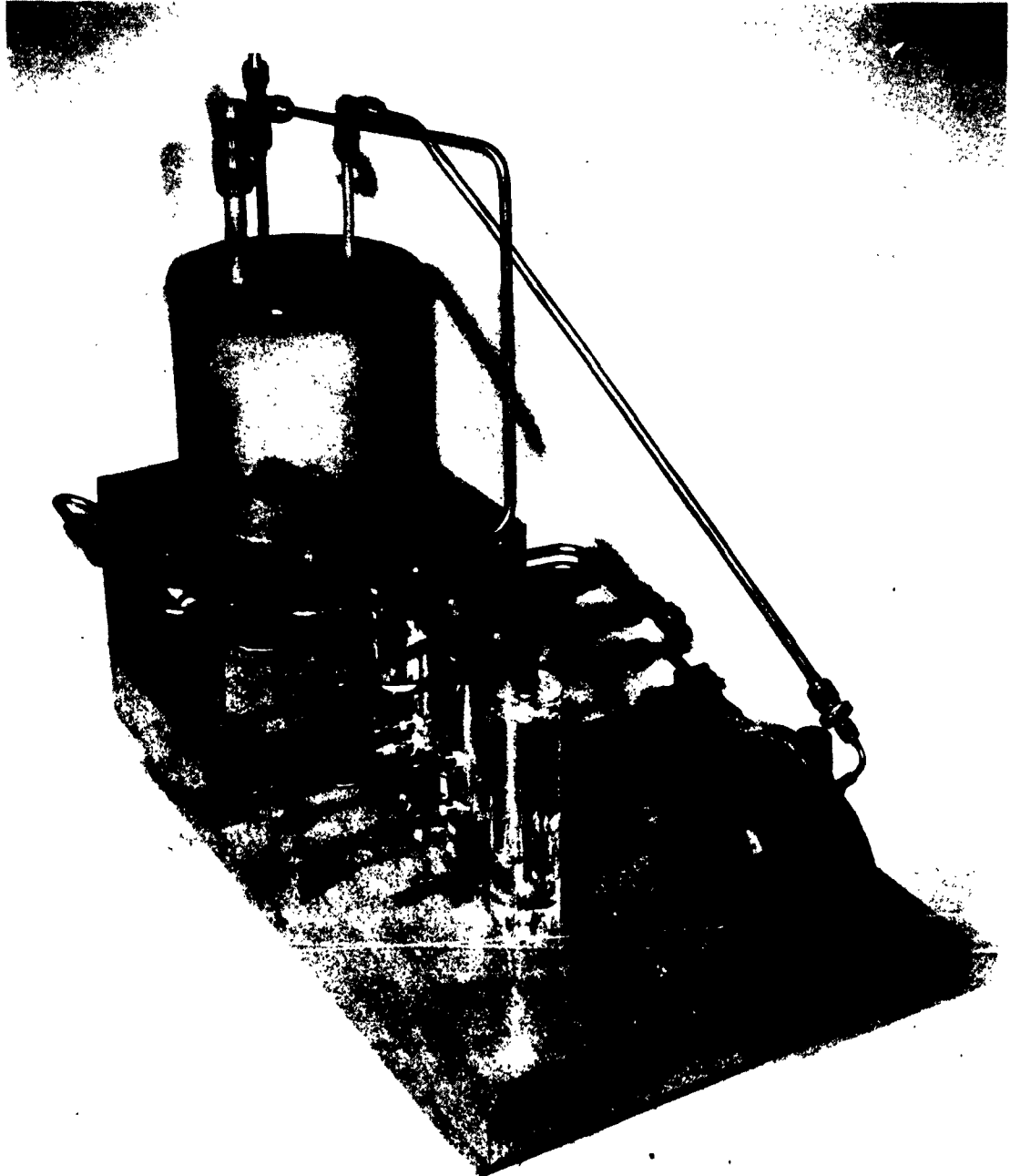


Figure 84. Mercury Feed System

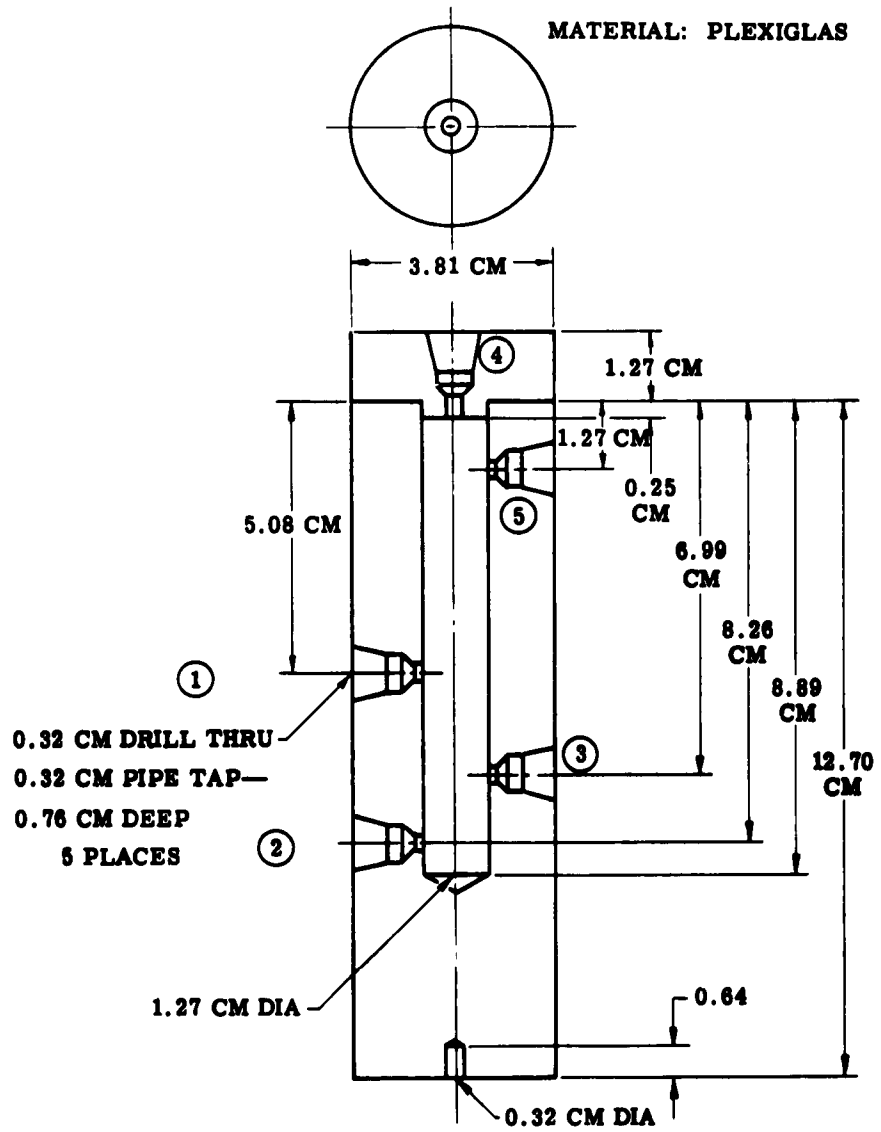


Figure 85. Detail of Mercury Weir

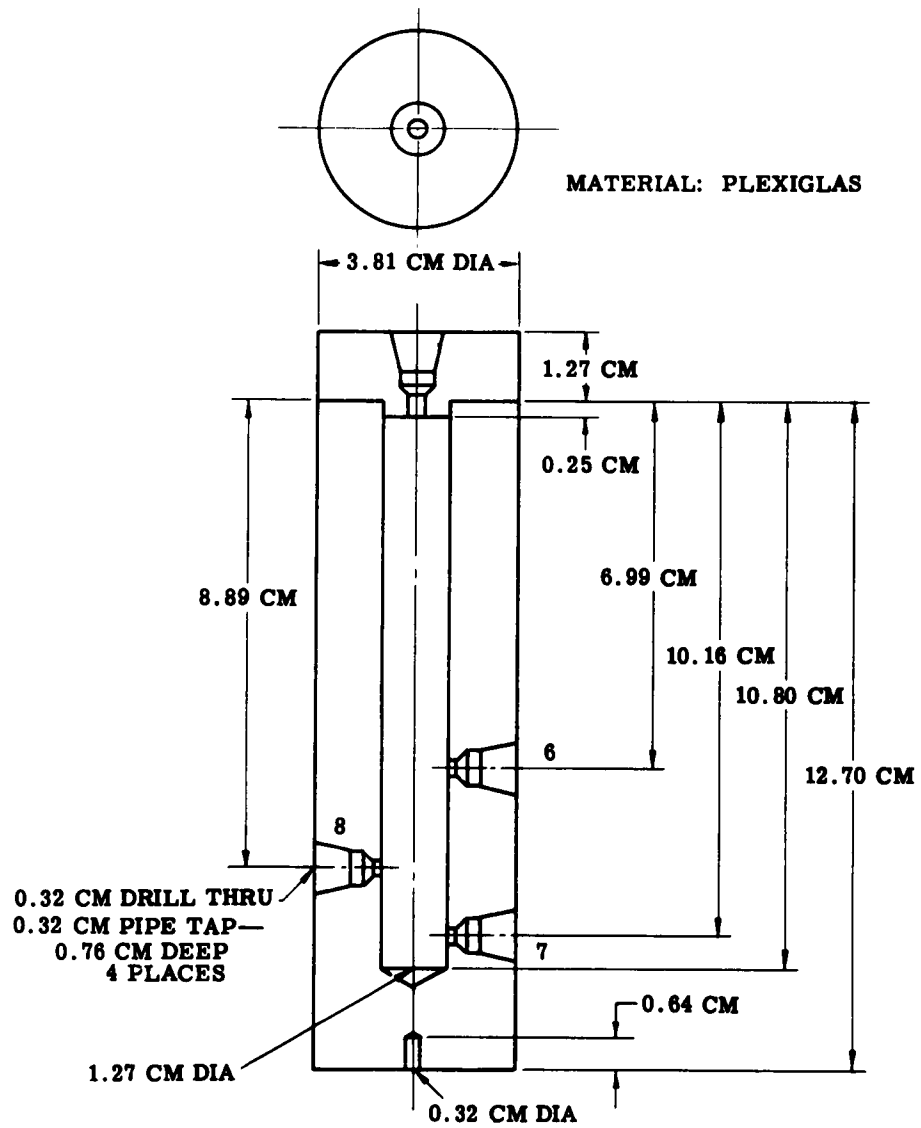


Figure 86. Detail of Consecutive Mercury Weir



Figure 87. Close-up of Mercury Weirs in Operation



Figure 88. Close-up of Exit End of Three Cell Stack with Mercury Flow

POTASSIUM FEED

The same requirements and principles which govern the successful feeding of mercury metal would also apply to the feeding of potassium. However, the behavior of potassium in any atmosphere but an inert one means that the whole system must be operated under a cover gas such as argon. Figure 89 is a detail of a potassium weir for a three-cell stack. Individual metal cylinders (substituting for the lucite cylinders) are insulated from the enclosing chamber which is kept inert. Potassium is admitted through the three-pronged header from the main feed pot. An insulated pipe from each potassium weir leads to a cell at a particular level, while the head is limited by the overflow pipe near the top of the cylinder. Any overflow passes from the inerted container into a collection tank, where it is pumped back to the main feed. The whole of the potassium feed system would need to be maintained above the melting point of the metal.

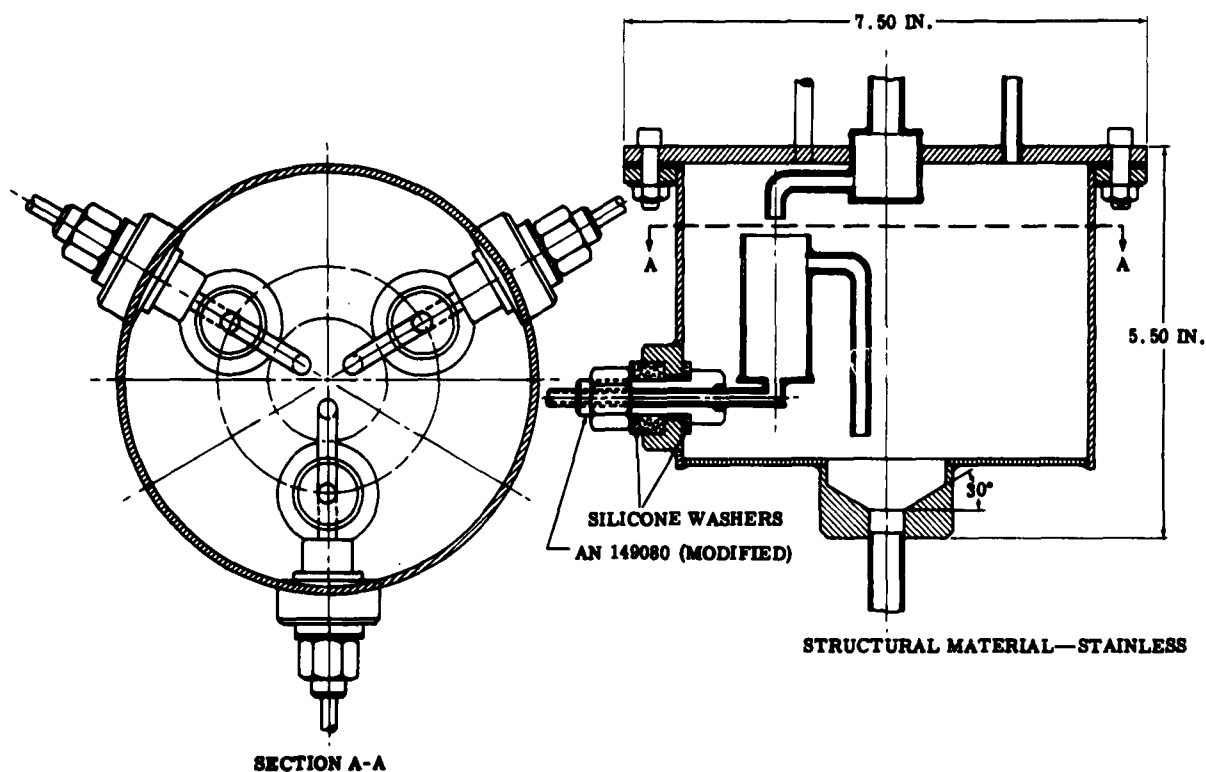


Figure 89. Detail of Potassium Weir



Figure 87. Close-up of Mercury Weirs in Operation



Figure 88. Close-up of Exit End of Three Cell Stack with Mercury Flow

HEAT BALANCE FLOWMETER

The heat balance flowmeter is to be used in experimentation or stack construction for monitoring flow rates of the liquid metals. It is interposed in the flow system so that the liquid metal, while flowing through, takes on heat from an electric heater of low capacity. Temperatures are measured at influent and effluent ends, and the temperature is changed in accordance with the flowrate. This temperature differential may be read on a potentiometric device. Thus, the slower the flowrate, the greater the temperature difference from entry to exit—the higher the flowrate, the lower the temperature differential.

To date, two flowmeters have been built for use with pure mercury as it would flow to or from the mercury weirs. Figure 90 is a view of the first flowmeter built before the insulation was placed around it. The liquid metal enters through the vertical tube and flows into the main chamber containing a 50-watt electrical heater (wires leaving from right). The temperature of the influent liquid metal is measured through the upper side arm, using a chromel-alumel thermocouple. The temperature differential is measured between the lower side-arm of the vertical tube and the thermocouple port on the main body of the device. The flowmeter was connected in the laboratory to a constant-head mercury feed tank, and an evaluation run was made using pure mercury at a 30-watt input to the heater. Initial results indicated that the flowmeter will function satisfactorily as a rate detection device, but results of the first test run suggested modifications to enhance the sensitivity of the device. Flowrates from 4 to 16 cm³/min (room temperature) were checked and it was found that the slope of a line calculated from the results of 53 separate measurements was:

$$\frac{d(\text{mv})}{dz} = \frac{-0.248 \text{ mv}}{\text{cm}^3/\text{min}}$$

The correlation factor for a straight line relationship was 0.949. The equation for the plotted curve was:

$$\text{mv} = 4.92 - 0.248 (z - 8.95) \quad (29)$$

where

$$\begin{aligned} \text{mv} &= \text{millivolts} \\ z &= \text{cm}^3/\text{min} \end{aligned}$$

Time response to a change in flowrate was very poor with this design—requiring eight or more minutes to detect a 2 cm³/min change in flowrate.

The improved design is shown in Figure 91. In this case the liquid metal passes directly through the 20-watt heater, and time response is nearly instantaneous. Seventy-nine separate readings were taken at flowrates from 2 to 20 cm³/min with a 20-watt heater input. Results are plotted in Figure 92. A semilogarithmic plot was used because of the exponential character of the data. A curve showing 95 percent assurance limits was then plotted for values of flow

up to $10 \text{ cm}^3/\text{min}$. Above this value, sensitivity is lost, and a larger heater should be substituted to increase the slope. The correlation coefficient for a straight line between these flow values is 0.990, and the equation for the curve is:

$$mv = 4.04 - 4.75 (\log z - 0.6948) \quad (30)$$

There is 95 percent assurance that the readout value will fall within 15 percent of the actual flow.



Figure 90. Heat Balance Flowmeter

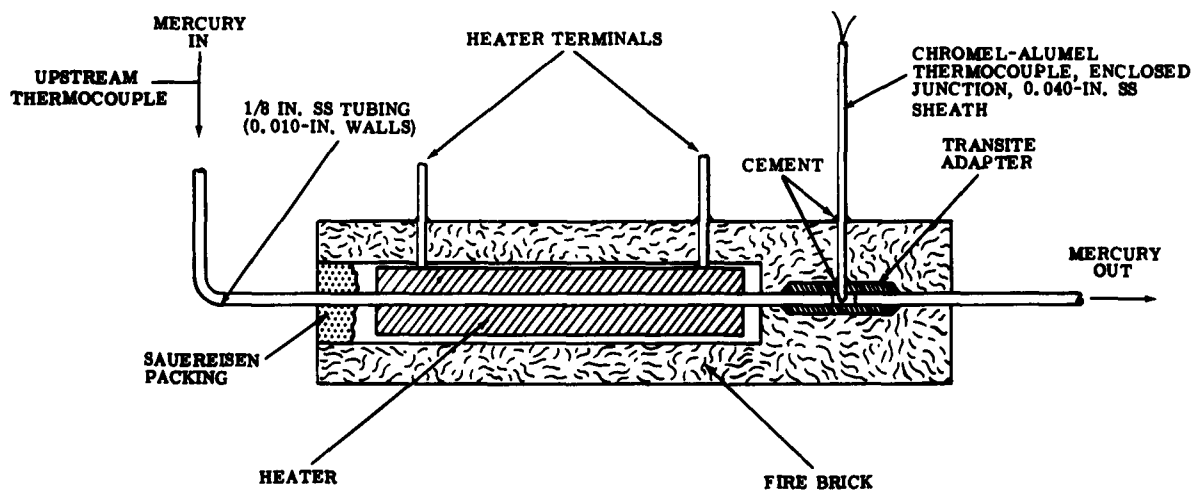


Figure 91. Improved Heat Balance Flowmeter

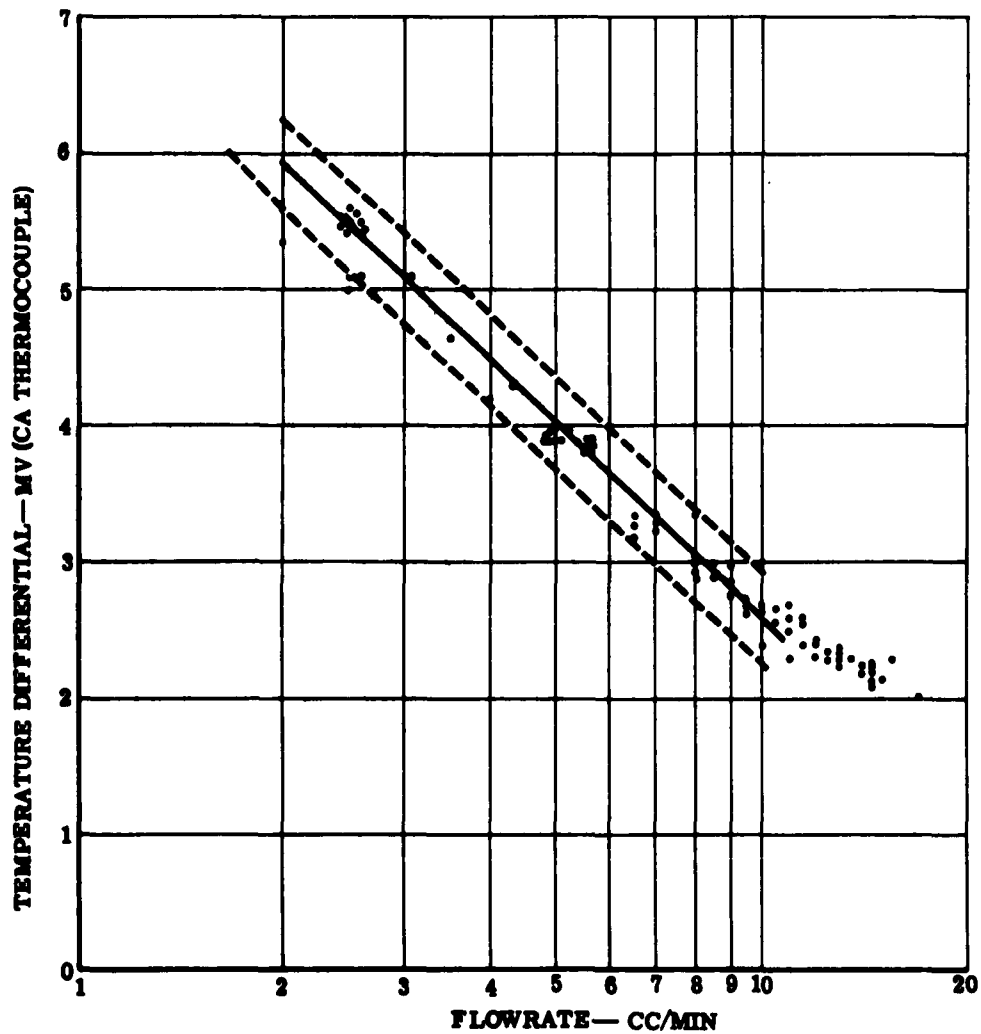


Figure 92. Temperature Differential vs Flowrate for Mercury Metal

EVALUATION OF FLOW EQUIPMENT

During the course of the work on the feed system, it became apparent that somewhat higher mercury feed rates might be desirable. The mercury feed was satisfactory at low rates ($3 \text{ cm}^3/\text{min}$), but to achieve good operation at higher rates, weir system would have to be modified from series to parallel feed and the overflow system would need to be revamped.

The unmodified flow equipment was tested at average flow rates of 5 to 6 cm^3 pure Hg/min. A Sargent recorder was connected to the cells of the simulated three-cell stack so that any electrical continuities produced would be recorded as an event on the recorder chart. The electrical hookup was such that an event in one direction indicated electrical parallelism between cells 1 and 2, and a blip in the other direction indicated parallelism between cells 2 and 3. At these flow rates the following continuities were recorded:

Between Cells 1 and 2	
Momentary	109
Short Duration	35
Between Cells 2 and 3	
Momentary	92
Short Duration	<u>61</u>
Total	297

This test was carried out so that there would be a basis for comparing performance of the modified and unmodified equipment.

The flow equipment was then modified and the experiment was repeated, measuring flow rates every two minutes on each of the three cell effluents. After one-half hour operation, flow rates were varied on individual lines to check the effect on flow to other cells. There was no mutual effect. This mode continued for the second half-hour period. The Sargent recorder was used to determine electrical parallelism. In 76 minutes, no blips were recorded even through flow rates reached $15.5 \text{ cm}^3/\text{min}$.

The heat balance flowmeter was connected into the line feeding cell 2. A calibration curve of log flow vs thermocouple output was determined to following the equation:

$$\text{mv} = 3.62 - 3.09 \log (z - 4.83)$$

A measure of flowmeter response and interrelation of individual cell feed rates is indicated in Figure 93.

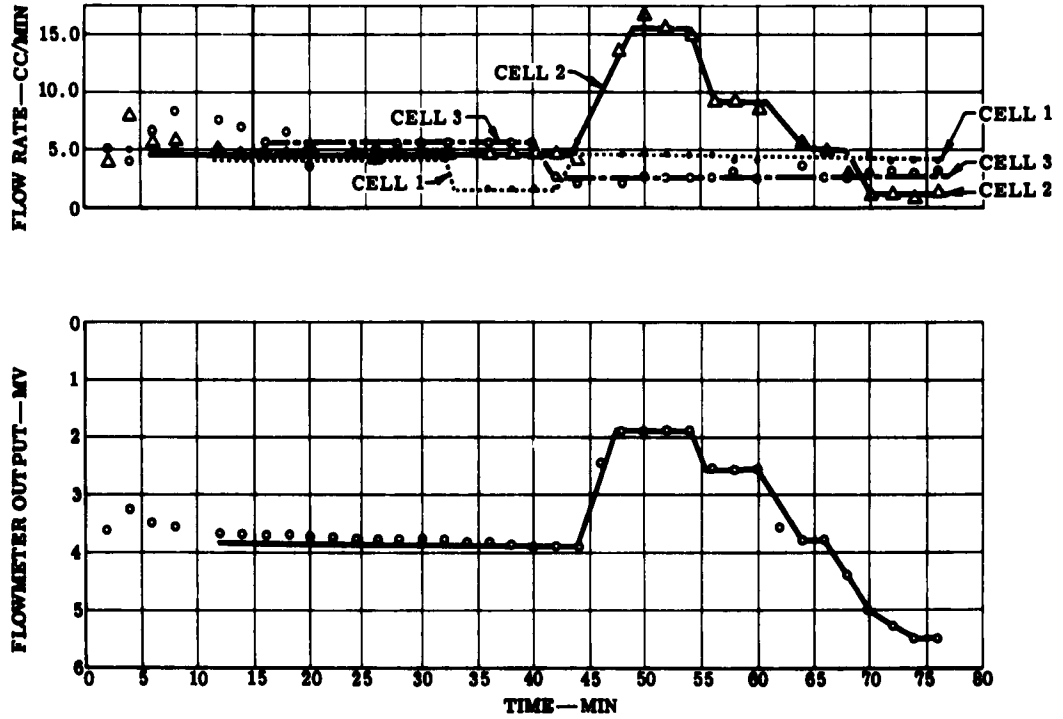


Figure 93. Flowmeter Response and Cell Feed Rate

The upper curves show flow rates for the three cells as a function of time. There was some initial unsteadiness until the rates were adjusted. Rate control was then good within limits of measurement. The lower curve is the millivolt output of the heat balance flowmeter which follows the flow profile of cell 2.

The modified flow system will satisfactorily handle requirements for operating a three-cell stack.

IX. DESIGN OF A MULTICELL STACK

Preliminary design work has been completed for a stack which has been arbitrarily chosen to have a power output of 310 watts, plus safety factor, since this was the original goal of this contract prior to the difficulties encountered with alumina matrices. The 81-cm² circular cell would be utilized in this construction.

ESTIMATION OF PERFORMANCE

With expected improvements in matrix materials—such as the unincreasing resistance exhibited by the magnesia matrix, Cell 19—it should not be unreasonable to plan for a 10-amp cell at an operating voltage of 0.5 volt. A 10-amp cell with an electrode area of 81 cm² would yield current densities of 123 ma/cm², or 114 amp/ft². At a V_c of 0.5 volt, this would yield power densities of 57 watts/ft².

At maximum power, this would require a V_o of 1.0 volt. Then the cell resistance would be

$$R_e = \frac{1.0 - 0.5}{10} = 0.05 \text{ ohm} \quad (31)$$

Reference to Table XXI, Single Cell Performance, yields the best figure available for resistivity of the electrolyte in an actual running cell (Differential Density Cell 17)— $\rho_e = 3.2$ ohm-cm. The best resistivity (ρ) for a matrix-electrolyte combination (Cell 14) is 15 ohm-cm. The best formation factor for a matrix-type cell would then be

$$(F) = \frac{\rho}{\rho_e} = \frac{15}{3.2} = 4.7 \quad (32)$$

To estimate the formation factor for a high porosity sintered matrix, reference is made to Cell 13 of Table XXI—an LA-830 matrix of 43 percent porosity. The resistivity of this cell was 32 ohm-cm. Thus, its formation factor was

$$(F) = \frac{\rho}{\rho_e} = \frac{32}{3.2} = 10.0 \quad (33)$$

Referring to Equation (23),

$$(F) = \frac{\rho}{\rho_e} = \frac{\tau^2}{\phi} \quad \text{where } \tau \text{ is tortuosity and } \phi \text{ is porosity.}$$

Then, for Cell 13,

$$\frac{\tau^2}{0.43} = 10.0, \text{ or } \tau^2 = 4.3 \quad (34)$$

Assume then a τ^2 of 4.3 for a high porosity sintered body (a reasonable assumption). It is estimated that porous magnesia bodies up to 65 percent porosity can be produced. Assume a

value of 50 percent. Then a formation factor for a 50 percent porous body of $\tau^2 = 4.3$ can be calculated.

$$(F) = \frac{\tau^2}{\phi} = \frac{4.3}{0.50} = 8.6 \quad (35)$$

Rearranging Equation (33):

$$\rho = \rho_e \times (F) = 3.2 \times 8.6 = 27.5 \text{ ohm-cm} \quad (36)$$

It should now be possible to calculate a matrix thickness sufficient to yield a resistance of 0.05 ohm. Using a ρ of 27.5 rather than the 4.7 of Cell 14, and substituting into

$$R_e = \frac{\rho t_e}{A} \quad (37)$$

then

$$t_e = \frac{0.05 \times 81}{27.5} = 0.15 \text{ cm thickness} \quad (38)$$

It should be possible to engineer a matrix of this thickness.

Looking at the possibility of using an unconsolidated matrix in the stack, reference is made to the best resistivity to date for an unconsolidated body—7.25 ohm-cm. Assume a value of 10 ohm-cm. The required maximum thickness would then be 0.41 cm.

STACK DESIGN

The arrangement of cells is shown in Figure 94. Using a 6.35-cm thick fire brick for furnace construction, the projected furnace size in the preliminary plan would be 96.5 cm wide, 42.3 cm deep, and 74.7 cm high. It should be emphasized that no great consideration was given to weight, compactness, or complexity in this design. The stack is designed primarily with the philosophy that any needed adjustments or repairs can be made without a complete shutdown, and that the instrumentation necessary to fully evaluate the operating characteristics of the cells and stack should be included. Future cell stacks will be more compact, lighter, and use less tubing than indicated in the preliminary design. The nomenclature in Figure 94 is identified as follows.

- No. 1 indicates the top view of the press which holds three units of seven cells each, or a total of 21 cells.
- No. 2 is an inerted collector-interrupter for the amalgam overflow from the anode compartment. It is planned that as potassium is drawn electrochemically to the cathode

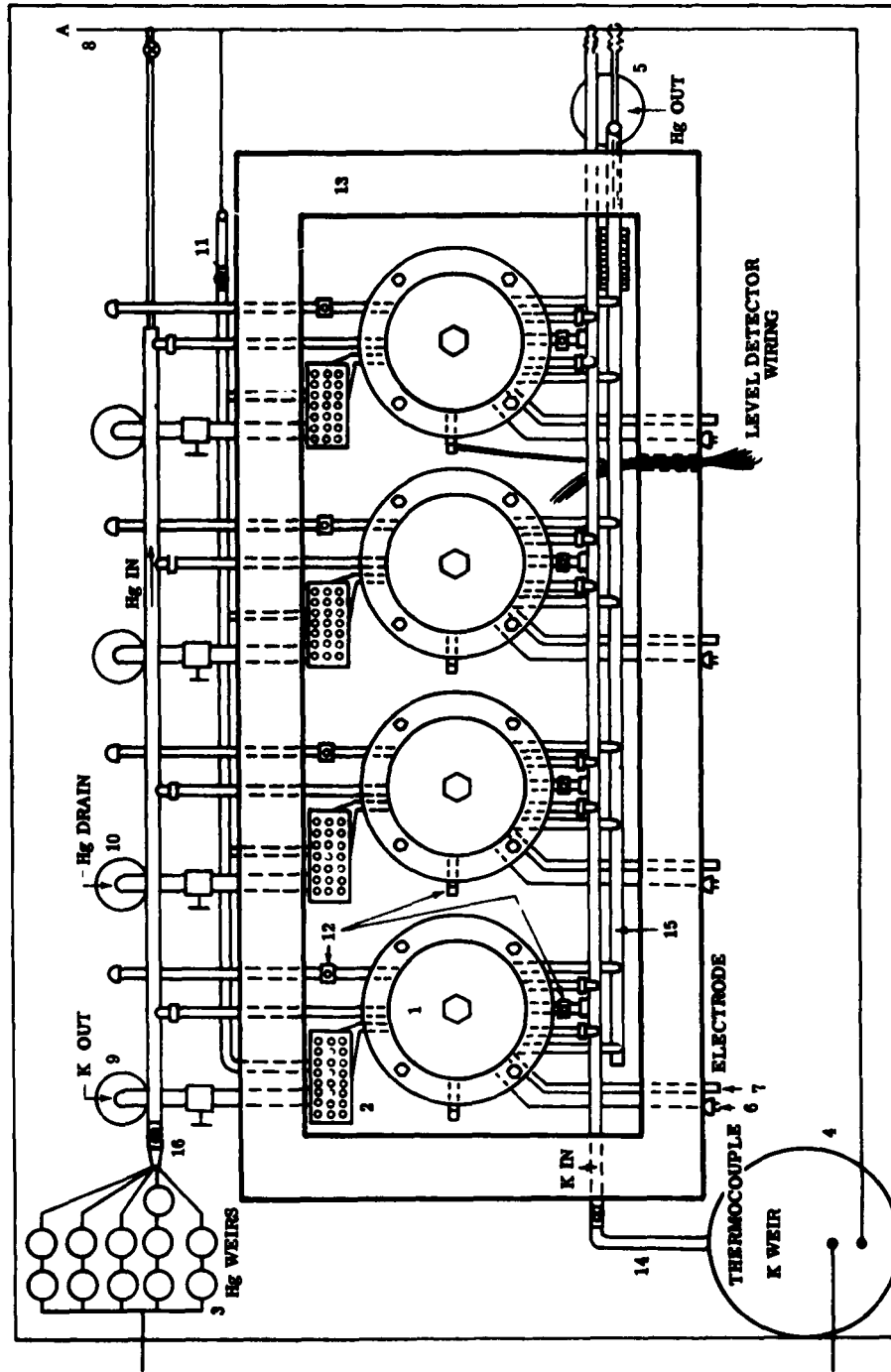


Figure 94. Top View of 310-Watt Stack

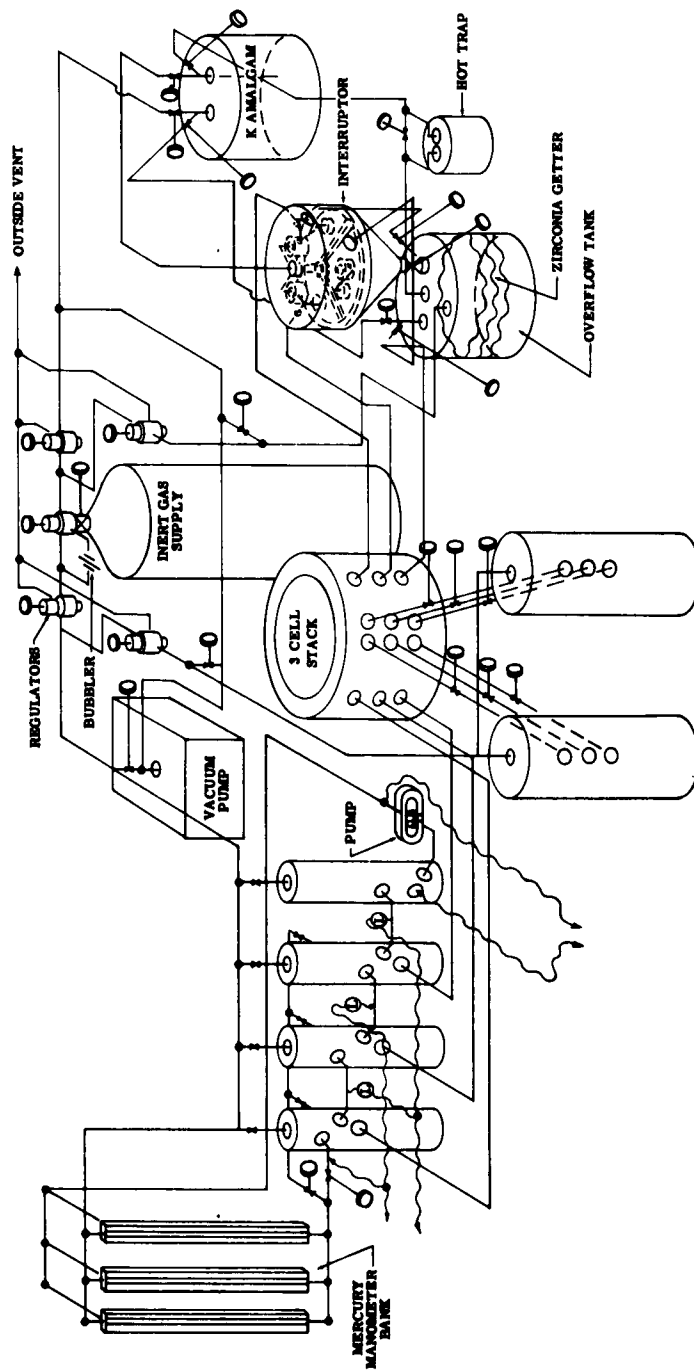


Figure 95. Schematic of Feed System for Liquid Metal Cell Stack

chamber, it will be replaced in the anode of the cell by periodic injections of pure potassium from the potassium feed rather than maintaining a steady flow of amalgam through the upper cell half. This will permit a more thoroughly cleaned and purified potassium feed—low in K_2O impurity.

- No. 3 indicates the mercury weirs to be fed from a large mercury feed pot. A detail drawing of the mercury weirs is shown in Figure 85. These weirs are also shown in Figure 95, which is a schematic of the feed system for the full stack. The weirs are used for control of the hydrostatic heads of mercury going into any particular horizontal layer of cells, eliminating the possibility of flexural damage to the matrix and minimizing the possibility of hydrostatic pressure forcing electrolyte from the pores. Each weir will have an upper and lower section serving a different layer of cells. A pipe from a weir to a particular layer will feed through one of the mercury feed manifolds, No. 16.
- No. 4 is a totally enclosed and inerted potassium feed weir (Figure 89).
- No. 5 indicates the collection pot for the mercury-rich amalgam feeding out of the cells through the mercury effluent manifold and collection weir (just inside the furnace). The mercury effluent manifold is indicated by No. 15. All manifolds in this system will be hooked to the cells by easily disconnectable joints so that if during operation a cell short should occur, the offending cell can be quickly disconnected from electrical parallelism, which would confine the loss to 5 watts. Otherwise, shorting of any one cell would result in a power loss of 20 watts.
- No. 6 indicates thermocouple outlets on the outside of the oven. There will be four thermocouples in each column of 21 cells—one located near the top, one located near the bottom, and two located near the center.
- No. 7 indicates the electrode leads coming to the outside from each cell. The leads in any particular layer will be connected externally to a bus bar, as shown in the schematic of the electrical system (Figure 96).
- No. 8 indicates an argon manifold. This manifold is tied into all the feed and effluent manifolds in the system so that, if it is desired to disconnect a particular cell, the valve linking the feed weir to a particular manifold can be closed. To clear the manifold, the valve admitting argon to the manifold can be opened and the material within the manifold forced into the cells. While still under positive pressure, the disconnection would be made and the joints would be capped. At this point the argon pressure would be reduced and feed for the other three cells would be restarted from the feed weir. The argon line

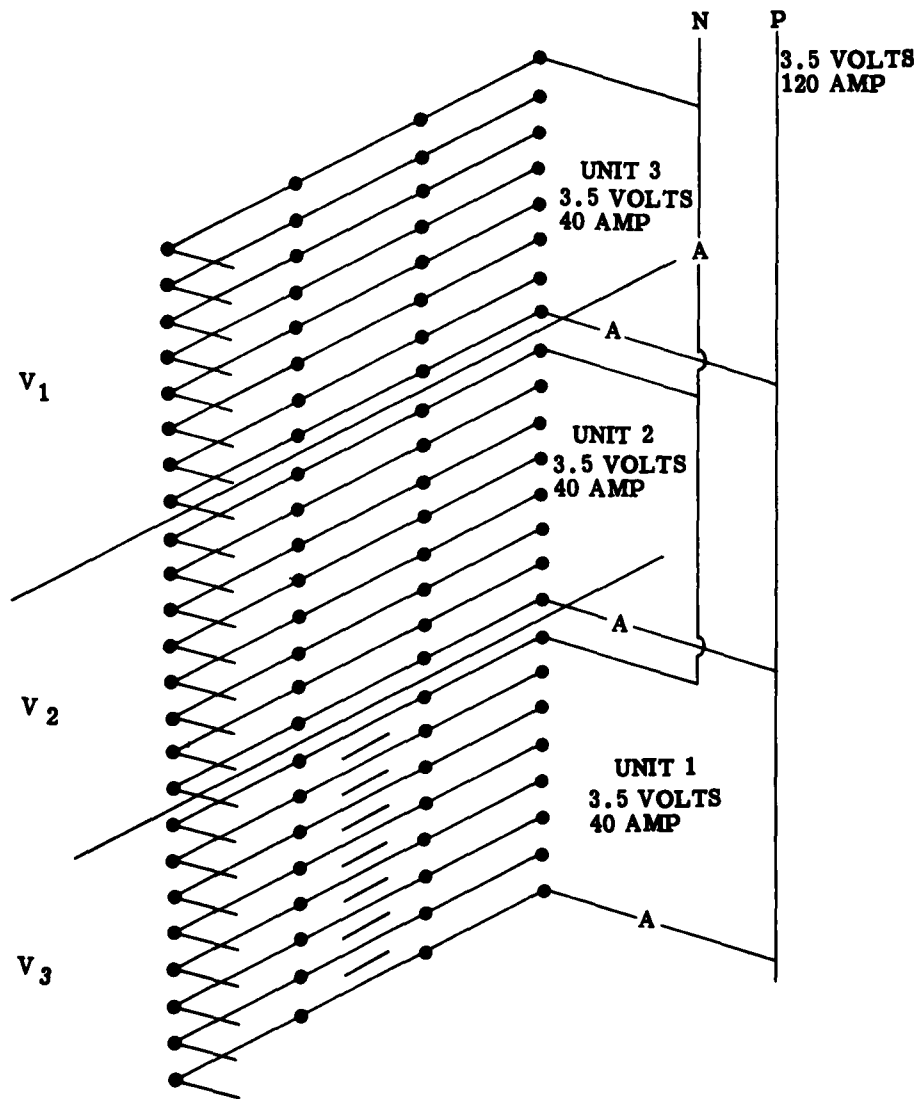


Figure 96. Schematic of Exterior Electrical Connections

will also serve to sweep out the cell before loading so that the last traces of air can be removed before the mercury or amalgams are loaded.

- No. 9 is the single drain from each of the collector-interrupters for the amalgam.
- No. 10 indicates the drains from the mercury side of the cell.
- No. 11 is the argon manifold which inerts the collector-interrupters.
- No. 12 indicates the three electrical level gauges previously mentioned.
- No. 13 is the furnace wall.
- No. 14 is the potassium feed manifold.
- No. 15 is the mercury effluent manifold.
- No. 16 is the mercury feed manifold.

It should be mentioned that if a short occurs through a matrix, it would not be necessary to disconnect the cell from the manifolds. The short could be interrupted merely by opening the mercury drain for that particular cell and allowing the mercury going into the cell to drain out rather than establishing contact with the matrix.

The feed system schematic shown in Figure 95 shows the argon source to be used in the cell layers or manifolds to pressure feed each of the weirs. The potassium would go from the initial potassium melting pot into the potassium weir and would overflow into the collection pot which contains zirconium metal, an oxygen getter. It is proposed that, before operation is begun, a full batch of potassium be purified by running it through the collection pot, pumping it back up to the feed tank and a hot trap, and then through the weirs into the cells. On the mercury side, prior to being fed into the weirs, the mercury can be vacuum degassed, removing any entrained air or moisture. It will then go from the feed tank into the weirs and then into the cells.

The schematic of the electrical system in Figure 96 shows the connections to the bus bars on the exterior of the furnace. The seven cells in Unit 1 would be in electrical series, as would the cells in Units 2 and 3. Each dot represents one of the four cells across the width of the furnace. The three units would be connected in parallel to produce 3.5 volts and 420 watts. One ammeter and a selector switch will be used to monitor the current output for the stack as a whole or the current output from each of the three units. One voltmeter will continuously

monitor the stack voltage; a separate voltmeter will monitor the voltage within each unit, and, by means of a selector switch, voltages can be measured either across the whole unit or between any two cells in the unit. Figure 97 is a view of the simulated three-cell stack and feed components.



Figure 97. View of Assembled Three-Cell Stack and Feed System

X. ACCOMPLISHMENTS AND TECHNICAL POSITION

Prior to this work, a few small liquid metal cells had been operated using the liquid metal systems sodium-tin and potassium-mercury. An electrolyte system, KOH-KBr-KI had recently been developed, but nothing was known of its electrical conductivity or compatibility with the system. Cells which had been run developed powers of approximately 15 milliwatts at 10 watts/ft². A total of perhaps 35 to 50 hours of running had been logged a few hours at a time. No cell had been run with the liquid metals flowing.

A summary of accomplishments during the course of this program follows:

1. Preliminary evaluation of cell feed characteristics was made.
2. Progress was made in sealing hot cells after earlier attempts led to gross leaks or cracked ceramics.
3. Initial problems in ceramic degradation and cell resistance were defined.
4. Vacuum impregnation techniques for ceramics were developed.
5. Improvements were made in matrix and cell design.
6. Six types of cells were operated for a total of 2300 hours.
7. Cycling life was extended to a maximum of 550 hours.
8. Necessary cell instrumentation was designed and initially evaluated.
9. A preliminary design was completed for a 310-watt multicell stack and support equipment, based on the flat-type circular cell.
10. A preliminary investigation and evaluation of other possible electrolyte systems was carried out.
11. Conductive properties of six-micron composite paste matrices were determined.
12. A satisfactory heat balance flowmeter was developed for flow rates up to 10 cm³/min.
13. A satisfactory electrical decoupler for one-g operation was developed.
14. The cell system was shown to be capable of producing power in a reversible manner.

15. A flowing potassium-mercury cell was run for six hours at 50 mw/cm^2 . A total time of 35 hours was accumulated for this type of operation.

Reference to Table XXI, Single Cell Performance, will help to establish certain milestones representative of the first year's work.

● Current Densities

Differential Density Cells (Pure Electrochemical System)

Static— 227 ma/cm^2 Flow— 109 ma/cm^2

Extrapolated to Maximum Power

Static— 225 ma/cm^2 Flow— 247 ma/cm^2

Matrix-Type Cells

Static— 150 ma/cm^2 Flow— 77 ma/cm^2

Extrapolated to Maximum Power

Static— 207 ma/cm^2 Flow— 78 ma/cm^2

● Power Densities

Differential Density Cells (Pure Electrochemical System)

Static— 87 mw/cm^2 Flow— 57 mw/cm^2

Extrapolated to Maximum Power

Static— 111 mw/cm^2 Flow— 128 mw/cm^2

Matrix-Type Cells

Static— 91 mw/cm^2 Flow— 41 mw/cm^2

Extrapolated to Maximum Power

Static— 107 mw/cm^2 Flow— 41 mw/cm^2

In many cases, the performance of flowing cells does not seem to match that of corresponding static-type cells. It is believed that the explanation to this phenomenon occurs in the fact that, with the exception of Cell 22 (for which no values were extrapolated), the mercury flowing into the cell was cold. It was thought originally that heatup would be rapid, but it is very likely (comparing Cells 21 and 22) that the entrance of the cold mercury reduced cell performance.

Figure 98 shows the program schedule.

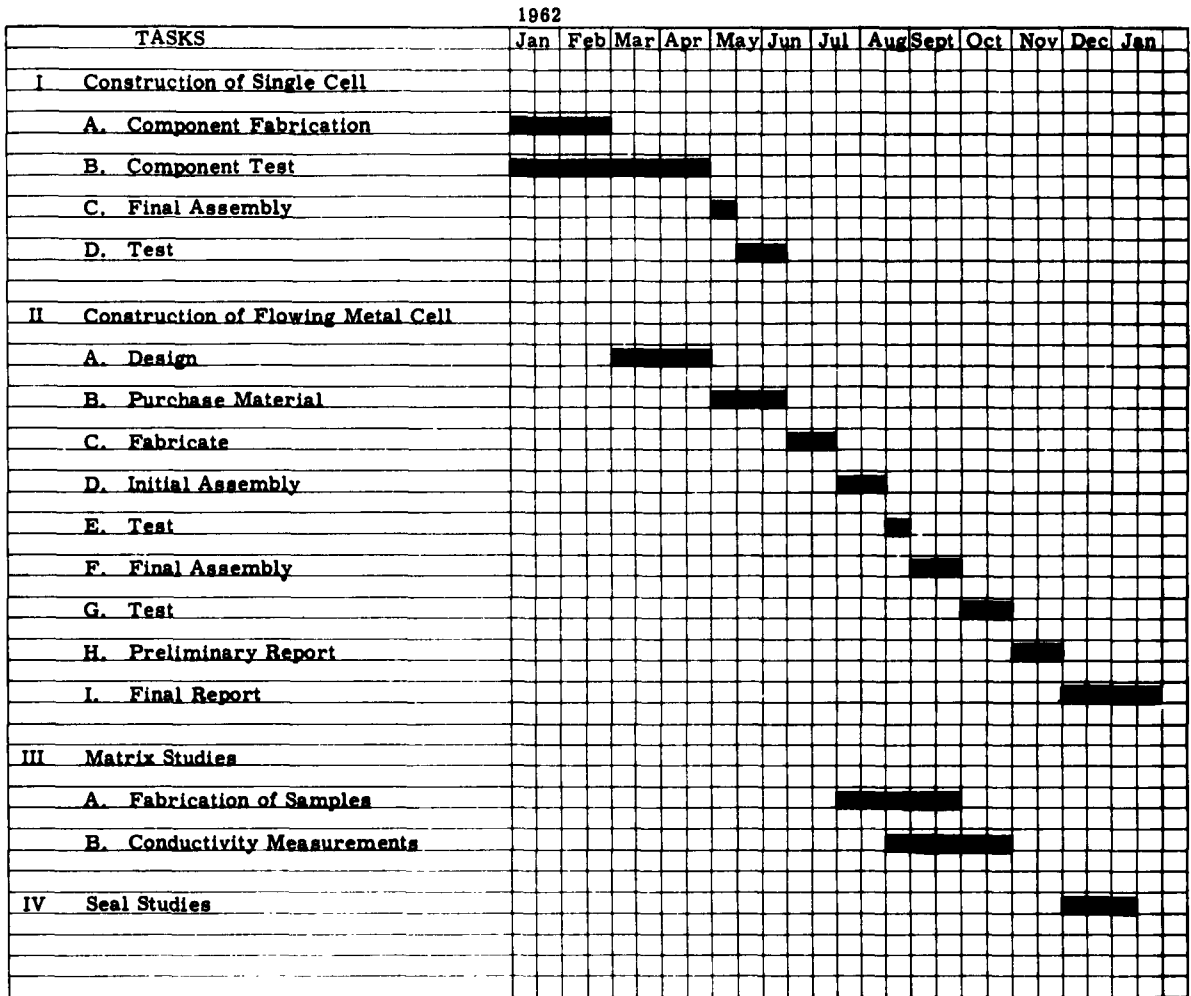


Figure 98. Program Schedule

XI. REFERENCES

1. Weaver, R. D. and Shriver, E. L. The Fuel Cell Literature. Allison Division, General Motors Corporation. APS 10 (1959).
2. Yeager, E. in Proceedings of the 12th Annual Battery Research and Development Conference. Asbury Park, New Jersey (1958) pp 2-4.
3. Caple, W. G. and Shriver, E. L. Thermally Decomposable Inorganic Compounds. Allison Division, General Motors Corporation. ACS 1 (1960).
4. King, J. Jr. and others, in Energy Conversion for Space Power. New York, Academic Press, 1961, pp 387-410.
5. Henderson, R. E., Agruss, B., and Caple, W. G. ibid. pp 411-423.
6. Laitinen, H. P. A. and others, in Journal of the Electrochemical Society. Vol 107 (1960) pp 546-555.
7. Parsons, R. Handbook of Electrochemical Constants, London, Butterworth's, 1959.
8. Kubaschewski, O. and Evans, E. L. Metallurgical Thermochemistry. New York, Pergamon Press, 1958, pp 6-72.
9. Selected Values for the Thermodynamic Properties of Metals and Alloys. Research Laboratory, Institute of Engineering Research, University of California, Berkeley, California (1959).
10. Liquid Metals Handbook. Atomic Energy Commission, Department of the Navy, Washington, D.C. (June 1950).
11. Handbook of Chemistry and Physics. 30th Edition. Cleveland, Ohio, Chemical Rubber Publishing Co., 1948.
12. Metals Handbook. American Society for Metals (1961).
13. Oxide Ceramics. New York, Academic Press, 1960.
14. Smith, T. P. Corrosion of Materials in Fused Hydroxides. Oak Ridge National Laboratories, Oak Ridge, Tennessee.

15. The Norton Company, Worcester, Massachusetts.
16. Whittemore, O. J. and Ault, N. N. in Journal of American Ceramics Society. Vol 39 (1956) p 443.
17. Morganite Incorporated, Long Island City, New York.
18. Benesi, H. A. and others. "Pore Volume of Solid Catalysts by Carbon Tetrachloride Absorption." Analytical Chemistry. Vol. 27 (1955) p 1963.
19. von Degenkolbe, J. and Sauerwald, F. "Das Volumen von schmelzflüssigen Kalium-Amalgamen." Zeitschrift für Anorganische und Allgemeine Chemie. Vol 270 (1952) pp 324-327.
20. von Degenkolbe, J. and Sauerwald, F. "Über die innere Reibung der schmelzflüssigen Kalium- und Natriumamalgame." Zeitschrift für Anorganische und Allgemeine Chemie. Vol 270 (1952) pp 317-323.
21. Muller, P. "The Electrical Conductivity of Metallic Alloys in Fluid Condition." Metallurgie. Vol 7 (1910) pp 730-740.
22. Mantell, C. L. Engineering Materials Handbook. New York, McGraw-Hill Book Co., Inc., 1958.
23. Mellor, T. A Comprehensive Treatise on Inorganic and Theoretical Chemistry. New York, Longmans-Green, 1956.
24. Williams, D. D. Solubility of Oxygen in Potassium Metal and Sodium-Potassium Alloys. Naval Research Laboratories, Washington, D. C. NRL Report 3894 (1952).
25. NASA-AEC Liquid Metals Corrosion Meeting. NASA-TDN 769. Washington, D. C. 1961.
26. International Critical Tables. Washburn, ed. Vol 4, 1920.
27. Moore, C. I. Liquid Metal Cell Electrolyte Matrices. Report for General Motors Institute, 1962.
28. Broers, G. H. J. and Schenke, M. Symposium on Recent Advances in Fuel Cells. Vol 6, No. 48, Chicago, Illinois (1961). (Sponsored by Division of Petroleum Chemistry, ACS)
29. Sundberg, K. "Geophysical Prospecting." AIME Transactions. (1932) p 367.

30. Wyllie, M. R. J. and Spangler, M. B. in Bull. Amer. Assoc. Petrol. Geol. Vol 36 (1952) p 359.
31. Winsauer, W. O. et al. in Bull. Amer. Assoc. Petrol. Geol. Vol 36 (1952) p 253.
32. Arndt, K. and Ploetz, G. in Z. für Physikalische Chemie. Vol 121 (1952) pp 439-455.
33. Jones, G. and Josephs, R. C. in Journ. Amer. Chem. Soc. Vol 50 (1928) p 1049.
34. Shedlovsky, T. J. in Journ. Amer. Chem. Soc. Vol 52 (1930) p 1793.
35. Edelson, D. and Fuoss, R. M. in Journ. Chem. Educ. (1950) p 610.

Aeronautical Systems Division, Dir/Aeromechanics, Flight Accessories Lab, Wright-Patterson AFB, Ohio. Rpt. No. ASD-TR-62-1045. DESIGN AND DEVELOPMENT OF A LIQUID METAL FUEL CELL. Final report, Dec 62, 155 pp. incl. illus., tables, 35 refs.

The electrochemical, physical, and chemical characteristics of potassium and potassium-mercury amalgams lend themselves to the successful operation of a liquid metal cell for space power. During the first year's work, substantial progress was made in the study and operation of potassium-mercury cells and in pointing up problem areas requiring solution. Six different types of cells were run, some utilizing a ceramic matrix while others operated on a differential density principle. Certain cells were operated with flowing cathode metal, so that steadiness of operation and regenerative capability could be studied. Results confirmed this regenerative capability up to 60 mw/cm², the operating level of the experiment. Liquid

(Over)

1. Liquid metal fuel cells
2. Potassium-mercury fuel cells
- I. AFSC Project 8173, Task 817303
- II. Contract No. AF33(657)-7847
- III. Allison Division, General Motors Corporation, Indianapolis, Indiana
- IV. Dr. B. Agruss, H. R. Karas, and V. L. Decker
- V. Allison Division EDR 3100
- VI. Aval fr OTS
- VII. In ASTIA collection

Aeronautical Systems Division, Dir/Aeromechanics, Flight Accessories Lab, Wright-Patterson AFB, Ohio. Rpt. No. ASD-TR-62-1045. DESIGN AND DEVELOPMENT OF A LIQUID METAL FUEL CELL. Final report, Dec 62, 155 pp. incl. illus., tables, 35 refs.

The electrochemical, physical, and chemical characteristics of potassium and potassium-mercury amalgams lend themselves to the successful operation of a liquid metal cell for space power. During the first year's work, substantial progress was made in the study and operation of potassium-mercury cells and in pointing up problem areas requiring solution. Six different types of cells were run, some utilizing a ceramic matrix while others operated on a differential density principle. Certain cells were operated with flowing cathode metal, so that steadiness of operation and regenerative capability could be studied. Results confirmed this regenerative capability up to 60 mw/cm², the operating level of the experiment. Liquid

(Over)

1. Liquid metal fuel cells
2. Potassium-mercury fuel cells
- I. AFSC Project 8173, Task 817303
- II. Contract No. AF33(657)-7847
- III. Allison Division, General Motors Corporation, Indianapolis, Indiana
- IV. Dr. B. Agruss, H. R. Karas, and V. L. Decker
- V. Allison Division EDR 3100
- VI. Aval fr OTS
- VII. In ASTIA collection

Aeronautical Systems Division, Dir/Aeromechanics, Flight Accessories Lab, Wright-Patterson AFB, Ohio. Rpt. No. ASD-TR-62-1045. DESIGN AND DEVELOPMENT OF A LIQUID METAL FUEL CELL. Final report, Dec 62, 155 pp. incl. illus., tables, 35 refs.

The electrochemical, physical, and chemical characteristics of potassium and potassium-mercury amalgams lend themselves to the successful operation of a liquid metal cell for space power. During the first year's work, substantial progress was made in the study and operation of potassium-mercury cells and in pointing up problem areas requiring solution. Six different types of cells were run, some utilizing a ceramic matrix while others operated on a differential density principle. Certain cells were operated with flowing cathode metal, so that steadiness of operation and regenerative capability could be studied. Results confirmed this regenerative capability up to 60 mw/cm², the operating level of the experiment. Liquid

(Over)

1. Liquid metal fuel cells
2. Potassium-mercury fuel cells
- I. AFSC Project 8173, Task 817303
- II. Contract No. AF33(657)-7847
- III. Allison Division, General Motors Corporation, Indianapolis, Indiana
- IV. Dr. B. Agruss, H. R. Karas, and V. L. Decker
- V. Allison Division EDR 3100
- VI. Aval fr OTS
- VII. In ASTIA collection

Aeronautical Systems Division, Dir/Aeromechanics, Flight Accessories Lab, Wright-Patterson AFB, Ohio. Rpt. No. ASD-TR-62-1045. DESIGN AND DEVELOPMENT OF A LIQUID METAL FUEL CELL. Final report, Dec 62, 155 pp. incl. illus., tables, 35 refs.

The electrochemical, physical, and chemical characteristics of potassium and potassium-mercury amalgams lend themselves to the successful operation of a liquid metal cell for space power. During the first year's work, substantial progress was made in the study and operation of potassium-mercury cells and in pointing up problem areas requiring solution. Six different types of cells were run, some utilizing a ceramic matrix while others operated on a differential density principle. Certain cells were operated with flowing cathode metal, so that steadiness of operation and regenerative capability could be studied. Results confirmed this regenerative capability up to 60 mw/cm², the operating level of the experiment. Liquid

(Over)

1. Liquid metal fuel cells
2. Potassium-mercury fuel cells
- I. AFSC Project 8173, Task 817303
- II. Contract No. AF33(657)-7847
- III. Allison Division, General Motors Corporation, Indianapolis, Indiana
- IV. Dr. B. Agruss, H. R. Karas, and V. L. Decker
- V. Allison Division EDR 3100
- VI. Aval fr OTS
- VII. In ASTIA collection

metal cell life was extended to as long as 550 hours to date. Current densities of 227 ma/cm² and power densities of 91 mw/cm² were achieved.

Composite matrices composed of 6- μ MgO particles were produced, and electrical conductivities of discs of various electrolyte/MgO ratios were measured. Results conform to requirements of liquid metal cell systems.

Preliminary measurements of those ceramic properties necessary for the design of a reliable cell seal were completed. Required support equipment was constructed.



metal cell life was extended to as long as 550 hours to date. Current densities of 227 ma/cm² and power densities of 91 mw/cm² were achieved.

Composite matrices composed of 6- μ MgO particles were produced, and electrical conductivities of discs of various electrolyte/MgO ratios were measured. Results conform to requirements of liquid metal cell systems.

Preliminary measurements of those ceramic properties necessary for the design of a reliable cell seal were completed. Required support equipment was constructed.



metal cell life was extended to as long as 550 hours to date. Current densities of 227 ma/cm² and power densities of 91 mw/cm² were achieved.

Composite matrices composed of 6- μ MgO particles were produced, and electrical conductivities of discs of various electrolyte/MgO ratios were measured. Results conform to requirements of liquid metal cell systems.

Preliminary measurements of those ceramic properties necessary for the design of a reliable cell seal were completed. Required support equipment was constructed.



metal cell life was extended to as long as 550 hours to date. Current densities of 227 ma/cm² and power densities of 91 mw/cm² were achieved.

Composite matrices composed of 6- μ MgO particles were produced, and electrical conductivities of discs of various electrolyte/MgO ratios were measured. Results conform to requirements of liquid metal cell systems.

Preliminary measurements of those ceramic properties necessary for the design of a reliable cell seal were completed. Required support equipment was constructed.

